USAAVRADCOM-TR-80-D-21

LEVEL # (12)

WIND TUNNEL TESTS OF LARGE- AND SMALL-SCALE
ROTOR HUBS AND PYLONS

A. H. Logan, R. W. Prouty, D. R. Clark
HUGHES HELICOPTERS
Division of Summa Corporation
Culver City, Calif. 90230

April 1981

Final Report for Period September 1977 - April 1980

Approved for public release;
distribution unlimited.

DTIC
ELECTE
MAY 7 1981
S A D

Prepared for

APPLIED TECHNOLOGY LABORATORY
U. S. ARMY RESEARCH AND TECHNOLOGY LABORATORIES (AVRADCOM)
Fort Eustis, Va 23604

81 5 04 170

APPLIED TECHNOLOGY LABORATORY POSITION STATEMENT

This report has been reviewed by the Applied Technology Laboratory, US Army Research and Technology Laboratories (AVRADCOM), and is considered to be technically sound.

The research described in this report is part of an ongoing program to reduce the drag and unsteady flow in the wake of helicopter components.

This effort was concentrated on the hub and pylon, although forces and moments were measured, and surface pressures measured and calculated for the entire body.

The scope of the entire drag program involves both a typical transport helicopter and a typical attack helicopter with modifications ranging from minor shape changes to the relocation of major components. However, during this contracted effort, only the proto-type attack helicopter was investigated with and without minor shape changes. In addition, these tests provided a measure of the relative importance of the effects of the presence of the rotor, hub rotation, engine inlet and exhaust flow, full versus partial-fuselage representation, and one-third-scale versus eight-tenths-scale tests.

This information is valuable not only to the present investigation but also for future, similar investigations. Comparisons of analytically determined pressures and measured pressures indicate the value of analysis in assessing the interference effects of body components on one another and on the determination of flow conditions which cause large differences in component drag.

The wind tunnel data resulting from this contract will be made available to qualified users upon request. Program DRAG, basis of the mathematical analysis used in this effort, is currently available through ATL.

Technical monitors for this contract were Mr. F. A. Raitch and 1LT D. D. Hollenbaugh, Aeromechanics Technical Area, Aeronautical Technology Division.

REPORT DOCUMENTATION PAGE	READ INSTRUCTIONS BEFORE COMPLETING FORM

1. REPORT NUMBER	2. GOVT ACCESSION NO.	3. RECIPIENT'S CATALOG NUMBER
USAAVRADCOM/TR-80-D-21	AD-A098510	

4. TITLE (and Subtitle)
WIND TUNNEL TESTS OF LARGE- AND SMALL-SCALE ROTOR HUBS AND PYLONS.

5. TYPE OF REPORT & PERIOD COVERED
Final Report.
September 1977 — April 1980

6. PERFORMING ORG. REPORT NUMBER
HH-80-15

7. AUTHOR(s)
A. H. Logan, R. W. Prouty, Hughes Helicopters
D. R. Clark, Analytical Methods, Inc.

8. CONTRACT OR GRANT NUMBER(s)
DAAJ02-77-C-0055

9. PERFORMING ORGANIZATION NAME AND ADDRESS
Hughes Helicopters
Division of Summa Corporation
Culver City, California 90230

10. PROGRAM ELEMENT, PROJECT, TASK AREA & WORK UNIT NUMBERS
62209A 1L262209AH76 00
213 EK

11. CONTROLLING OFFICE NAME AND ADDRESS
Applied Technology Laboratory, U.S. Army Research and
Technology Laboratories (AVRADCOM)
Fort Eustis, Virginia 23604

12. REPORT DATE
April 1981

13. NUMBER OF PAGES
134

14. MONITORING AGENCY NAME & ADDRESS(if different from Controlling Office)

15. SECURITY CLASS. (of this report)
Unclassified

15a. DECLASSIFICATION/DOWNGRADING SCHEDULE

16. DISTRIBUTION STATEMENT (of this Report)

Approved for public release; distribution unlimited.

17. DISTRIBUTION STATEMENT (of the abstract entered in Block 20, if different from Report)

18. SUPPLEMENTARY NOTES

19. KEY WORDS (Continue on reverse side if necessary and identify by block number)

Air Flow	Fuselages	Vorticity Panel Models
Boundary Layer Flow	Helicopters	Wind Tunnel Models
Computerized Simulation	Hubs	Wind Tunnel Tests
Drag Reduction	Model Tests	
Flow Fields	Pylons	

20. ABSTRACT (Continue on reverse side if necessary and identify by block number)

The Army YAH-64 and UH-60A helicopters were studied to determine optimum wind tunnel test procedures and to expand the experimental data base on drag reduction for rotor hubs and pylons. Full- and reduced-scale models of these helicopters were fabricated. The Hub Pylon Evaluation Rig (HPER) and the Generalized Rotor Modeling System (GRMS) were used for the experimental testing, conducted in the NASA/Langley V/STOL wind tunnel. Only the YAH-64 models underwent wind tunnel testing during this contracted effort. Plans are under way for testing of the UH-60A models. All configurations were subjected to viscous analysis using

DD FORM 1473 EDITION OF 1 NOV 65 IS OBSOLETE
1 JAN 73

409164

Block 20.   Abstract - Continued.

Program DRAG, a configuration modeling program. This effort included evaluation of hub fairings, pylon fences, rotor wake flow, hub rotation, engine air flow, fuselage parasite drag, empennage flow, and stabilators. The DRAG program was validated by correlation of predicted and experimentally obtained surface pressures. All test data will be retained as background material and made available upon request. This data includes HPER and GRMS wind tunnel force and moment data, and surface pressure data recorded during the wind tunnel testing.

PREFACE

Accession For

NTIS GRA&I ☑
DTIC TAB ☐
Unannounced ☐
Justification

Distribution/

Availability Codes

Avail and/or
Special

A

TABLE OF CONTENTS

LIST OF ILLUSTRATIONS

LIST OF ILLUSTRATIONS (CONT)

LIST OF TABLES

INTRODUCTION

A full understanding of airflow characteristics near the main rotor hub and upper fuselage is essential in order to attain the operational improvements desired in future Army helicopters. The main rotor hub and upper fuselage area contributes from 20 to 40 percent of the total aircraft drag and directly affects aircraft performance, power requirements, fuel consumption, and rotor blade loads. Drag is a measure of interference effects and flow separation that impacts handling qualities, vibration, and tail disturbances. An understanding of the main rotor hub and upper fuselage airflow will allow the effects of drag and separation to be controlled and reduced.

The understanding of the helicopter fuselage flowfield and the subsequent prediction of drag have always been very difficult tasks (Reference 1). Due to the limited capabilities of early analytical techniques, the traditional method of investigating these areas has been experimental testing. Testing, however, has drawbacks in that it is time-consuming, costly, and usually conducted at scales considerably under full size. This results in questions of Reynolds number scaling and questions of adequate model physical representation. Whenever full-scale tests were conducted, they were only on parts of the helicopter configuration, mounted in too-small wind tunnels where wall and floor constraints and the absence of the rest of the aircraft contaminated the results. Common to both model and full-scale testing were questions concerning the requirement for hub rotation and rotor wake representation.

Recent analytical modeling work has reduced reliance on testing by providing analytical methods that model the complex flowfield of the main rotor hub and upper fuselage area, permitting the timely and efficient pretest evaluation of alternate hub and fuselage configurations. Correlations to date have shown good agreement between analytical predictions and the limited available experimental data up to the point of boundary layer separation. Current methods have extended the analysis into areas of extensive flow separation.

In order to answer the questions about wind tunnel testing, to provide a more consistent experimental data base, to expand the analysis, and to answer the questions regarding the equivalence of model and full-scale test data, a combined experimental and analytical program was undertaken. As outlined in Figure 1, typical Army helicopters were analytically and experimentally

1. Special report presented to the American Helicopter Society, 31st Annual National Forum, by the Ad Hoc Committee on Rotorcraft Drag, Washington D.C., 21 May 1975.
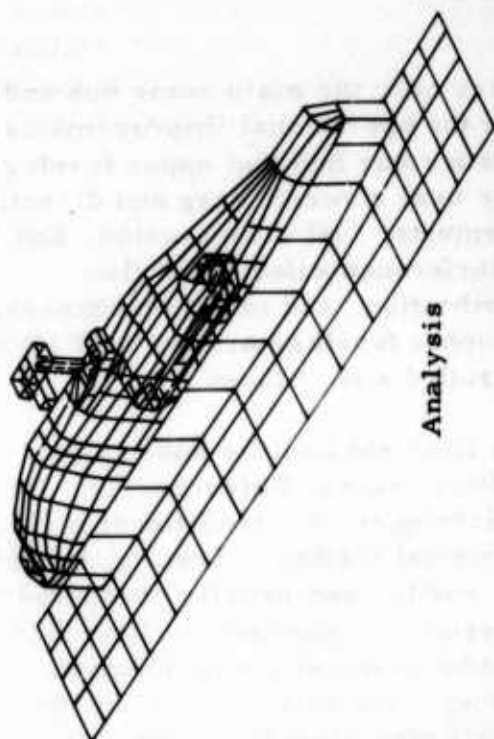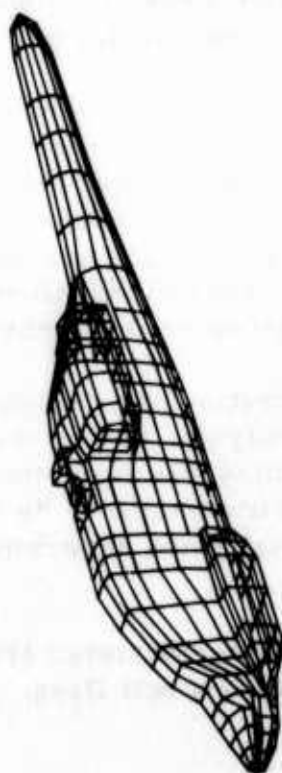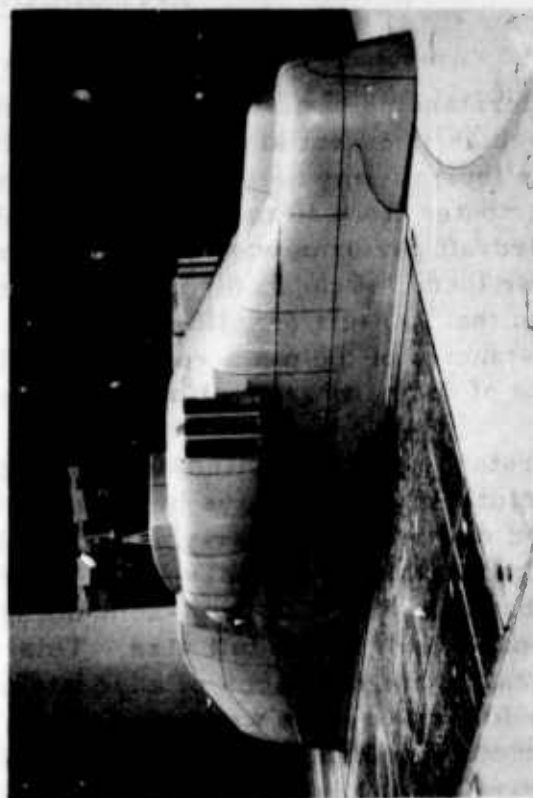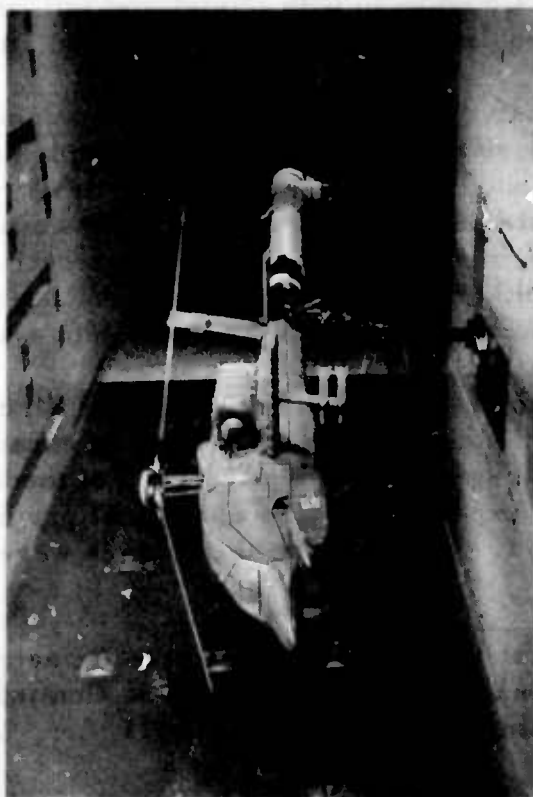
GRMS Testing   HPER Testing

Figure 1. Large- and Small-Scale Tests Combined with Analysis.

studied at model scale (approximately 25 percent) and as close to full scale as wind tunnel test facilities would allow (80 percent). All configurations tested were examined using a configuration modeling analysis that included viscous effects. The results of these tests were correlated with the computer analysis to verify the ability of the analysis to model complex helicopter configurations.

The YAH-64 and UH-60A Army helicopter configurations used in the investigation are representative of an armed attack helicopter and a utility helicopter. Both aircraft were studied analytically, and 80 and 25 percent scale models were fabricated. Only the YAH-64 armed attack helicopter models were tested in the NASA/Langley V/STOL tunnel. The UH-60A models are scheduled to be tested at a future date.

The experimental models were fabricated to be installed on the Hub Pylon Evaluation Rig (HPER) for the large-scale testing (80 percent of full size) and the General Rotor Modeling System (GRMS) for the reduced-scale testing (25 percent). The HPER models represented the upper half of the YAH-64 and UH-60A fuselage and pylon configurations, while the GRMS models represented the complete helicopter, which for the YAH-64 included the nose sighting system, wing, and tail empennage. For the YAH-64 GRMS model, a four-bladed rotor system was tested to evaluate the effect of main rotor wake. At both model scales, the model hubs represented realistically the components on the actual hub, up to the blade attachment. The main hub body; lead-lag dampers; pitch housing; and pitch and scissors links, both rotating and nonrotating, were represented. In addition, the hubs were designed to be rotated at scale speeds. For both the YAH-64 and UH-60A, the HPER and GRMS hubs were identical except for size.

The computer program used in the design analysis is a completely viscous procedure that couples potential flow, streamline, boundary layer, and separated flow analysis in an iterative procedure, using the potential flow solution as input to the viscous analysis. The viscous analysis includes boundary layer growth and large areas of shed separated wake as well as the effects of the engine inlet and exhaust flow.

The testing of the YAH-64 HPER and GRMS models covered the full range of helicopter operating conditions. Test conditions include speeds up to 145 knots, fuselage angles of ±10 degrees, full and partial rotor wake simulation, variation of hub advance ratio, full and partial fuselage representation, and engine airflow/exhaust simulation. In addition to the basic configurations, low-drag fairings for the YAH-64 hub and pylon were tested at both model scales.

15

In the YAH-64 model tests, the forces and moments on the hub, pylon, and fuselage were measured independently by a system of internal balances. Pressure taps were installed on the fuselage and pylon surfaces, and were located close enough together to define boundary layer separation areas as well as differentiate between left- and right-hand fuselage surface pressures caused by model yaw and main rotor wake effects. A one-to-one correlation between the location of the pressure taps on the models and the calculation points of the computer program facilitated an extensive comparison of analytical and experimental pressures.

Wake surveys were taken for the small-scale YAH-64 model in several configurations. The wake velocity deficit and direction were mapped in the plane of the stabilizer, both with and without main rotor downwash. The effects of main rotor hub fairings and the wing/rocket pod were also determined.

EXPERIMENTAL MODELS

The YAH-64 and UH-60A HPER models are 80 percent of full scale (Figures 2 and 3). The YAH-64 HPER model is 25 feet long, 6 feet 10 inches wide, and 5 feet 8 inches tall. The centerline of the hub is located 7 feet 5 inches from the floor of the tunnel and has an overall diameter of 5 feet 4 inches. The UH-60A HPER model is 25 feet long, 6 feet 6 inches wide, and 5 feet 6 inches tall. The centerline of the hub is located 7 feet from the tunnel floor and has an overall diameter of 4 feet 1 inch.

The HPER models are divided into three major components: fuselage, pylon, and hub. The fuselage and pylon are anchored independently to the HPER, with the pylon forces recorded on a balance and the nonmetric fuselage rigidly attached. The hub is secured to the HPER driveshaft with four bolts, and forces are measured independently from the pylon.

The YAH-64 and UH-60A GRMS models (Figures 4 and 5) are 30 and 25 percent of full scale respectively. The YAH-64 GRMS model fuselage is 156 inches long, 32 inches wide, and 25 inches tall. The hub diameter is 24 inches. The UH-60A GRMS model is 120 inches long, 24 inches wide, and 23 inches tall. The hub diameter is 15 inches.

Both the YAH-64 and UH-60A GRMS models are divided into four major components: fuselage, pylon, tail, and hub (Figure 6). The fuselage and pylon components are anchored independently to the GRMS. The fuselage attaches to the wing mount and is supported by the 748 balance. The pylon is attached to the GRMS frame by a steel machine fitting and is supported by the 731 balance. The tail component is attached to the GRMS sting using a steel machine fitting and is supported by the VST-2 balance. The hub is secured to the GRMS driveshaft, which is supported by the SIK-2.5 balance.

The pylon areas of the HPER and GRMS models were identical. The YAH-64 pylon area, which was defined as all nonrotating elements above Waterline 145 and between Stations 160 and 370 (Figure 7), includes the engine nacelles and the stationary mast. The UH-60A pylon area was defined as all nonrotating elements above Waterline 250 and between Stations 235 and 507.

_____

2. Wilson, John C., A GENERAL ROTOR MODEL SYSTEM FOR WIND TUNNEL INVESTIGATION OF ROTORCRAFT AERODYNAMICS AND ACOUSTICS, Journal of Aircraft, Vol. 6, 1974.
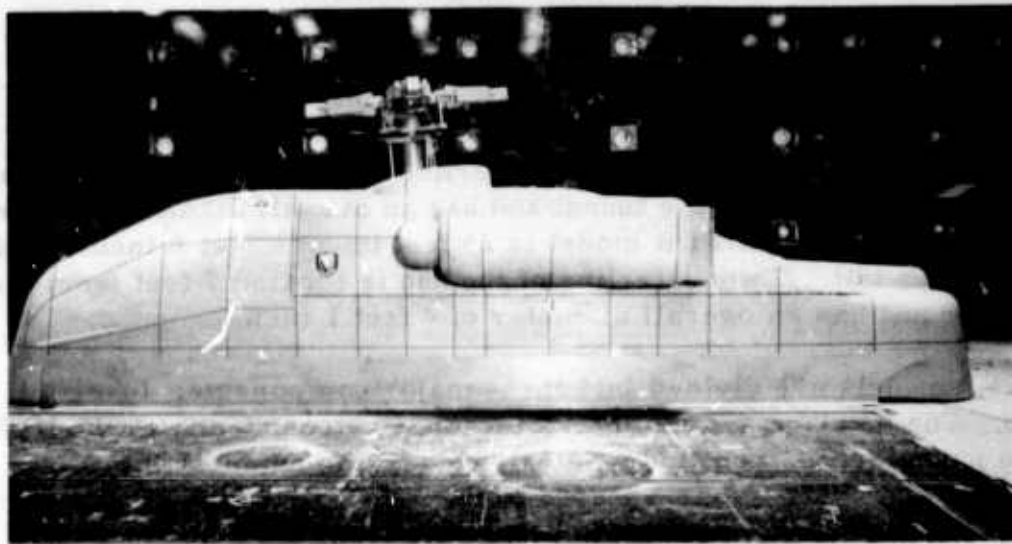
(a) Side View
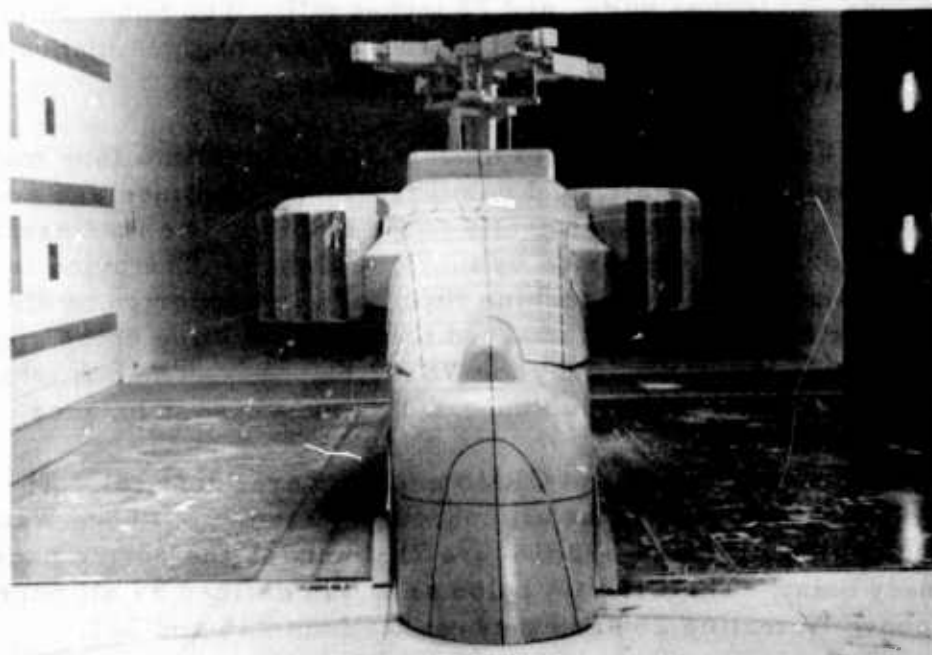
(b) Rear View

Figure 2. YAH-64 HPER Model, Shown in the NASA/Langley V/STOL Tunnel.

18
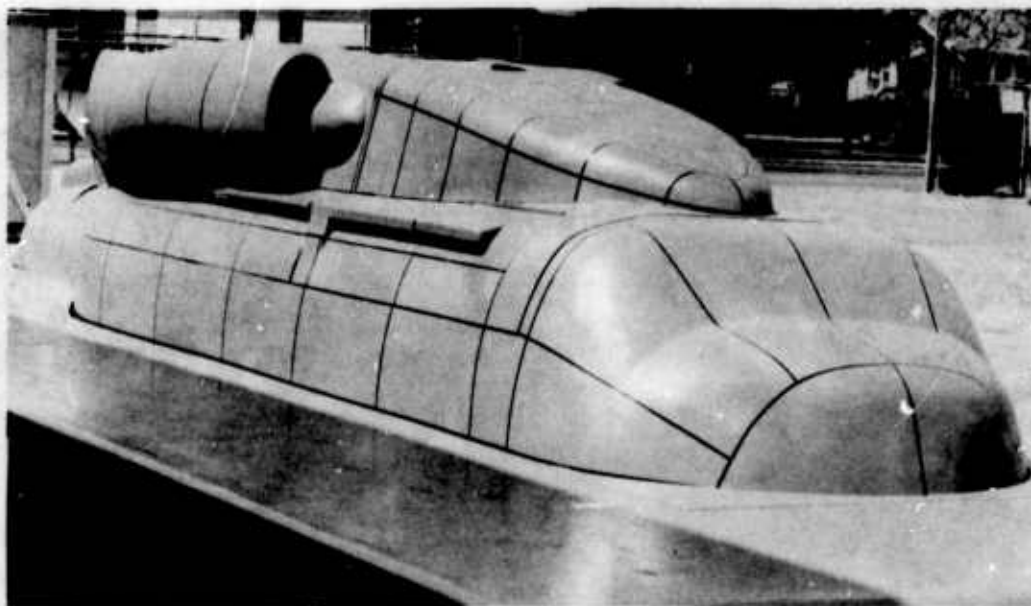
(a) Front View
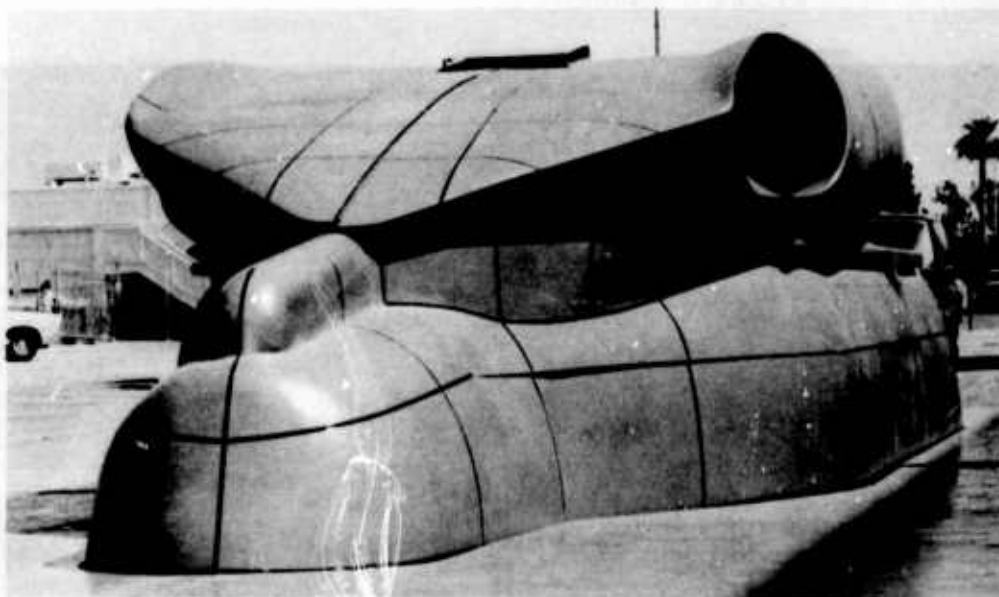
(b) Rear View

Figure 3. UH-60A HPER Model, Shown without Hub and with Splitter Plate.

19

Figure 4.   YAH-64 GRMS Model, Shown in the NASA/Langley
V/STOL Tunnel.
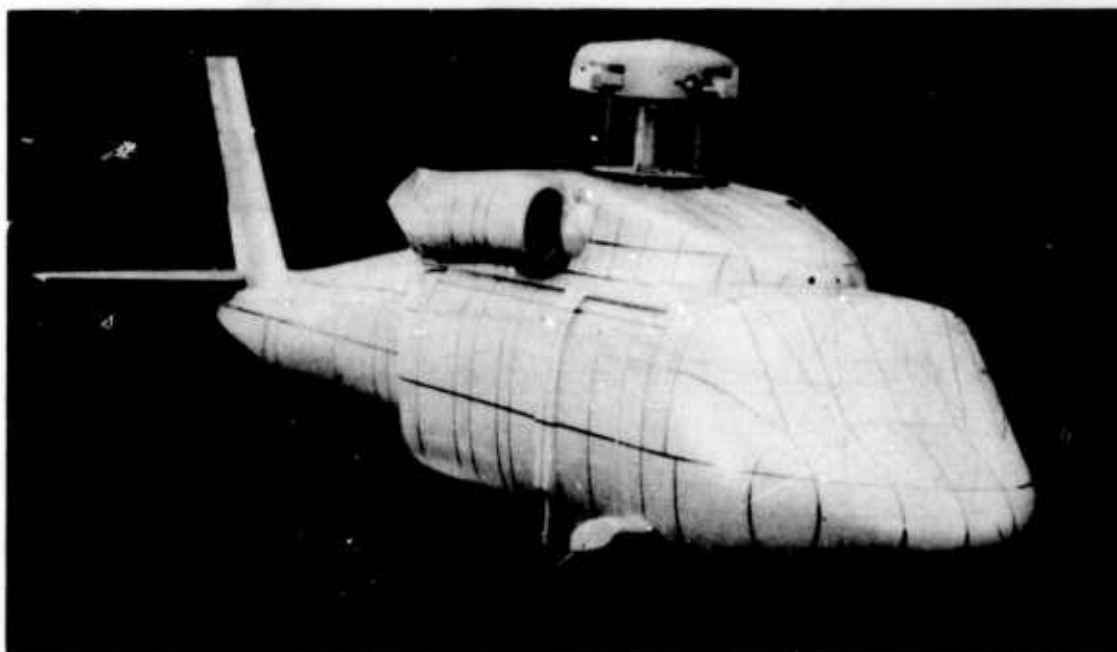
Figure 5.   UH-60A GRMS Model, Shown with
Faired Hub.

20
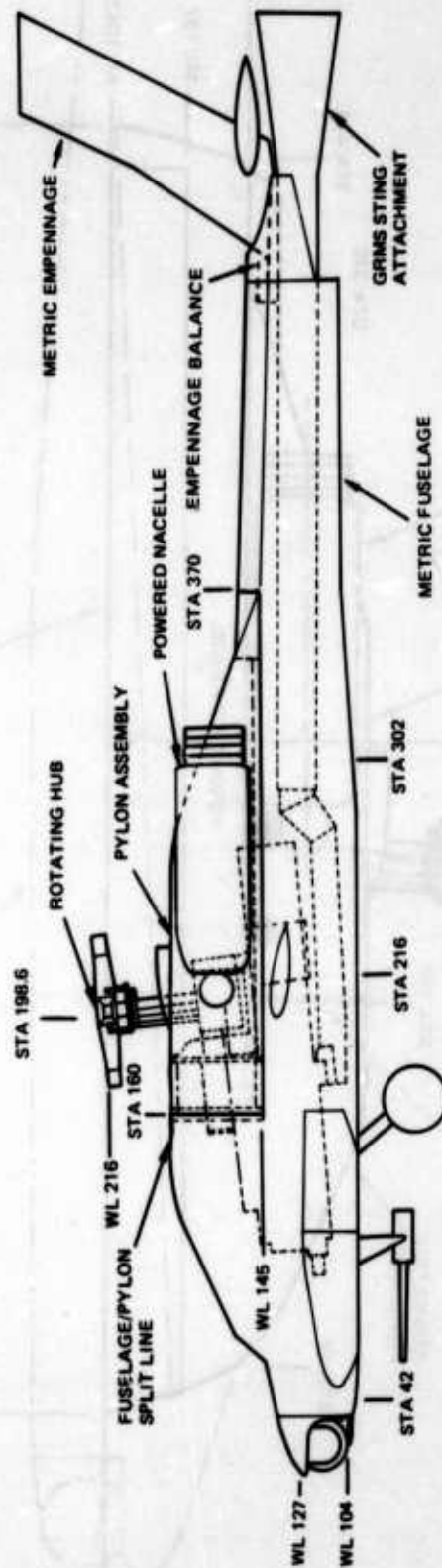
Figure 6. General Arrangement of GRMS YAH-64 Model.
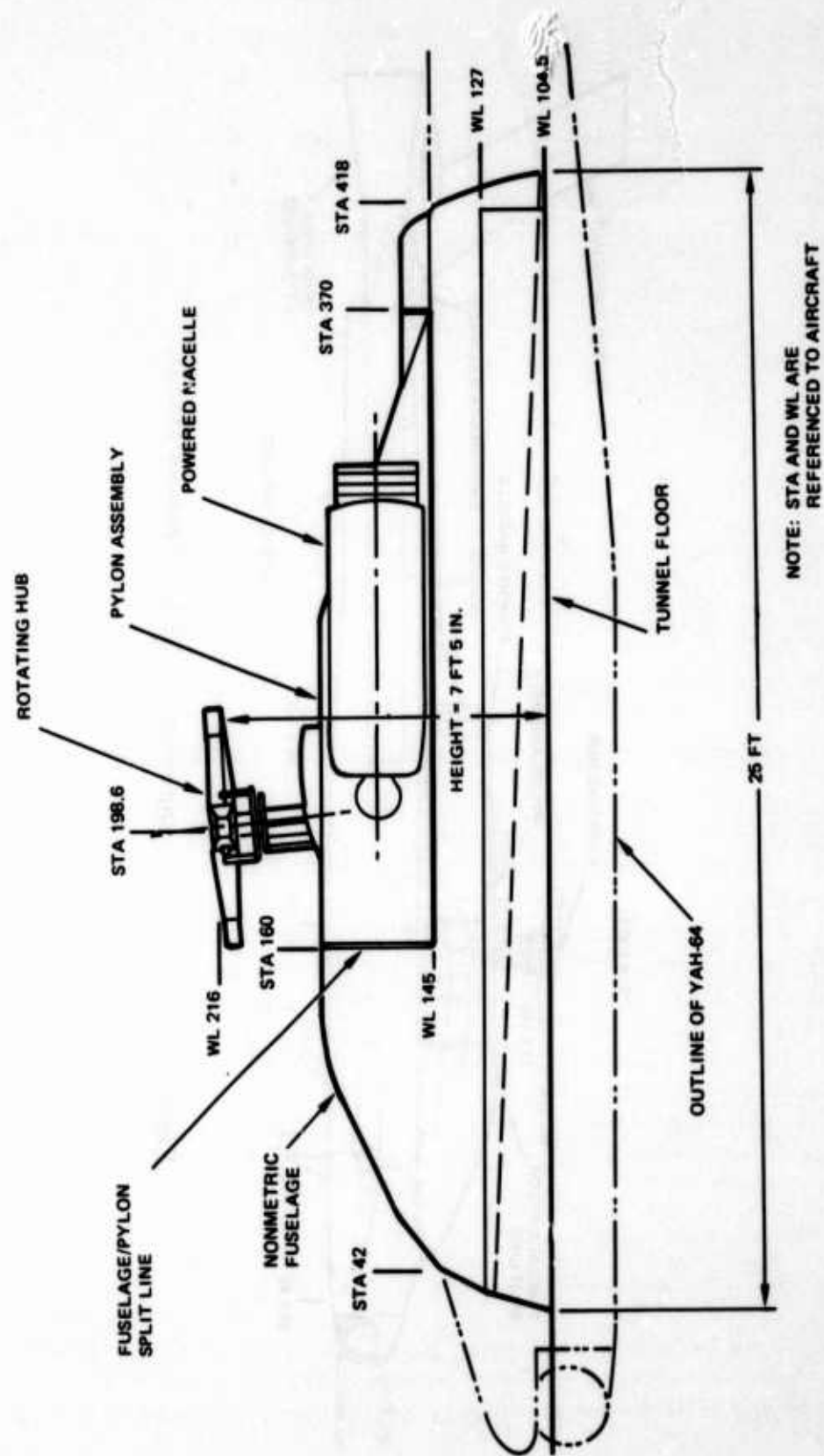
Figure 7. General Arrangement of HPER YAH-64 Model.

ROTATING HUB

FUSELAGE/PYLON
SPLIT LINE

PYLON ASSEMBLY

POWERED NACELLE

STA 198.6

NONMETRIC
FUSELAGE

WL 216

STA 160

STA 42

STA 370

STA 418

WL 127

WL 104.5

WL 145

HEIGHT = 7 FT 5 IN.

TUNNEL FLOOR

25 FT

OUTLINE OF YAH-64

NOTE: STA AND WL ARE
REFERENCED TO AIRCRAFT

The HPER models were configured to allow the simulation of inlet and exhaust airflow. During the tests, four 292-1C tip turbine fans were used to simulate model engine nacelle and mast airflow in the YAH-64 HPER model. Two 292-1C tip turbine fans were used to simulate engine nacelle airflow, and an airline was used to simulate oil cooler airflow in the UH-60A model. The fan support structure is nonmetric and is mounted to the HPER fuselage support frame.

The GRMS models were also configured to permit the simulation of inlet and exhaust airflow. On the YAH-64, four Model 897 turbine fans were used to simulate engine nacelle and main rotor mast airflow. On the UH-60A, two Model 897 tip turbine fans were used to simulate engine nacelle airflow, and an airline was used to simulate oil cooler airflow. On both helicopter models, the fans are mounted to the internal bulkheads of the pylon, and fan forces are included in the pylon balance measurement. The fan drive air is provided by a 3/8-inch, S-shaped stainless steel tube that serves as a bridge from the sting side to the model side.

The HPER models were originally designed to be tested with a splitter plate located 18 inches above the tunnel floor. (The splitter plate is shown fitted around the UH-60A HPER model in Figure 3.) During the course of model development, however, work at the V/STOL tunnel indicated that large boundary layer growth could be controlled by suction on the tunnel floor upstream of the test section. Consequently, the splitter plate was not used to reduce tunnel blockage.

The YAH-64 GRMS model was tested with the four-bladed GRMS rotor system (Figure 4). Relative to the full-size YAH-64, the rotor system was built to 21 percent of scale and was therefore undersized for the body (built to 30 percent of scale). Since the objective of the testing was not rotor performance but an evaluation of the effect of rotor wake on the fuselage forces, the mismatch in rotor fuselage scaling was acceptable, and reduced the program cost by making use of available hardware. During testing the rotor system was trimmed at 7 pounds per square foot disc loading and zero flapping relative to the rotor shaft, which was tilted forward 5 degrees to match the YAH-64.

Surface pressure taps and a grid system were installed on the HPER and GRMS models. For each model, approximately 200 pressure taps were located along the waterline and section lines and, wherever possible, at the central points used in the mathematical analysis. The grid system is used to locate the paneling used in the mathematical analysis and is the same for both the GRMS and HPER models of each helicopter, YAH-64 or UH-60A.

Testing of the YAH-64 HPER and GRMS models was conducted in the 14.5- by 21.75-ft closed test section of NASA's V/STOL tunnel at Langley Research Center in Hampton, Virginia. The large model was bolted to the steel tunnel floor, with the HPER aligned along the centerline of the front portion of the 60-ft-long test section, immediately behind the boundary layer suction slot. The small model was attached to the pitch and yaw sting of the V/STOL tunnel, aligned with the tunnel centerline and with the hub centered in the tunnel.

The YAH-64 HPER tests were run at free-stream airspeeds of 30, 60, 90, 120, and 145 knots. All testing was conducted in the closed test section with the boundary layer suction in operation.

The YAH-64 GRMS tests were run at 40, 80, and 120 knots. Generally, testing was conducted in the closed test sections except for some low-speed stabilator runs with the GRMS rotor system.

The basic YAH-64 rotor hub for both the HPER and GRMS models is shown in Figure 8. For the HPER, rotor hub rotation was varied from 0 to 289 rpm (which represented 100 percent power), while for the GRMS the hub rotation was varied from 100 to 770 rpm. The rotational tip speed was thus the same in both models, and the engine inlet and exhaust mass flows for both models were adjusted to properly simulate the appropriately scaled engine mass flow as a function of tunnel speed. It is not possible to simultaneously match the inlet and exhaust mass flows of a gas turbine engine with an air-driven simulator, and separate runs were therefore made in which the inlet and exhaust flows were alternately modeled. The engine exhaust mass flow was simulated using a cold flow technique that matches dynamic pressure between hot and cold exhaust.

The basic YAH-64 aircraft utilizes inlet airflow obtained through the rotor mast opening as well as through the nacelle inlet, and both flowpaths were represented on the models. Inlet mass flows were computed by utilizing data from the inlet pitot/static rakes, and drive/air mass flows were determined from the tunnel flowmeter data. The total mass flow out of the exhaust was simply the total of the fan inlet mass flow and the drive/air mass flow. Force and moment data have been corrected for momentum drag and internal forces due to air mass flow.

For HPER and GRMS testing, a data run generally consisted of an angle-of-attack sweep for a given combination of airspeed, hub rotation speed, and engine mass flow. At each angle of attack, 10 complete samples of all force, moment, and pressure data were automatically recorded over a 5-second interval by the digital data acquisition system, and the raw data were stored
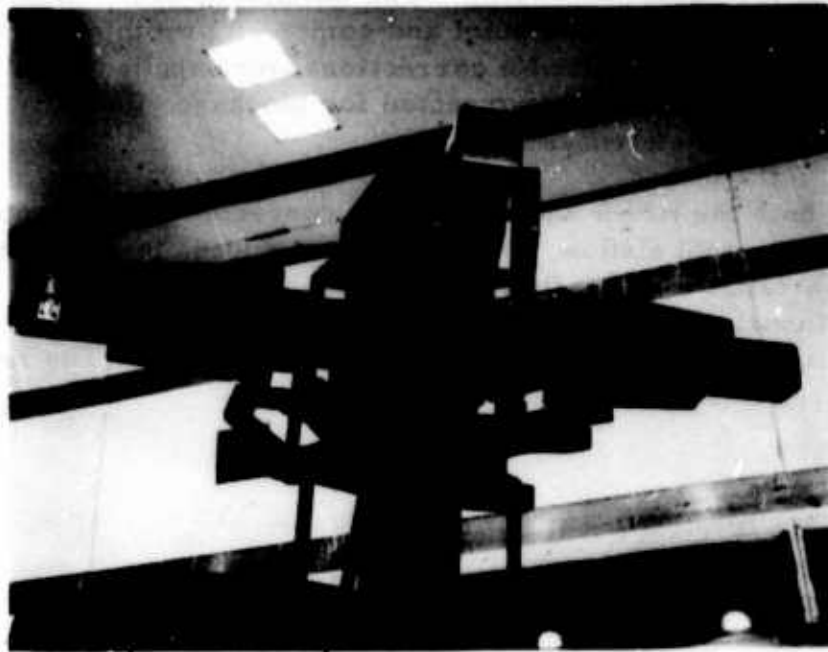
(a) HPER
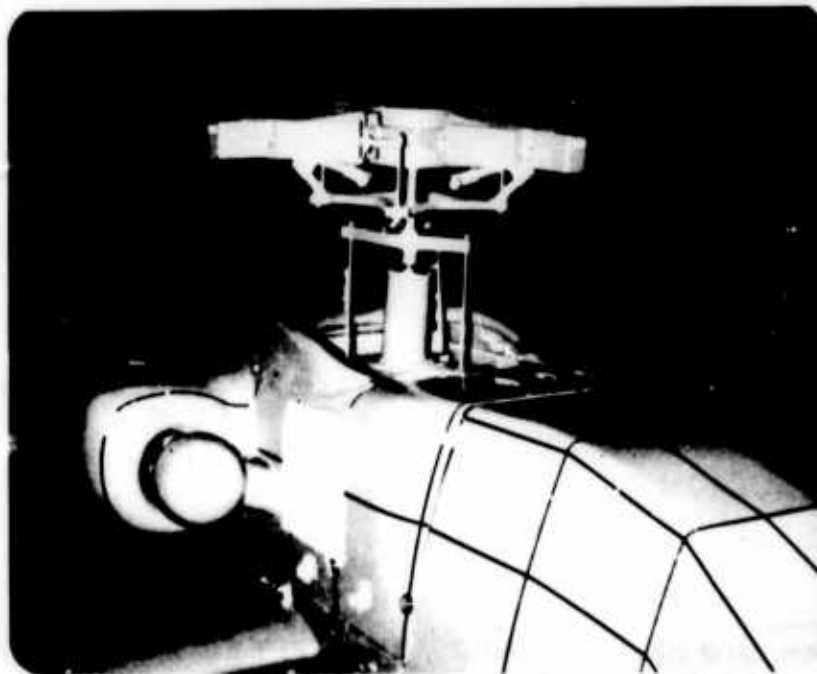
(b) GRMS

Figure 8. YAH-64 Basic Hub for the HPER and GRMS Models.

25

on magnetic tape for batch processing. The on-line computer averaged the raw data to produce a single data point and computed preliminary data in coefficient form for each point. No corrections were applied to the on-line data, but all final data have been corrected for blockage effects by the methods presented in References 3 and 4.

Pylon drag for both the HPER and GRMS was corrected for both momentum drag and engine internal airflow. Without tunnel speed, the internal fans were run over a range of mass flows, and pylon balance data were recorded. For runs with tunnel speed, this static tare was removed from the pylon data to account for internal losses as well as momentum thrust. The inlet ram drag was also removed.

3. Pope, Allen, and Harper, John J., LOW-SPEED WIND TUNNEL TESTING, John Wiley and Sons, Inc., New York, 1966.

4. Hess, John L., CALCULATIONS OF POTENTIAL FLOW ABOUT ARBITRARY THREE-DIMENSIONAL LIFTING BODIES, Report No. J5679-01, McDonnell Douglas Corp., October 1972.

ANALYTICAL METHODS

The mathematical analysis was carried out using the Wing and Body
Aerodynamics with Boundary Layer Effects (WBABL) and DRAG programs
described in References 5 and 6. These programs were developed from the
basic WBAERO program (Reference 7), which used a panel model representa-
tion with source and vortex singularities to calculate surface flow effects and
distributed and integrated airloads (Figure 9). The earlier WBAERO pro-
gram modeled the presence of separated flow by changing the effective surface
boundary condition in the separation zone. This was adequate provided that
the extent of the separation was known ahead of time and that accurate pre-
diction of the airloads in the separated region was not required. Its use was
also limited, however, by a requirement imposed by the streamline tracing
routine then used for a regular panel network. This combination of problems
precluded a realistic drag calculation, especially when irregular shapes were
involved (as with most helicopter configurations).

To overcome these problems, Program DRAG was developed. In this pro-
gram, paneling flexibility was recovered by using patches of panels. This
was done to allow panel density to vary with the variation in body surface
curvature and still retain the rectangular grid of panels, required by the
streamline tracing, within each patch. At the same time the streamline
tracing routine was enhanced, and the singularities used to represent the
body panels were changed from constant-source to variable-vorticity ele-
ments to better model the local airloads close to separation. A method of

5. Dvorak, F., Maskew, B., and Woodward, F., INVESTIGATION OF
    THREE-DIMENSIONAL FLOW SEPARATION ON FUSELAGE CONFIGU-
    RATIONS, Analytical Methods, Inc.; USAAMRDL-TR-77-4, Eustis
    Directorate, U.S. Army Air Mobility Research and Development
    Laboratory, Fort Eustis, VA, March 1977, AD A039382.

6. Clark, D., Dvorak, F. Maskew, B., Summa, J., and Woodward, F.,
    HELICOPTER FLOW FIELD ANALYSIS, Analytical Methods, Inc.;
    USARTL-TR-79-4, Applied Technology Laboratory, U.S. Army Research
    and Technology Laboratories, Fort Eustis, VA, April 1979, AD A069542.

7. Woodward, F., Dvorak, F., and Geller, E., A COMPUTER PROGRAM
    FOR THREE-DIMENSIONAL LIFTING BODIES IN SUBSONIC INVISCID
    FLOW, Flow Research, Inc.; USAAMRDL-TR-74-18, Eustis Directorate,
    U.S. Army Air Mobility Research and Development Laboratory, Fort
    Eustis, VA, April 1974, AD 782202.

SURFACE SOURCE PANELS

HORSESHOE VORTEX SYSTEM

Figure 9. Source and Vortex Panel Arrangement
on Wing/Body Combination.

modeling the separated flow that was developed for predicting post-stall airfoil behavior is used in the DRAG program. This allows the calculation of airloads in the separation zone and, hence, permits accurate calculation of drag.

For applications that require only the prediction of regions of separated flow without full modeling, Program WBABL can be used. WBABL has the panel/patch flexibility and the improved streamline tracing capability of DRAG but retains the simpler source singularity. WBABL therefore provides a tool for predicting viscous effects to the same level as Program DRAG but, because of the simpler singularity, with considerable savings in execution time and cost. Both programs were used in this study.

Two basic configurations were modeled, the YAH-64 and the UH-60A. Each aircraft was modeled as it would appear on the HPER for large-scale testing (80 percent of full size) and on the GRMS for reduced-scale testing (25 percent). Although the testing in this first phase was to be restricted to the YAH-64 models, all four basic configurations were constructed and analyzed. The panel models are shown in Figures 10 through 13.

28
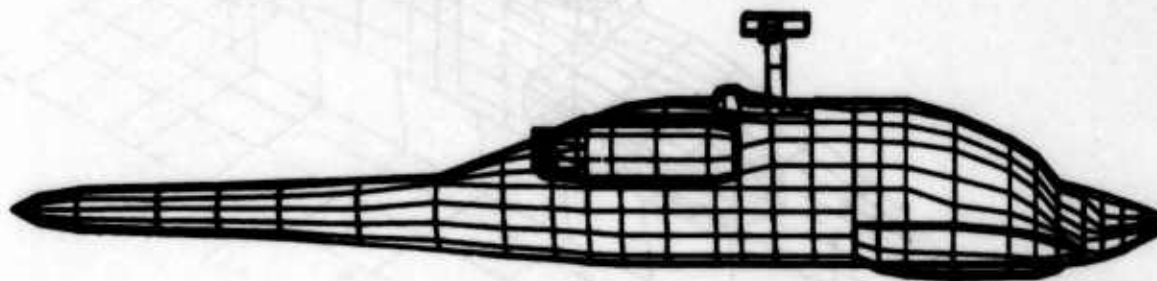
Figure 10. YAH-64 GRMS Panel Model.
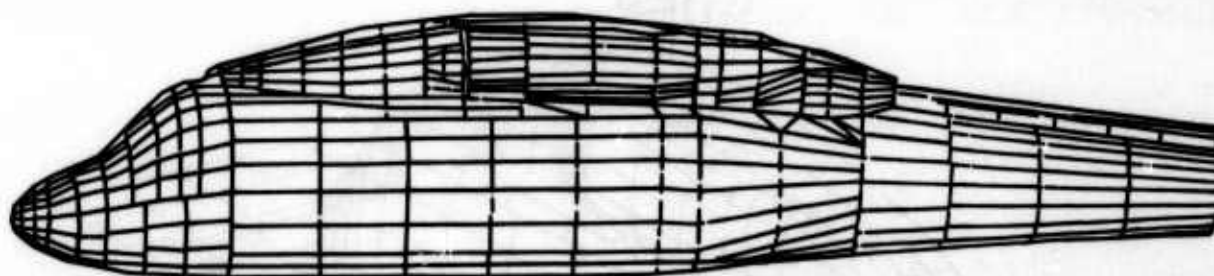
Figure 11. UH-60A GRMS Panel Model.

29
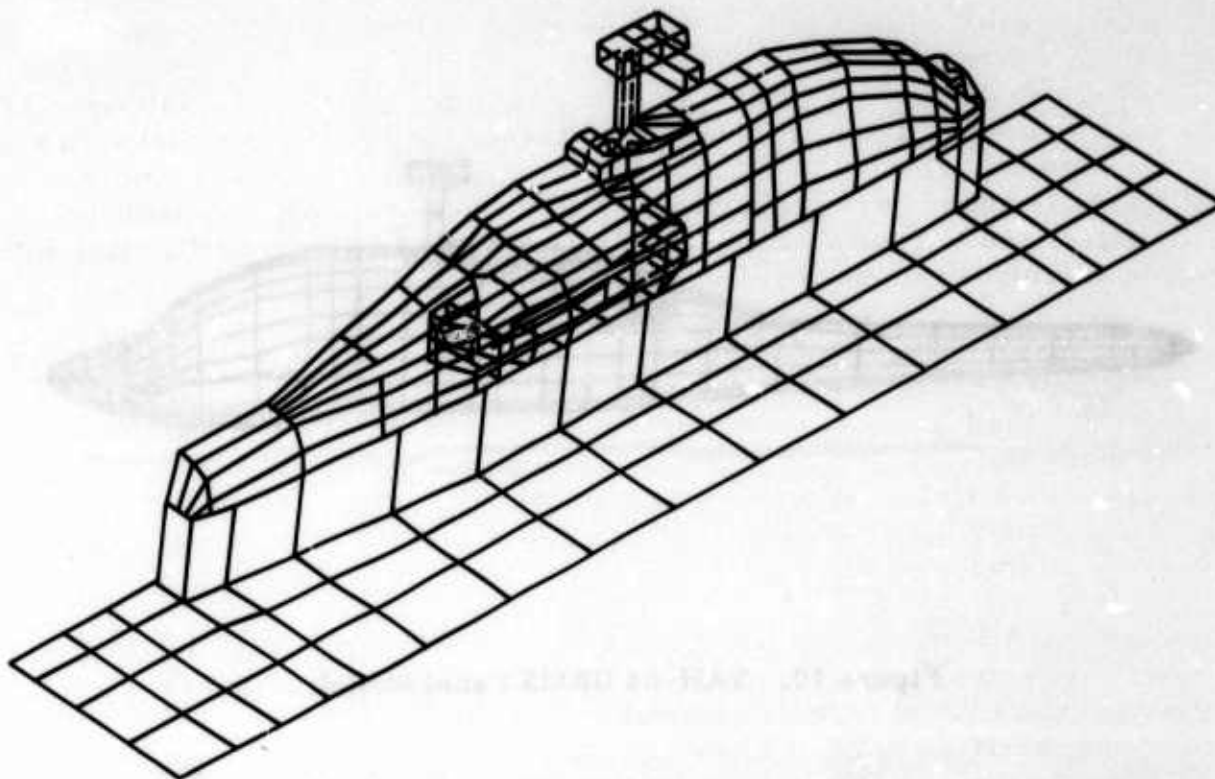
Figure 12. YAH-64 HPER Panel Model.
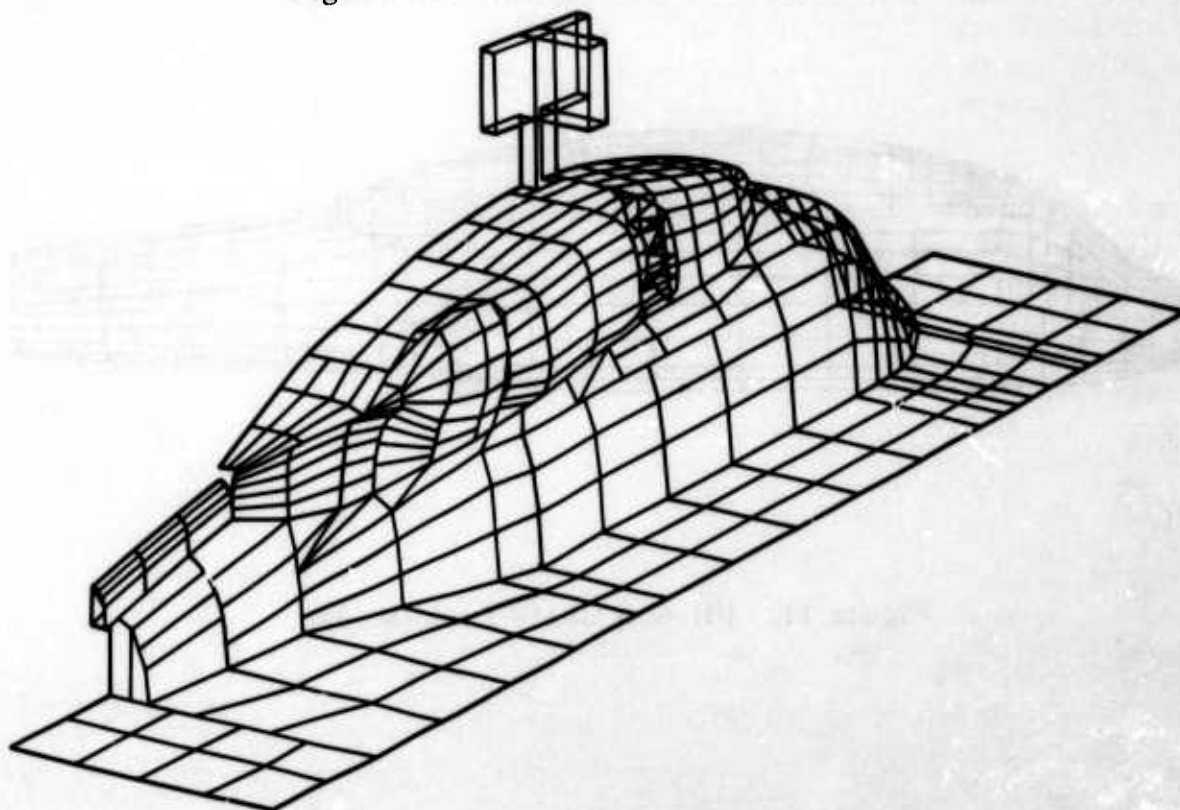
Figure 13. UH-60A HPER Panel Model.

30

The GRMS panel models (Figures 10 and 11) represented the complete helicopter, which for the YAH-64 included the nose sighting system and the forward avionics bays (FABs). The UH-60A panel model shown in Figure 11 is drawn without a complete tailboom, although the analytical model used had a complete tailboom (as is shown in Figure 10). The HPER panel models (Figures 12 and 13) were half models with the nose rounded, the tailboom truncated, and (for the YAH-64) the FABs deleted. These modifications were made to provide remote angle-of-attack change capability.

While not shown on the panel models pictured in Figures 12 and 13, the wind tunnel walls were included in the calculation. This was felt to be necessary because of the large size of the test hardware relative to the wind tunnel cross section. (The method of representing the tunnel is given in detail in Reference 5.) In an attempt to keep computation time and computer core requirements to a reasonable level, a relatively spare panel model of the tunnel was employed.

The basic YAH-64 and UH-60A models were paneled by HH and Sikorsky respectively for execution in their own codes. In neither case was this a problem since HH operates with a version of Program WBAERO and the Sikorsky paneling scheme, described in detail in Reference 8, can be accepted by the WBABL and DRAG programs with no modification. Only minor adjustments were made to the original panel models. In the case of the UH-60A model, this was limited to repaneling the joint between the pylon and fuselage to minimize the patch joint information that has to be carried over from aerodynamics to streamline tracing routines.

For these baseline configurations, the paneling density was deliberately left relatively open — 423 panels for the YAH-64 GRMS and 326 panels for the YAH-64 HPER — to allow for increased densities in the regions of interest as modifications of increased complexity were incorporated. The equivalent numbers for the UH-60A aircraft were 508 and 426 panels respectively. No attempt was made to model in detail the rotor hub/shaft/control linkage assemblies. Although this is theoretically possible, the number of panels required would have absorbed the entire program capacity and left none available for the airframe. Instead, a momentum model of the assemblies was developed based on the good correlation between hub frontal area and drag noted in Reference 8.

---

8. Sheehy, T. W., and Clark, D. R., A METHOD FOR PREDICTING HELICOPTER HUB DRAG, Sikorsky Aircraft Div., United Technologies Corp.; USAAMRDL-TR-75-48, Eustis Directorate, U. S. Army Air Mobility Research and Development Laboratory, Fort Eustis, VA, January 1976, AD A021201.

Knowing the frontal area of the swept volume of the hub/shaft assembly, a drag coefficient can be determined from Reference 8. With this known, a crude panel model of the volume can be developed (Figure 14), and the boundary conditions on the forward and aft panels can be set to permit a through flow with a momentum deficit (the difference between inflow and outflow) adjusted to match the empirical drag. The strengths of the singularities on the other faces, calculated in the normal manner, provide the displacement effect of the flow moving aside to pass around the volume. With the momentum deficit known, a vortex sheath can be tacked on around the edges of the aft-facing panels (as is done with the engine efflux, described in Reference 5).

The program used for the study has the ability to model inlet and exhaust flows and to represent exhaust efflux effects. Inlet/exhaust modeling is done simply by specifying a boundary condition at the inlet or exhaust face other than the zero normal velocity of a solid surface. With the exhaust mass flow and energy level defined from the engine parameters, a vortex sheath having
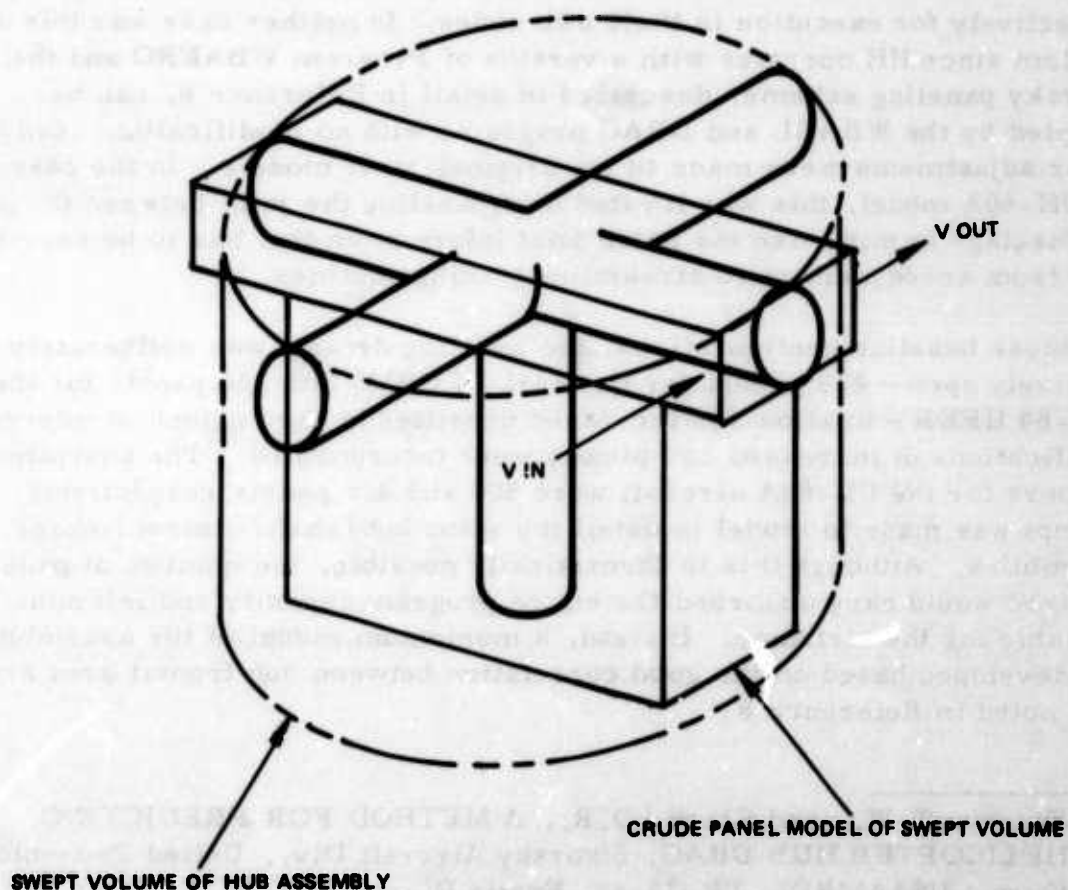
Figure 14. Hub Analysis Model.

32

strength equal to the energy jump from the efflux to the outside can be tacked on around the efflux. On both the GRMS and HPER versions, inlet and exhaust flows were specified. This included the mast inlet flow as well as the power plant inlet and exhaust. No attempt was made to model in detail the Black Hole infrared radiation suppressor on the YAH-64, and a simple block model was used. Modeling the details of the flow between the elements of the exhaust system, while possible, would have compromised the number of panels required for the more significant hub/pylon region.

In addition to the engine exhaust, the air mass drawn in around the YAH-64 mast was also modeled. The procedure is similar to that for the engine exhaust model.
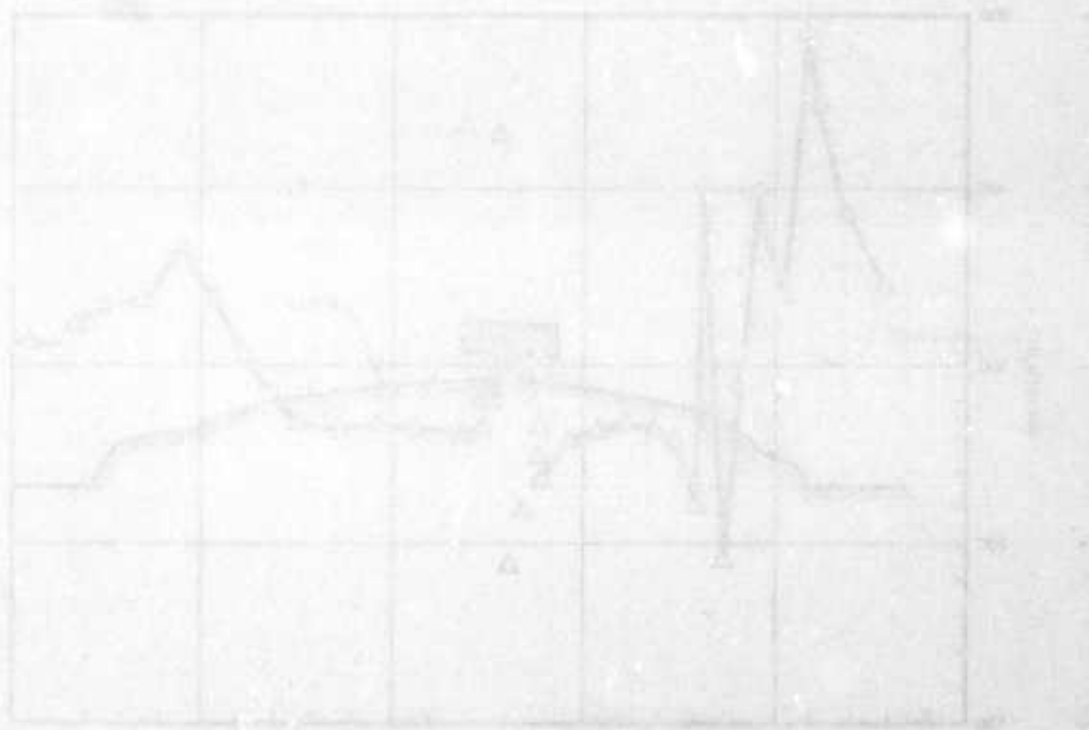
Based on the fuselage pressure distributions predicted by Program DRAG, alternate pylon and hub modifications were developed for the YAH-64 and UH-60A aircraft. The guideline for the alternative pylon configuration was to enclose all mechanical elements within the pylon fairing of the baseline configuration, making every effort to shape the fairing for optimum airflow conditions. Movement of the mechanical elements was not allowed. Another important but unstated guideline was to minimize the projected frontal area of the aircraft, since previous studies have shown that aircraft drag rises almost linearly with projected frontal area. For the present baseline pylons, it is particularly difficult to minimize the frontal area without rearranging mechanical elements because the space between the present pylon and existing components is minimal.

An examination of the UH-60A HPER baseline pressure distribution (Figure 15) reveals two problem areas. First, there is a series of secondary stagnation points as the airflow accelerates over the nose, over the canopy,
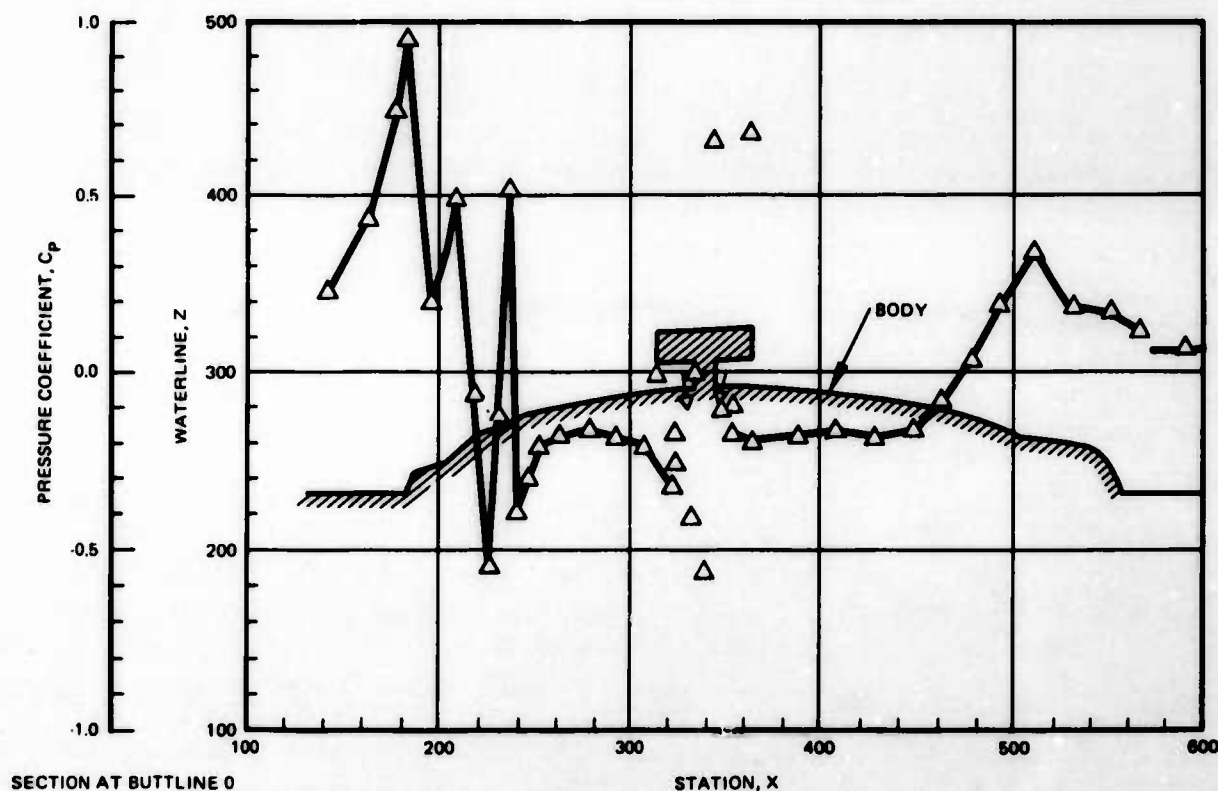
Figure 15. Basic UH-60A HPER Pressure Distribution along Centerline (Analytical Data).

34

and on to the pylon. An area of particularly rapid pressure gradient change is found at the juncture of the pylon and the canopy at approximately Station 235. These fluctuations perturb the boundary layer at the canopy/pylon juncture. Second, an adverse pressure gradient exists along the aft pylon between Stations 440 and 510. This gradient is predicted even though the baseline UH-60A oil cooler flow is included in the analysis; however, that flow is at about Station 400, well upstream of the adverse pressure gradient.

The UH-60A alternative pylon configuration ameliorates the problems in these two areas. First, the pylon is extended forward so the canopy line now flows smoothly onto the pylon (Figure 16). (This requires placing an additional fairing between Stations 230 and 260.) Second, the oil cooler lid is replaced with a fairing that ducts the oil cooler exhaust back to Station 450 and spreads it over the entire width of the aft pylon (Figure 17). This should provide boundary layer control over the aft pylon and make the sharp aft pylon lip more effective.

An examination of the YAH-64 HPER pressure distributions (Figure 18) indicates that the salient feature is the adverse pressure gradient over the aft pylon between Stations 270 and 320, indicating an area of boundary layer separation. There are three general solutions to this problem: First, the gradient could be reduced by reducing the aft pylon taper ratio. This would result in extending the pylon onto the tailboom and increasing the projected area in sideward flight, an undesirable effect. Second, the aft pylon could be isolated from the body flow by extending the isolation provided by the engine nacelles, which now extends to Station 320. Third, the boundary layer could be energized at the beginning of the adverse gradient so it could withstand the region without separation. The boundary layer could be energized by either of two approaches, active or passive. The active approach would require an additional air source, and the passive approach would collect high-energy upstream air and duct it back to the beginning of the adverse gradient. The passive approach was selected for the YAH-64.

On the YAH-64, the alternative pylon consists of an additional cowl that fits around the existing mast cowl and extends downstream to Station 280. Forward-facing scoops on both sides of the existing cowl collect the air and duct it back to a narrow exit slot. This slot extends the full width of the pylon at Station 280, where the air is ejected in a thin sheet in much the same way as is done using slotted high-lift devices. This modification, referred to as the "aft doghouse fairing," is shown installed on the model in Figure 19. At 170 knots the scoop area is sized to ingest the air at approximately 6800 cubic feet per minute and the exit area is sized to eject the air at approximately 200 knots. The exit velocity was designed to be higher than free-stream to provide good mixing.
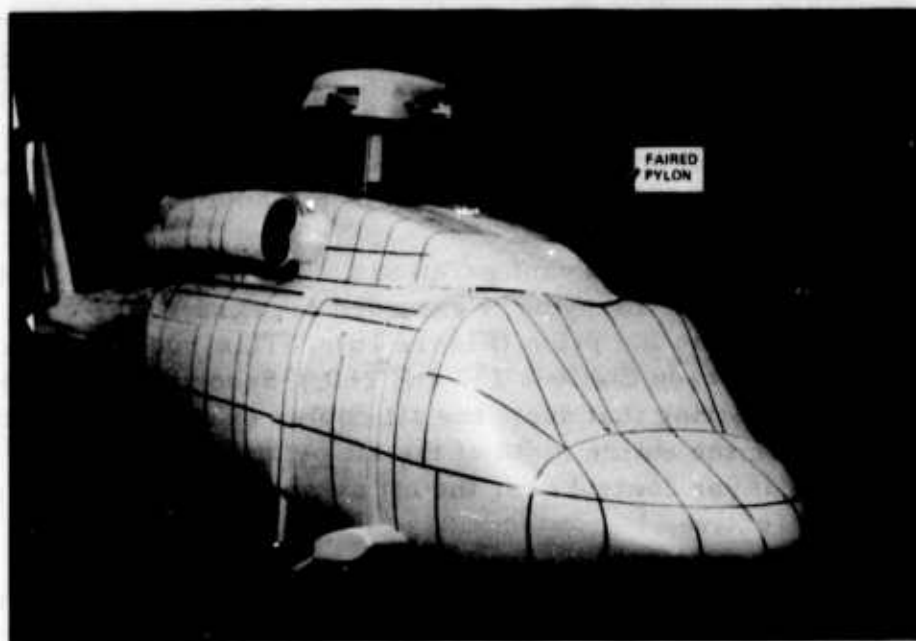
Figure 16. UH-60A Alternate Pylon with Faired Hub,
Shown on GRMS.
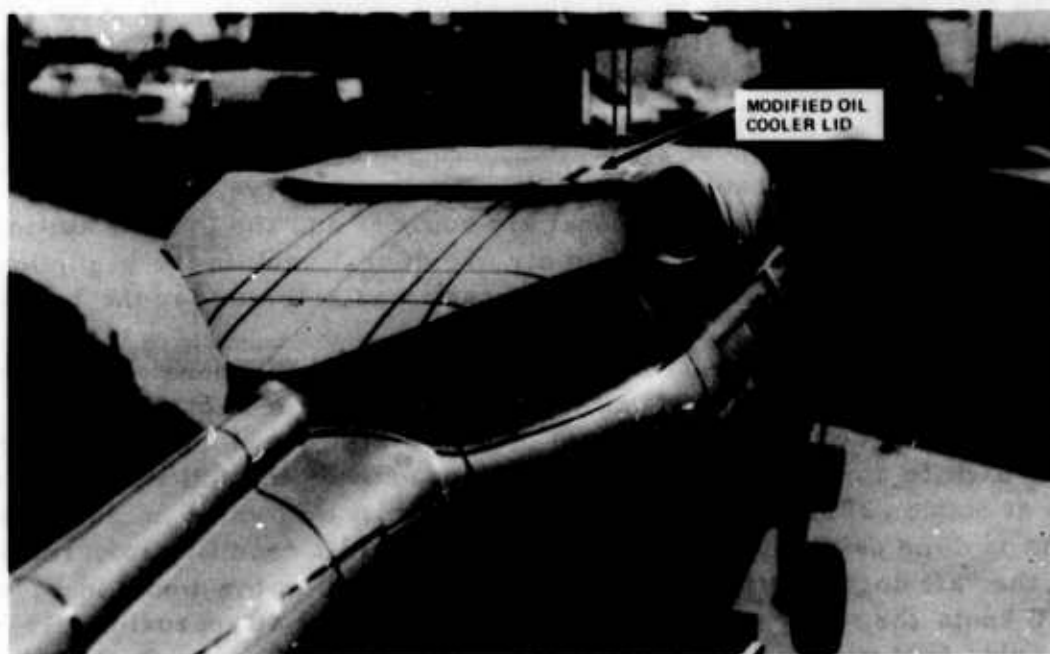
Figure 17. Modified UH-60A Oil Cooler Lid.
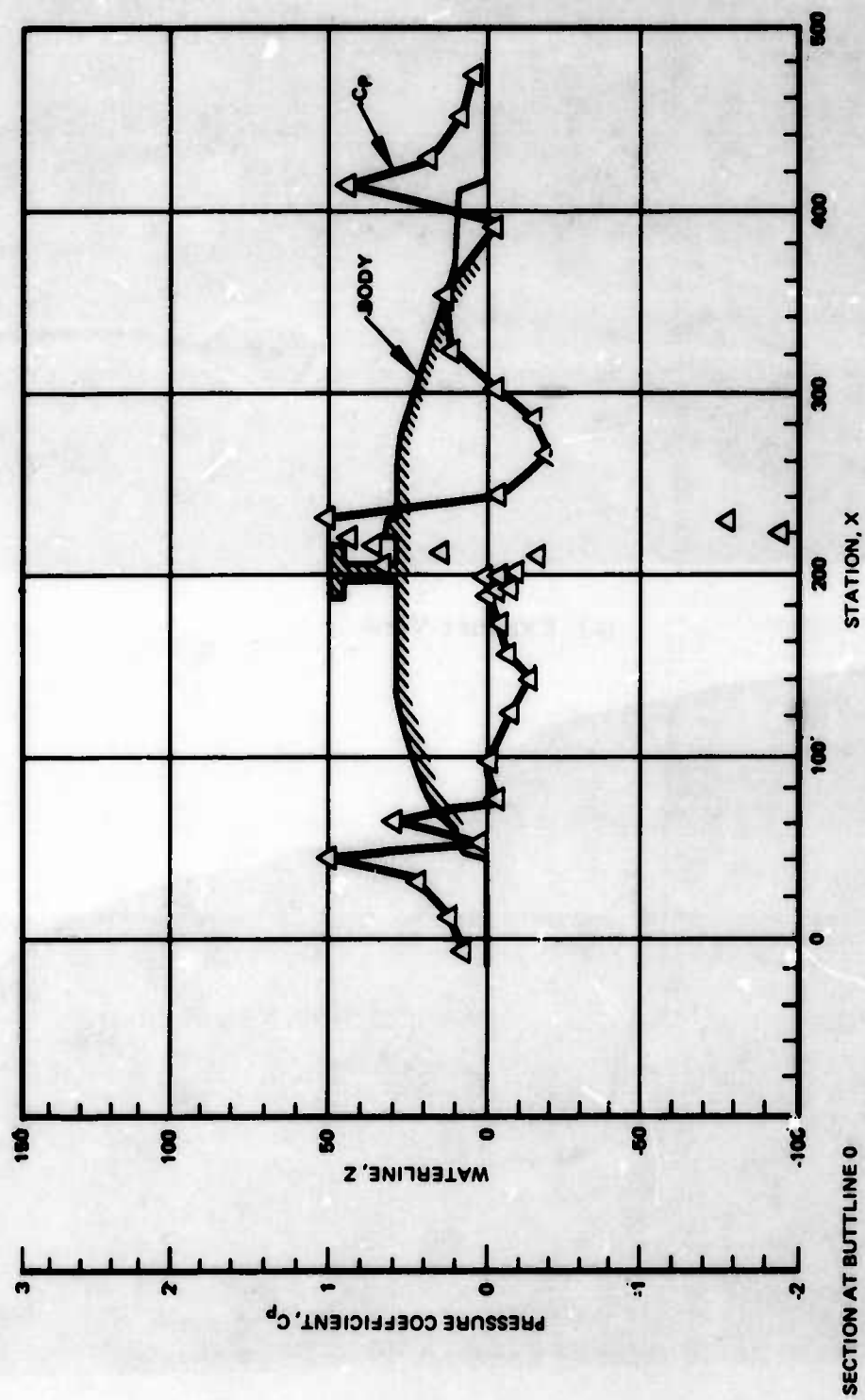
Figure 18. Pressure Coefficient Versus Station at Constant Buttline for YAH-64 HPER.

37
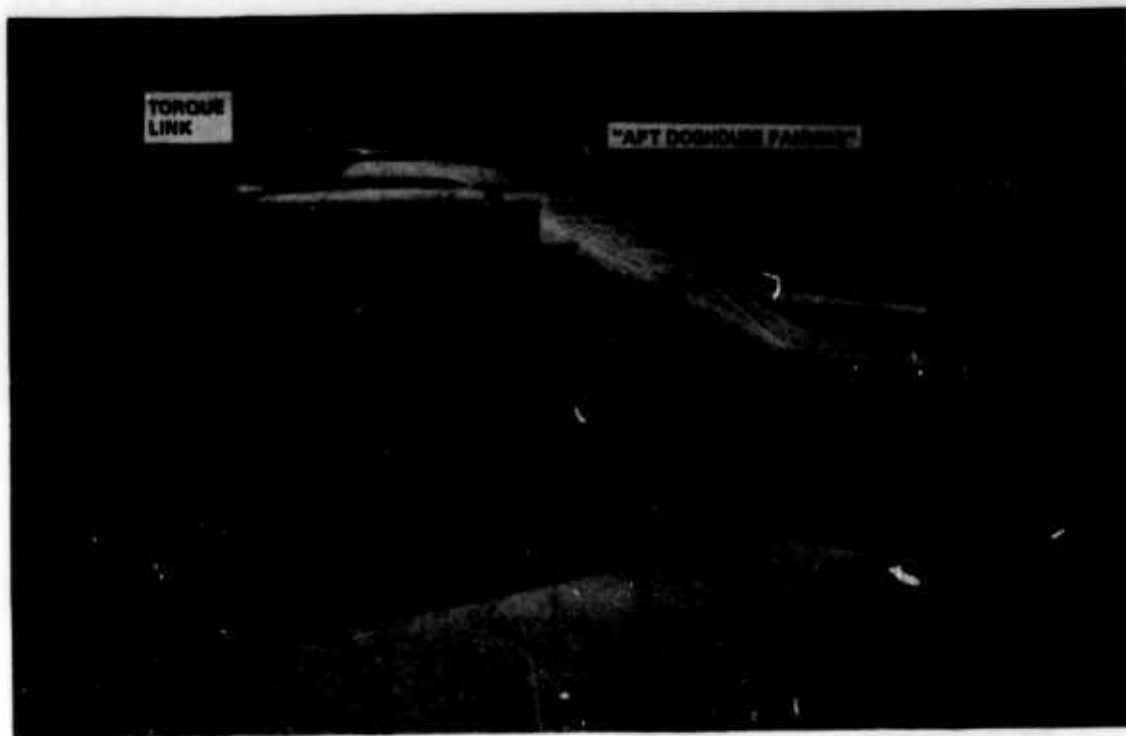
(a) Exhaust View
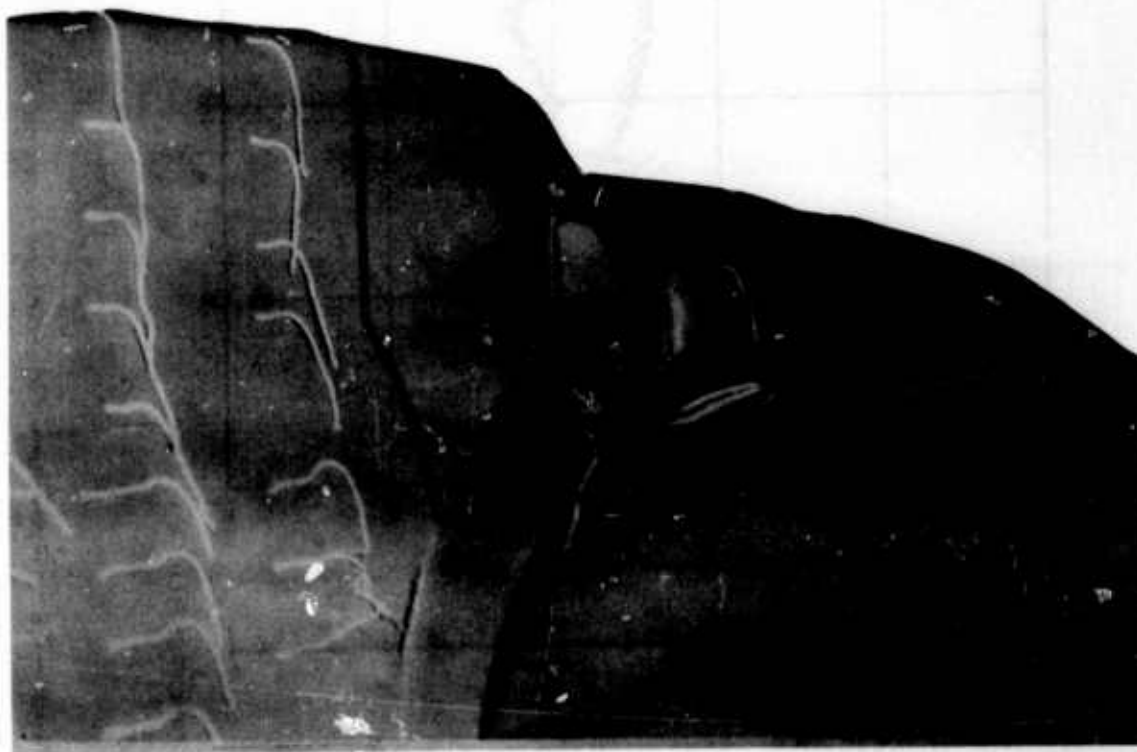
(b) Inlet View

Figure 19. YAH-64 Modified "Aft Doghouse Fairing," Shown on HPER.

A second modification was to put fences along the aft shoulders of the pylon, to isolate the separation region behind the engine nacelles. These fences extend from the aft nacelle/pylon juncture to the tail cone/pylon juncture (Figure 20).

Figure 20. YAH-64 Aft Pylon Fences.

39

Alternate hub configurations have been designed for the YAH-64 and the
UH-60A. The UH-60A alternate hub consists of a two-stage fairing. The
first-stage fairing covers the top of the hub and the vibration isolators
(Figure 21), and the second stage is an additional skirt attached to the first-
stage fairing and extending down to the bottom of the hub. Cutouts are pro-
vided for the blade attachment arms. This two-stage fairing was designed
so that the drag contribution of each area of the hub could be identified.
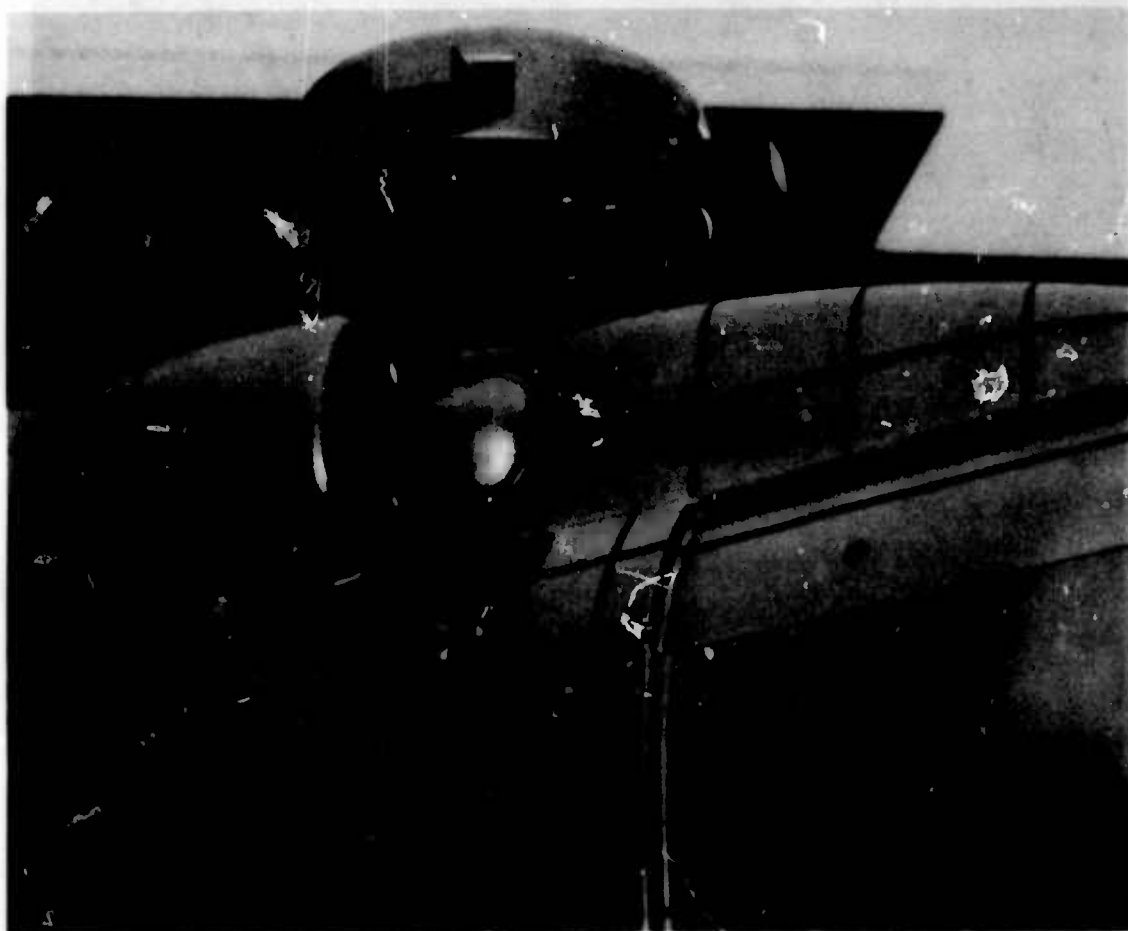
Figure 21. First-Stage UH-60A Faired Hub.

The alternate hub fairing for the YAH-64 was designed to treat the individual elements of the hub for aerodynamic improvement and to require minimum modification of the basic hub. This hub fairing, shown in Figure 22, consists of damper fairings over the lead-lag dampers on each blade pitch arm. In addition, the centerbody of the hub is covered with a "beanie" type of centerbody fairing. The rotating swashplate and scissors remain unchanged from the baseline configuration.
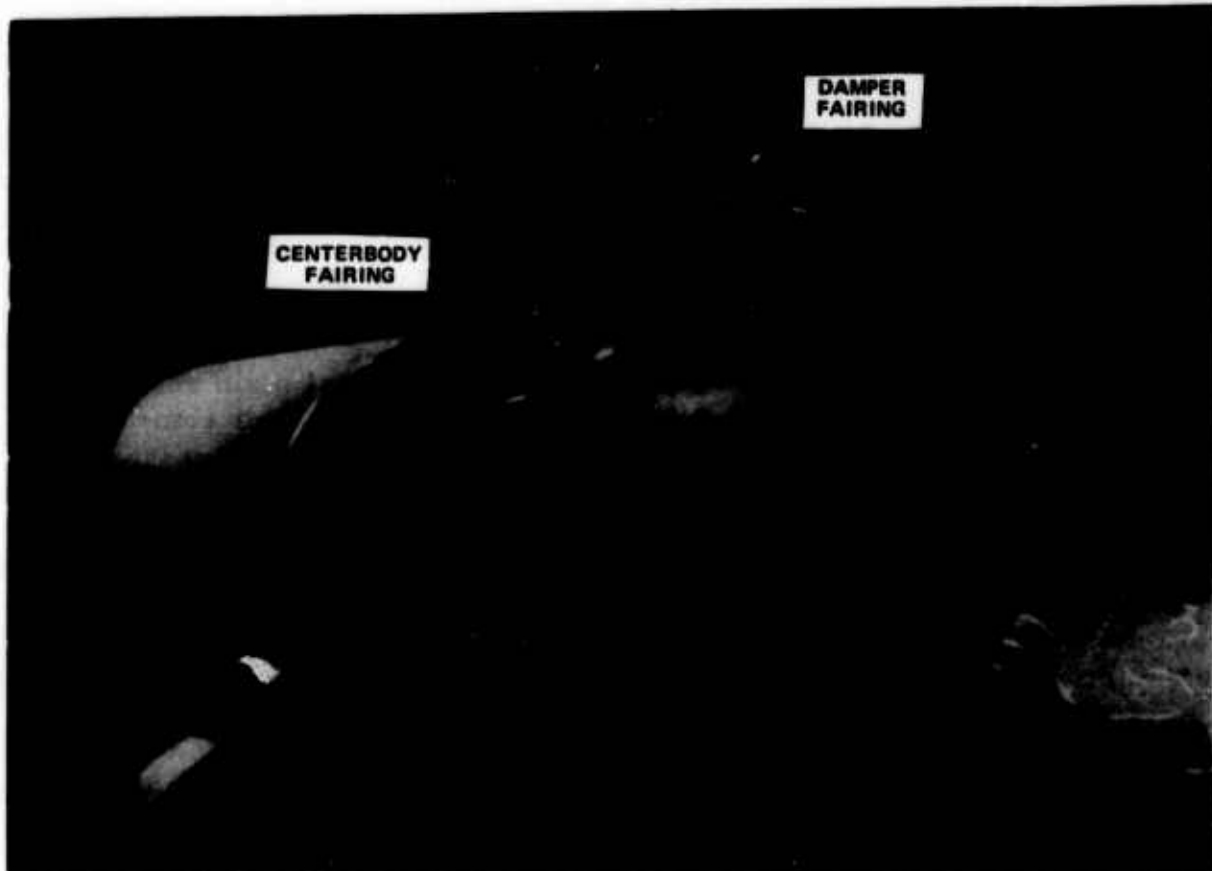
Figure 22. YAH-64 Faired Hub Configuration.

ANALYSIS OF RESULTS

The discussion of the data recorded during the YAH-64 testing is divided into four parts: wind tunnel modeling effects, hub and airframe modifications, experimental and analytical pressures, and empennage testing. Run logs and test configurations are presented in the appendix.

WIND TUNNEL MODELING EFFECTS

As a background to the discussion of wind tunnel modeling effects, a summary of the drag of the major YAH-64 components is presented in Table 1. As can be seen, the GRMS and HPER scale models developed similar drag levels for the hub and pylon. In addition, the total vehicle drag measured by the GRMS agrees closely with drag measured by an HH-developed 1/7-scale model tested in a pressurized wind tunnel.

Full/Partial Main Rotor Wake

The effect of full and partial main rotor wake representation was examined for several YAH-64 configurations. In this case the partial main rotor wake is the GRMS rotor system without the rotor blades while the full rotor wake is with the rotor blades, thrusting at 7 pounds per square foot, and the rotor trimmed perpendicular to the main rotor shaft. The effects of the main rotor wake on the drag of the basic YAH-64 configuration with the wing and simulated Hellfire missiles are presented in Figure 23 for the pylon, fuselage, and tail empennage. The drag in increments is referenced to a clean configuration with no mast or hub. All the data are presented at 120 knots and at the same exhaust flow simulation. The results show that the variation in drag is less than 1 square foot for either the full or partial (hub alone) rotor wake. The full or partial rotor wake decreased pylon and tail empennage drag while increasing the fuselage drag. The benefits of the full rotor wake are largest at positive fuselage angles, probably because higher-energy air is provided downstream of the maximum fuselage cross section and the main rotor hub.

It is interesting to note that the difference between full and partial rotor wake simulation is smallest for the pylon and tail empennage. In a later discussion it is shown that adding the main rotor wake produces no appreciable reduction in drag for a variety of pylon modifications. In addition, analysis of the pressure distributions indicates that the rotor wake has little impact on the pylon but does alter the pressure distribution over the nose.

TABLE 1. YAH-64 COMPONENT DRAG SUMMARY

Component	Drag,[1] D/q, ft^2	
	GRMS	HPER
Basic Hub	5.42	5.44
Pylon		
Without Wing/Rocket Pod	4.97	5.26
With Wing/Rocket Pod	2.57	
Wing/Rocket Pod	5.46	
Fuselage	7.45	
Empennage	2.50	
Total Vehicle		
Without Wing/Rocket Pod	20.34	
With Wing/Rocket Pod	23.40	
Stationary Controls/Mast[2]	1.40	

NOTES:

1. V_T = 120 kn, α_f = 0 deg, engine exhaust simulation, hub rotating.

2. Stationary controls/mast drag is included in pylon drag.

43
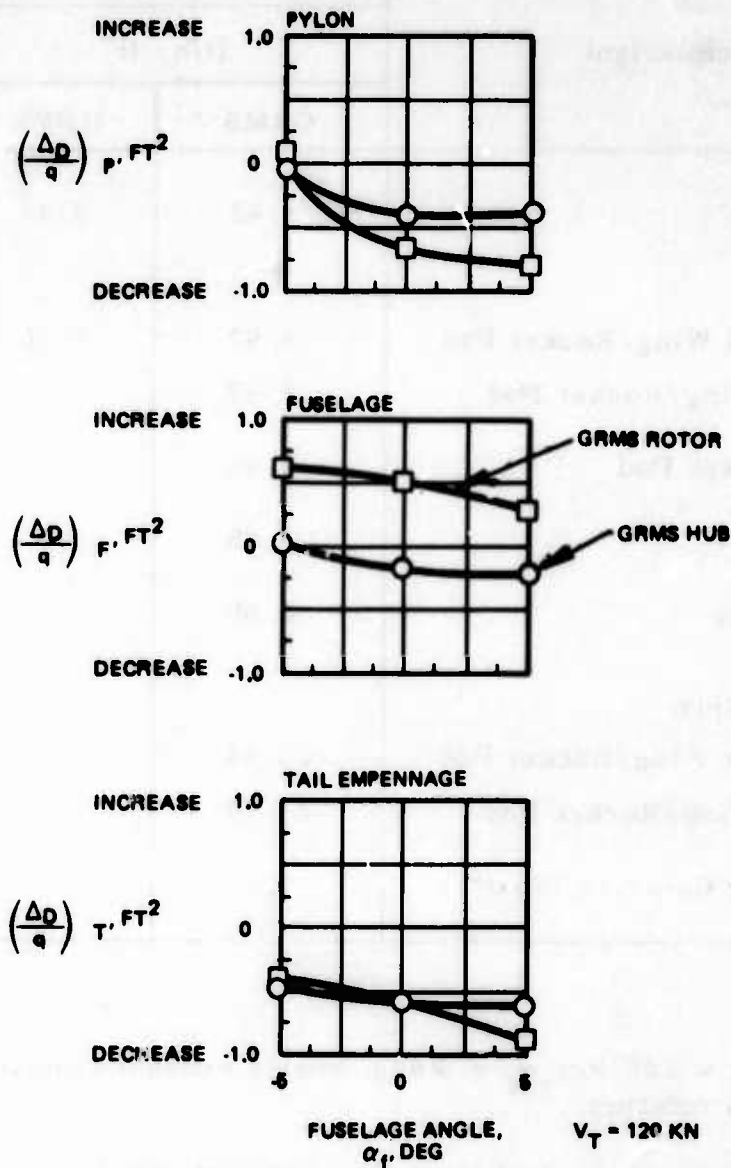
Figure 23. Effect on Pylon, Fuselage, and
Tail Empennage Drag of Full
and Partial Rotor Wake.

44

The rotor wake effect on fuselage and pylon combined lift was shown to be equivalent to a reduction in fuselage angle of attack (Figure 24). As compared to the baseline configuration with no rotor system, the addition of the GRMS rotor hub alone did not alter the fuselage or pylon lift. The addition of the thrusting blades reduced the lift by an amount equivalent to a 2.5-degree reduction in fuselage angle of attack. Using momentum theory, the rotor-induced angle of attack is calculated to be -2.06 degrees, indicating that, for lift, the addition of the thrusting rotor had the effect of a simple induced angle-of-attack change for the body.

Hub Rotation

An analysis of the large- and small-scale data indicates that hub rotation had a distinct effect on hub drag and that the effect was modified by both scale and fuselage angle of attack.
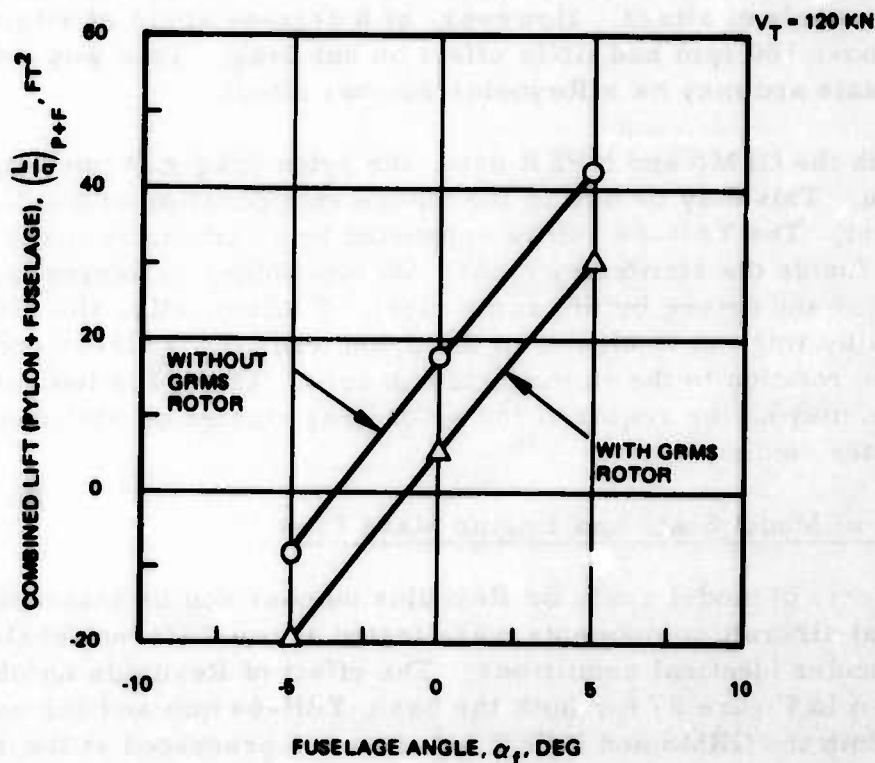
Figure 24. Effect of Full Rotor Wake Simulation on Combined Pylon and Fuselage Lift.

45

The effect of hub rotation on the large-scale HPER data is shown in Figure 25 for the basic hub and for the sealed, faired hub. The data are presented at 60 knots, but due to data recording problems only one fuselage angle is shown for each hub configuration. As can be seen for both hub configurations, the rotation of the hub resulted in a 0.5-square-foot increase in hub parasite drag at 60 knots. This drag increment was fairly consistent over the complete range of tunnel speeds, including 145 knots. For the basic hub at a particular tunnel speed, the drag increment due to rotation increased linearly with rotational speed. For the sealed, faired hub the drag increment was linear in two stages with a transition at the mid-rpm range, indicating a transition phenomenon. The hub drag data were also examined on the basis of the hub advance ratio (the ratio of tunnel speed to hub rotation speed), but the analysis produced no clear trend.

A similar trend of increased drag with hub rotation is shown in Figure 26 for the small-scale GRMS data. For the GRMS hubs, however, angle of attack modifies the effect. For both the basic and the sealed, faired hubs, an approximate 0.5-square-foot increase in hub drag is shown at ±10 degrees fuselage angle of attack. However, at 0 degrees angle of attack, hub rotations above 100 rpm had little effect on hub drag. This was not seen in the HPER data and may be a Reynolds number effect.

For both the GRMS and HPER data, the pylon drag was unchanged by hub rotation. This may be due to the unique configuration of the YAH-64 rotor and mast. The YAH-64 hub is supported by a stationary mast and driven by a shaft inside the stationary mast. On most other helicopters the hub is supported and driven by the same mast. Consequently, the disturbance created by rotation is closer to the pylon while the YAH-64 configuration confines rotation to the immediate hub area. This does indicate that hub rotation may not be required for pylon drag studies on stationary mast helicopter configurations.

Effects of Model Scale and Engine Mass Flow

The effects of model scale or Reynolds number can be isolated because identical aircraft components were tested at two different scales in the same tunnel under identical conditions. The effect of Reynolds number on hub drag is shown in Figure 27 for both the basic YAH-64 hub and the sealed, faired hub. Both the GRMS and HPER hub data are presented at the same hub tip speed. The Reynolds number in this case is based on the tunnel speed and model scale factor. It can be seen that the hub data correlate well with a sharp rise in hub drag beginning between a Reynolds number of 250,000 and 300,000. The same Reynolds number behavior is shown for the sealed, faired hub. The drag reduction due to sealing the fairing is consistent over the whole Reynolds number range except at the highest speed, where the drag

46
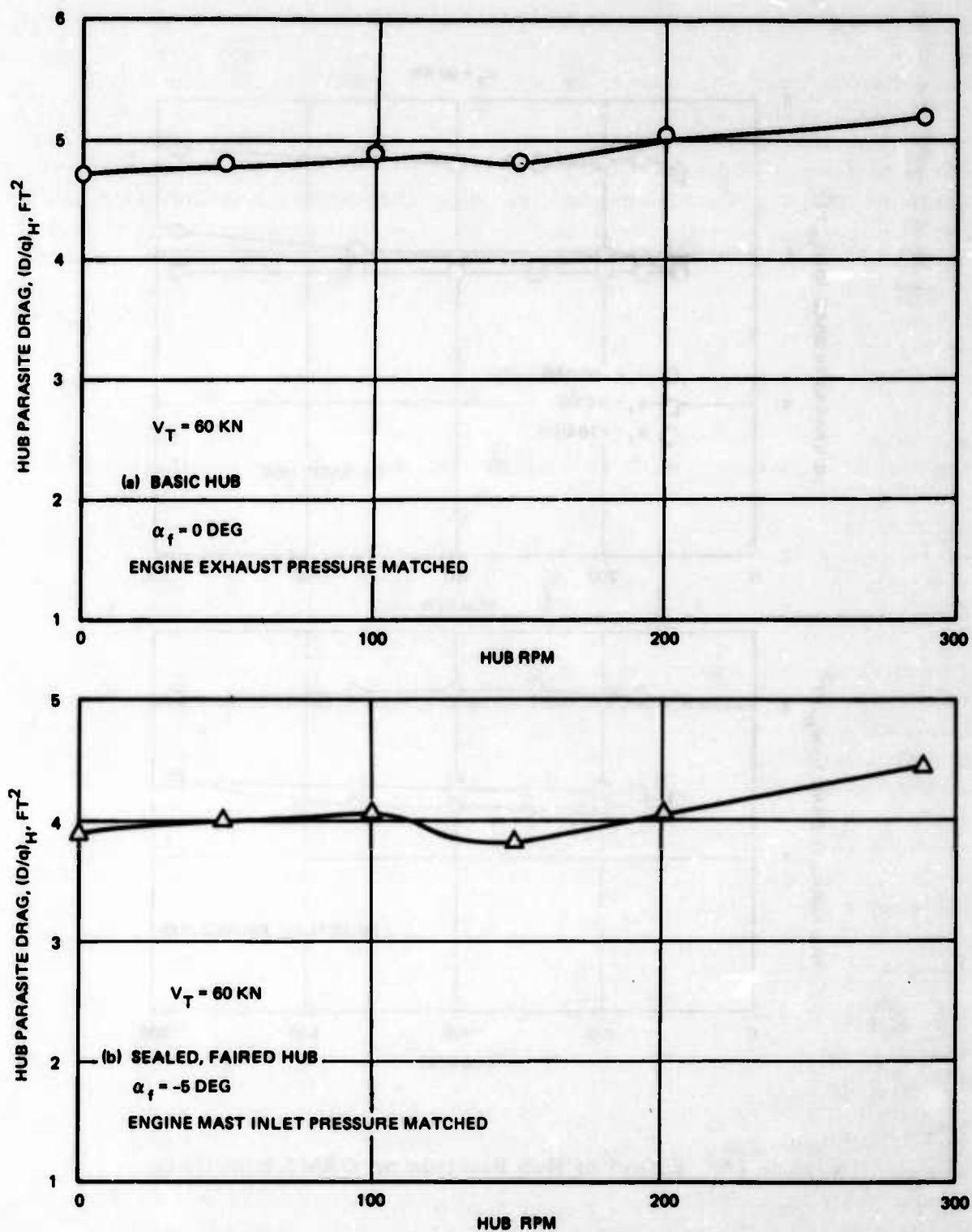
Figure 25. Effect of Hub Rotation on HPER Hub Drag.

$V_T = 80$ KN

(a) BASIC HUB

$\alpha_f = -10$ DEG
$\alpha_f = 0$ DEG
$\alpha_f = +10$ DEG
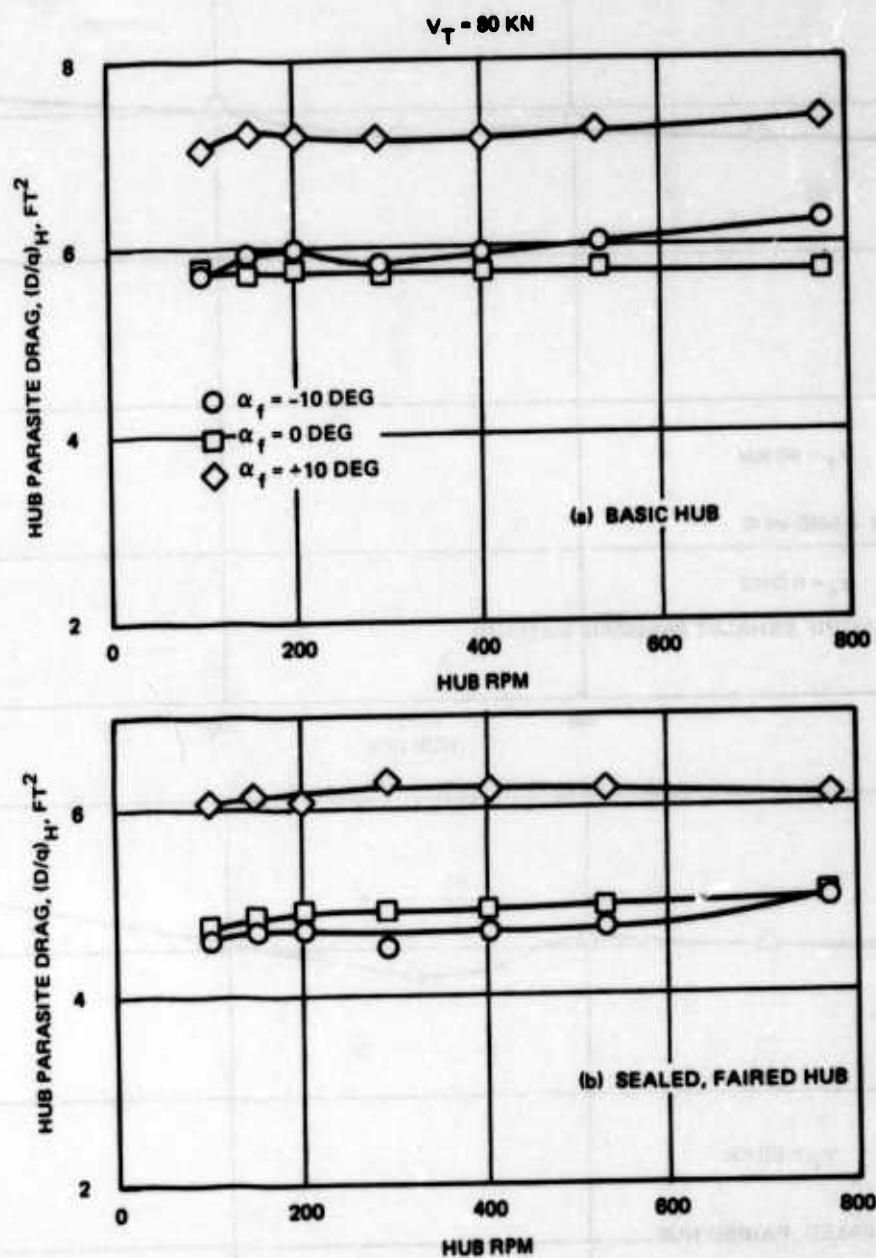
(b) SEALED, FAIRED HUB

Figure 26. Effect of Hub Rotation on GRMS Hub Drag.

48
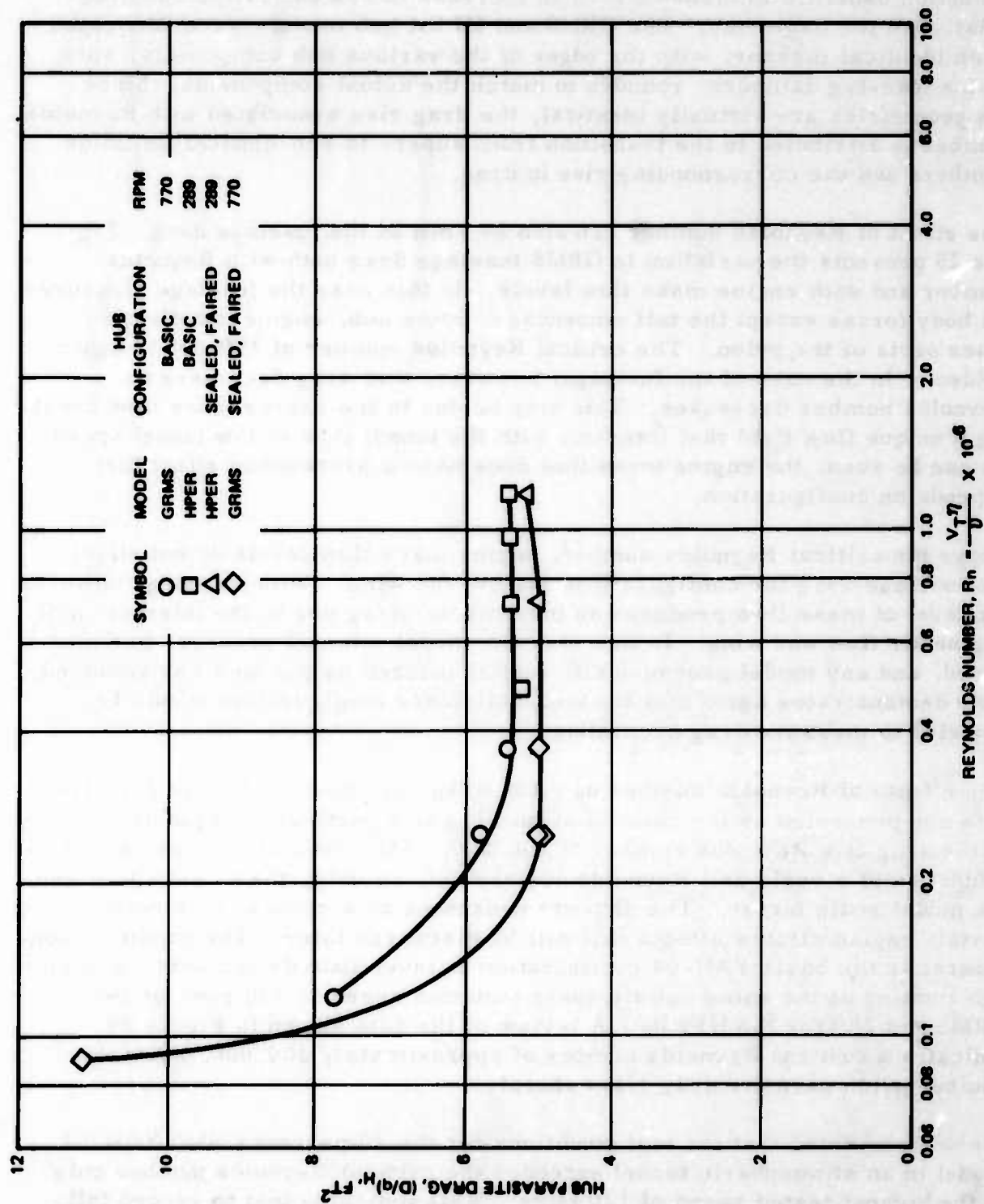
Figure 27. Effect of Reynolds Number on Hub Drag.

reduction benefit diminishes due to an increase in sealed, faired hub drag relative to the basic hub. The GRMS and HPER hub models were fabricated in an identical manner, with the edges of the various hub components, such as the lead-lag dampers, rounded to match the actual components. Since the geometries are virtually identical, the drag rise associated with Reynolds number is attributed to the transition from super- to sub-critical Reynolds numbers and the corresponding rise in drag.

The effect of Reynolds number can also be seen in the fuselage drag. Figure 28 presents the variation in GRMS fuselage drag both with Reynolds number and with engine mass flow levels. In this case the fuselage measures all body forces except the tail empennage, rotor hub, engine nacelles, or other parts of the pylon. The critical Reynolds number of 250,000 is again evident. In the case of the fuselage, however, this drag decreases as Reynolds number decreases. This may be due to the engine mass flow creating a unique flow field that interacts with the tunnel flow at low tunnel speeds. As can be seen, the engine mass flow does have a pronounced effect that depends on configuration.

Above the critical Reynolds number, engine mass flow levels do not affect the fuselage drag for configurations without the wing. With the wing, however, the level of mass flow produces an incremental drag due to the interaction of engine air flow and wing. In this case the model internal pressure was measured, and any model pressure differential induced by the fans was removed. This demonstrates again that the total helicopter configuration should be modeled to measure drag accurately.

The effects of Reynolds number on pylon drag are shown in Figure 29. The data are presented as the ratio of pylon drag at a particular Reynolds number to the drag at a Reynolds number of 400,000. This ratio is then presented as a function of a scale unit Reynolds number defined using the tunnel speed and the model scale factor. The data are presented as a ratio to eliminate certain engine airflow effects that will be discussed later. The condition considered is the basic YAH-64 configuration at level attitude and with the basic hub rotating at the same hub tip speed (rotation speed is 770 rpm for the GRMS and 289 for the HPER). A review of the data shown in Figure 29 indicates a critical Reynolds number of approximately 300,000; below this number pylon parasite drag rises sharply.

It should be noted that the test conditions for the 30 percent GRMS YAH-64 model in an atmospheric tunnel exceeded the critical Reynolds number only at the highest tested speed of 120 knots. This indicates that to record full-scale baseline drag data on a small-scale model, the tunnel should be pressurized to achieve a scale unit Reynolds number of 300,000. However, comparative data on different configurations under the same tunnel conditions may be acceptable without tunnel pressurization.

50
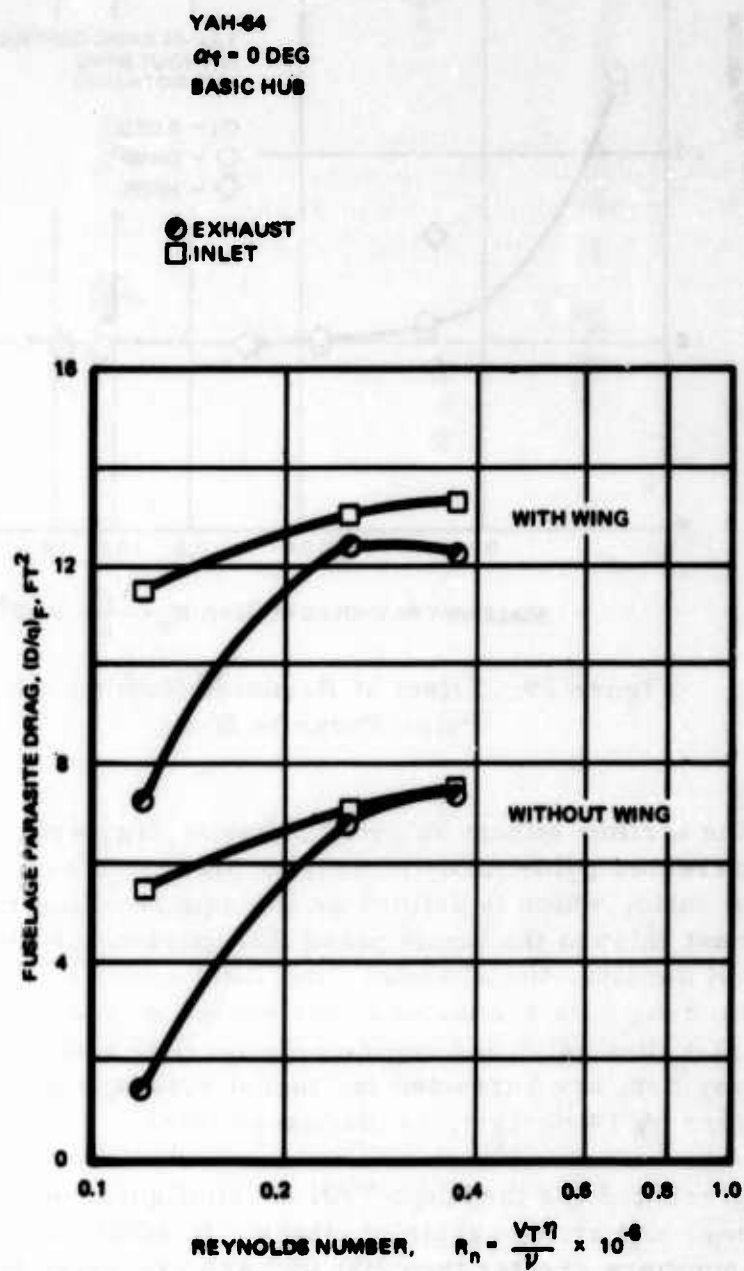
Figure 28. Effect of Reynolds Number on
Fuselage Drag (GRMS).
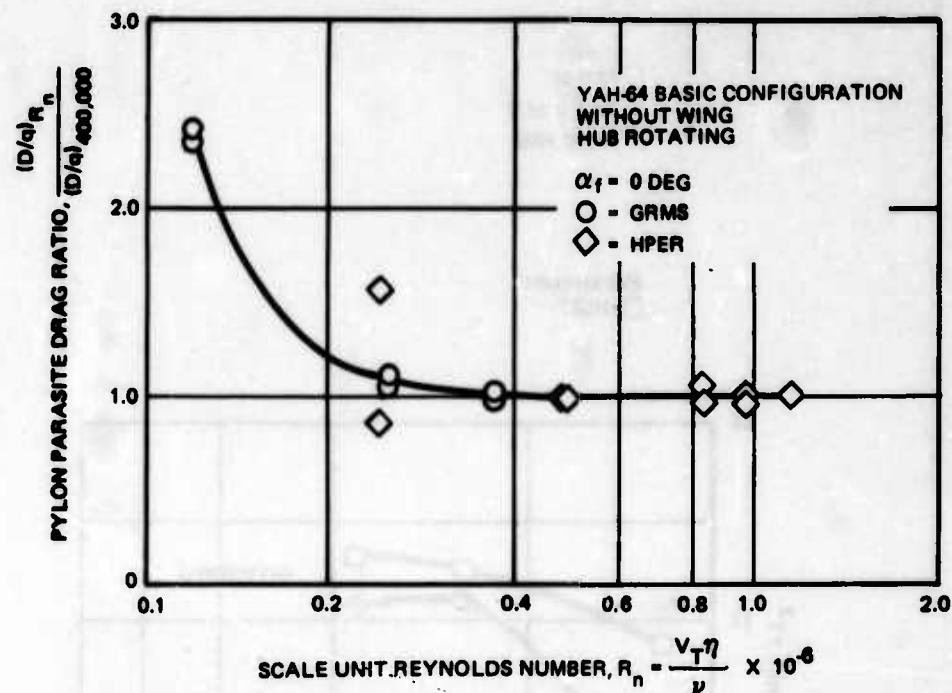
Figure 29. Effect of Reynolds Number on
Pylon Parasite Drag.

Simulated engine airflow effects on pylon parasite drag are shown in
Figure 30. Corrected pylon parasite drag is presented as a function of mast
inlet mass flow ratio, which is defined as the square of the ratio of the mass
flow into the mast inlet to the tunnel mass flow parameter formed by multi-
plying the tunnel density, tunnel speed, and BHO exhaust area. Both GRMS
and HPER pylon drag data are included for sealed engine/mast inlets, fan
windmilling, inlet flow rate, and engine exhaust flow rate conditions. The
HPER pylon drag data are corrected for tunnel blockage by increasing
dynamic pressure by 14 percent, as discussed later.

The data are presented for the basic YAH-64 configuration without a wing,
with hub rotating, and at zero angle of attack. In addition, only data at scale
unit Reynolds numbers greater than 200,000 are presented (a run number is
presented at each data point for reference). The data include HPER runs from
60 to 145 knots and GRMS runs from 80 to 120 knots.

The pylon drag data indicate that there is a strong effect of inlet mass flow,
particularly at low mass flows. Generally, the pylon drag is approximately
5.25 square feet, but below a mast inlet flow ratio of 0.04 the pylon drag
rises sharply to a value of 9.3 square feet for sealed HPER conditions.
For typical YAH-64 mast inflow conditions at 145 knots, the pylon parasite
drag is 6.6 square feet.
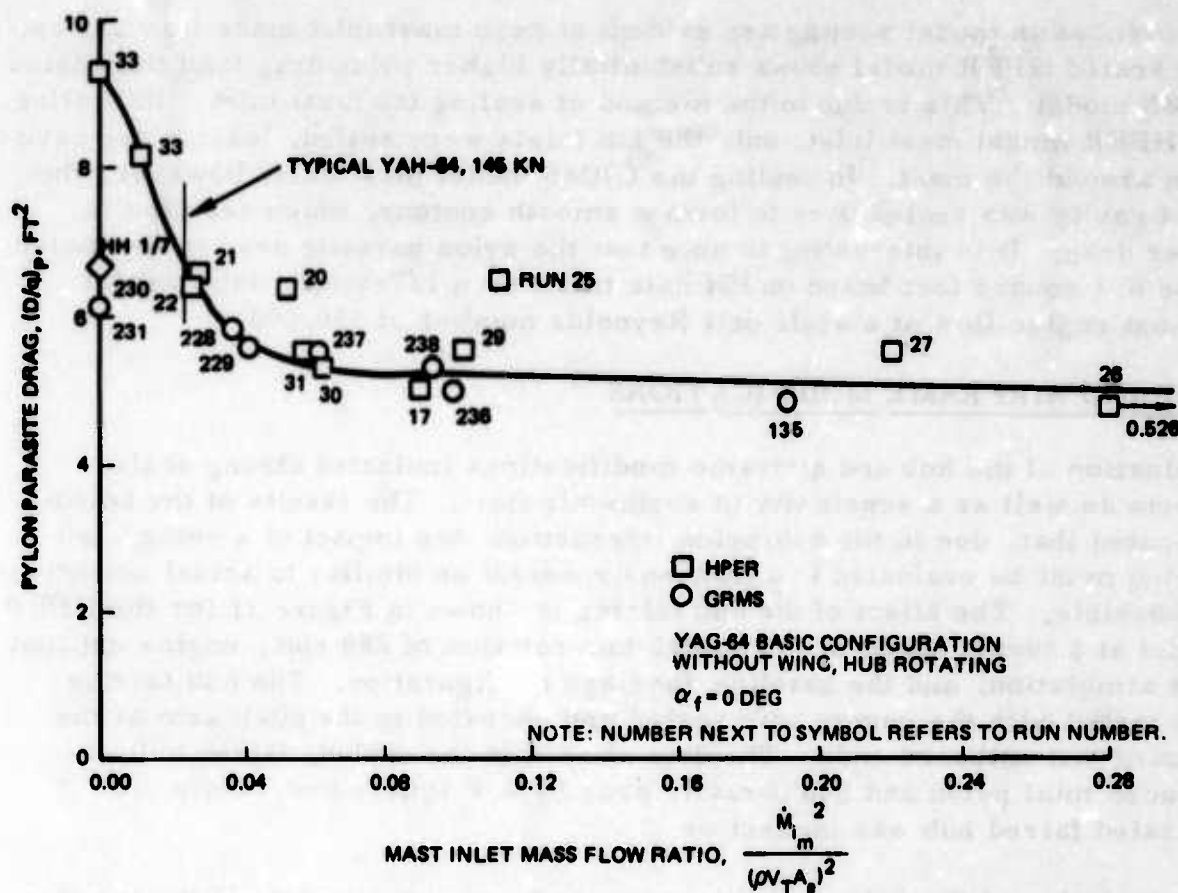
Figure 30. Effect of Mast Inlet Mass Flow on Pylon Parasite Drag.

Several parameters were used in an attempt to correlate the HPER/GRMS
pylon drag data, and only the mast inlet mass flow ratio was used success-
fully. The data showed a great deal of scatter when total mass flow or
nacelle mass flow was used, probably due to the manner in which mass flow
level was varied. To simulate exhaust mass flow levels, the fans drawing
air in both the engine nacelle inlet and the mast inlet were set at maximum
settings. To simulate inlet mass flow levels, the reduction in fan setting
was greater for the fans drawing air from around the mast than for the fans
drawing air from around the nacelle inlet. Consequently, the flow changes
were greatest through the mast inlet, and this flow parameter proved
dominant. This indicates that when powered models are tested, extreme care
should be taken in accurately simulating the full-scale vehicle airflow
environment.

53

Differences in model sealing are evident at zero mast inlet mass flow ratios. The sealed HPER model shows substantially higher pylon drag than the sealed GRMS model. This is due to the method of sealing the mast inlet. In sealing the HPER model mast inlet, only the fan inlets were sealed, leaving the cavity open around the mast. In sealing the GRMS model mast inlet, however, the mast cavity was sealed over to form a smooth contour, which resulted in lower drag. It is interesting to note that the pylon parasite drag is estimated to be 6.7 square feet based on HH data taken on a 1/7-scale, solid model without engine flow at a scale unit Reynolds number of 350,000.

HUB AND AIRFRAME MODIFICATIONS

Evaluation of the hub and airframe modifications indicated strong scale effects as well as a sensitivity to engine air flow. The results of the testing indicated that, due to the hub/pylon interaction, the impact of a rotor head fairing must be evaluated in a flow environment as similar to actual conditions as possible. The effect of the hub fairing is shown in Figure 31 for the HPER model at a tunnel speed of 145 knots, hub rotation of 289 rpm, engine exhaust flow simulation, and the baseline fuselage configuration. The hub fairing was tested with the covers both sealed and unsealed to the pitch arm at the inboard and outboard ends. The data show that the sealed, faired hub reduced total pylon and hub parasite drag by 0.8 square foot, while the unsealed faired hub was ineffective.

The isolation of the pylon and hub components of parasite drag indicates that, for the HPER, most of the benefit of the sealed, faired hub came from the reduction in pylon parasite drag and not the reduction in hub parasite drag. This occurred even though there was no discernible change in the surface flow patterns on the pylon area of each configuration. The tufts applied to the pylon surface indicated no change in the separation regions behind the mast collar or the engine nacelle/pylon juncture. The surface pressure distributions also showed little difference. Similar results were shown for the nonrotating hub case.

In the GRMS testing, similar drag reductions were demonstrated, but the distribution between hub and pylon was reversed. As shown in Figure 32, the sealed, faired hub reduced the total pylon and hub drag by approximately 0.8 square foot as measured during the HPER test. However, the majority of the drag reduction came from the hub. The drag reduction benefits of the sealed, faired hub in the GRMS scale were also shown by wake surveys at the tail empennage station. The data shown in Figure 33 indicate that the sealed, faired hub increased the wake dynamic pressure and reduced the sidewash angles. At planes below the centerline of the pylon the benefits of the sealed, faired hub are reduced.

54
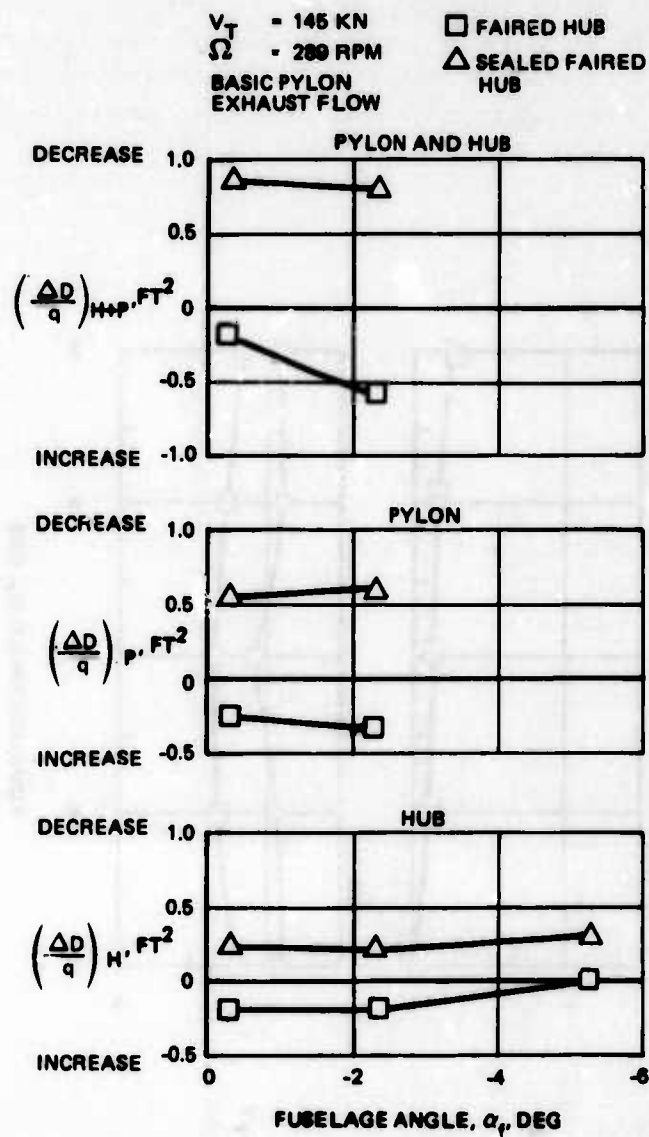
Figure 31.   HPER Hub and Pylon Drag Reduction
Due to Hub Fairing.
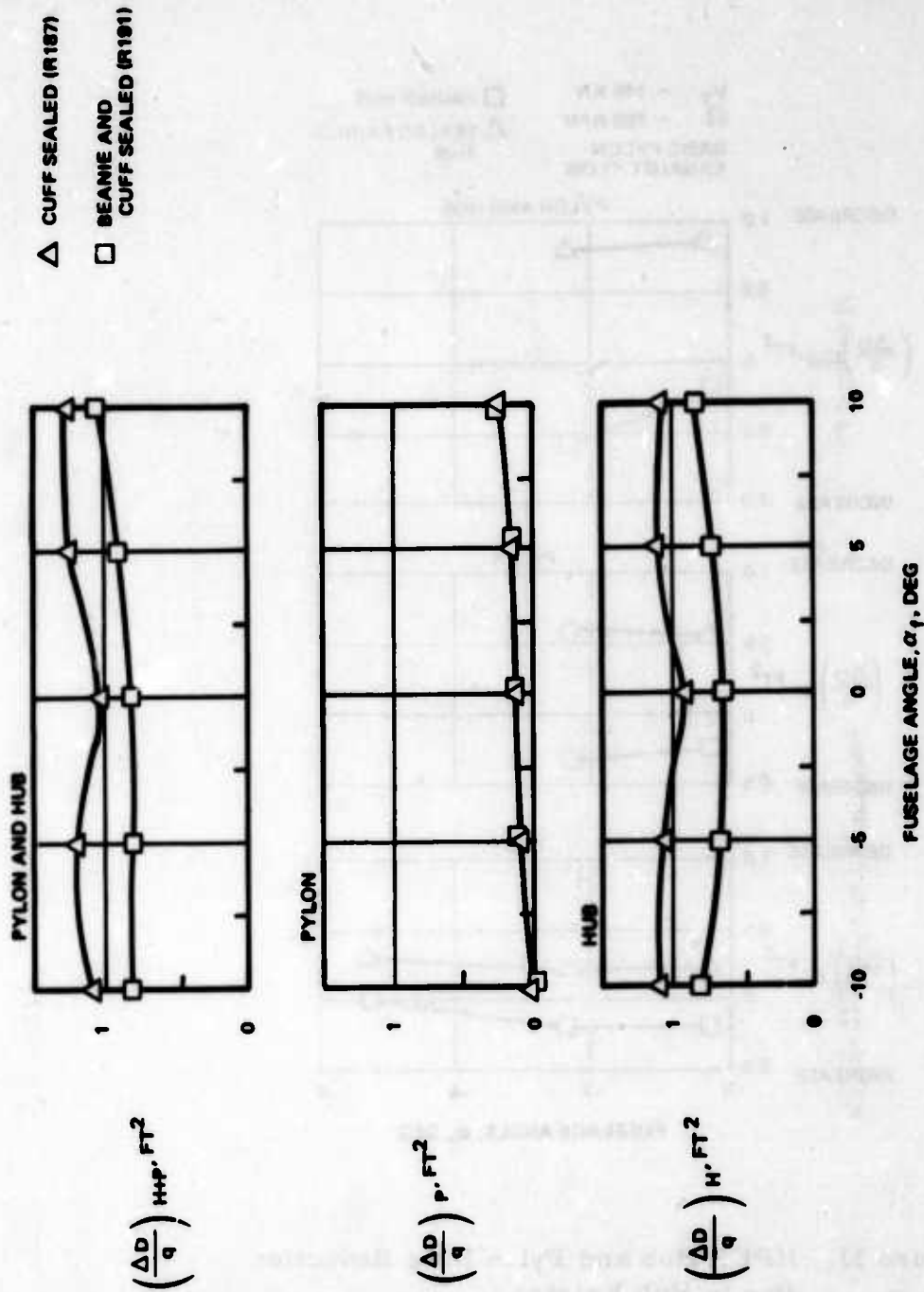
Figure 32. GRMS Hub and Pylon Drag Reduction Due to Hub Fairing.
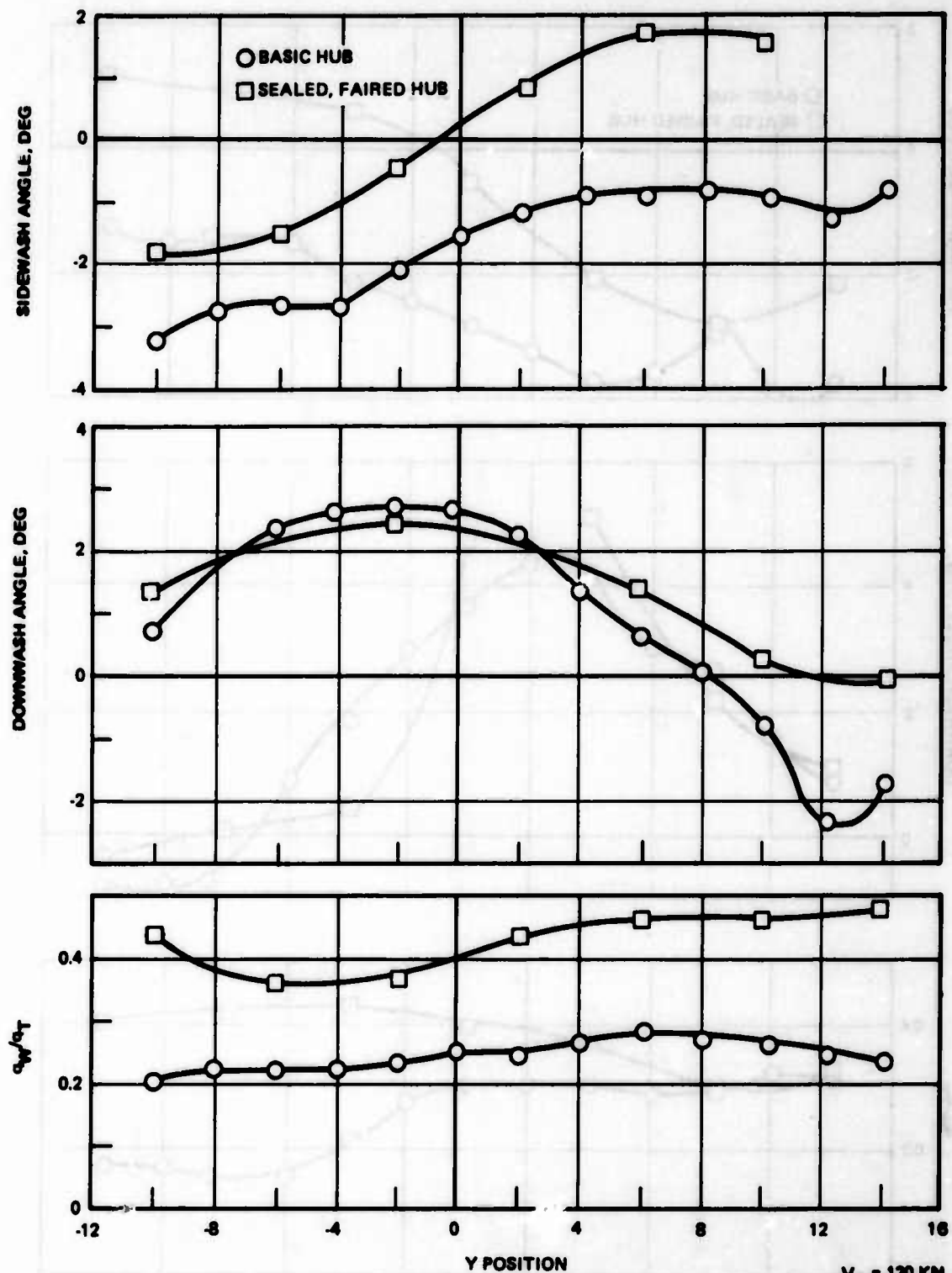
(a) Stabilizer Position + 18 inches

V_T = 120 KN
α_f = 0 DEG

Figure 33. Effect of Hub Fairing on Flow at Tail Empennage
of YAH-64 GRMS.
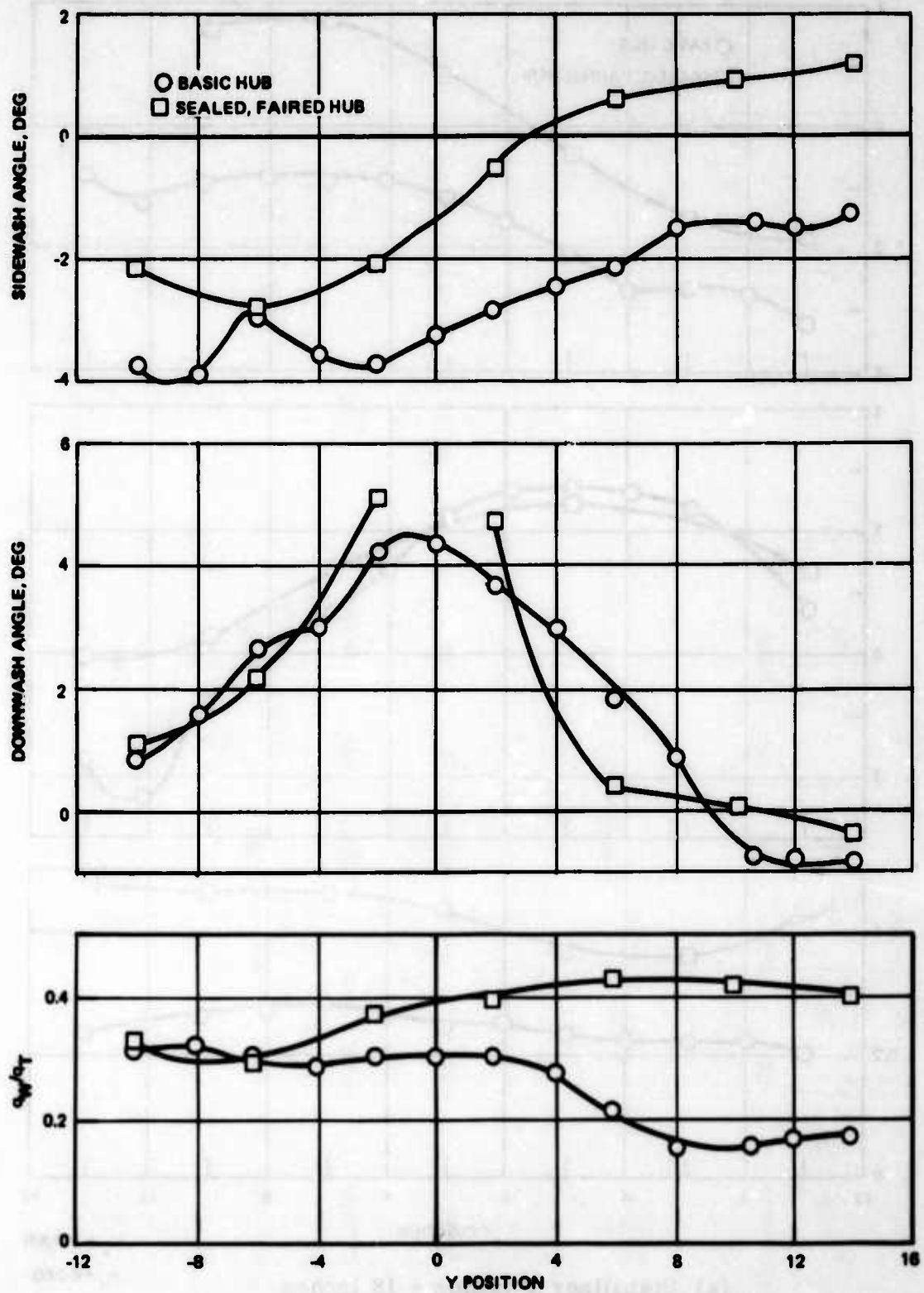
(b) Stabilizer Position + 12 Inches

Figure 33. (Continued).

58
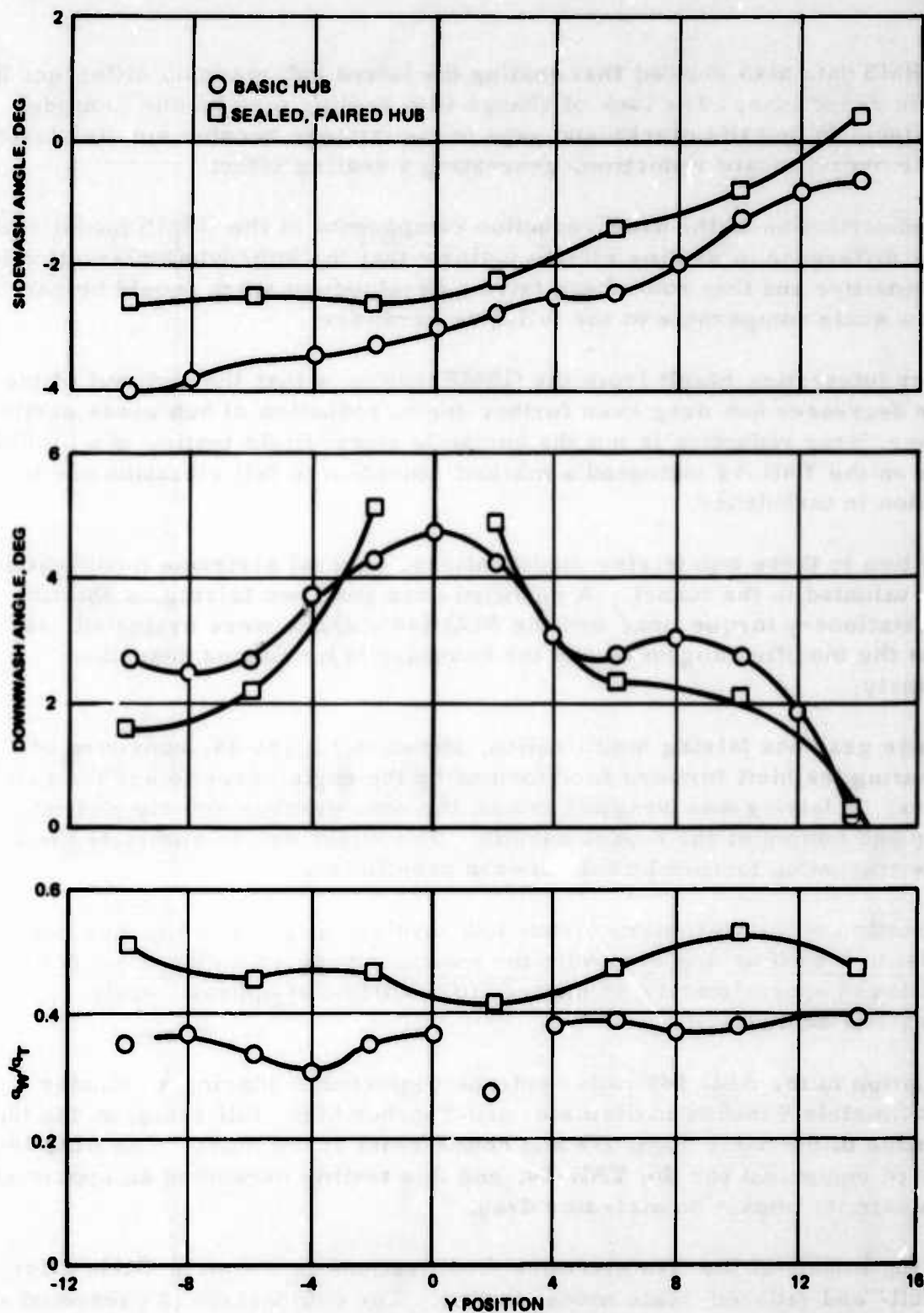
(c) Stabilizer Position + 6 Inches

Figure 33. (Continued).

The GRMS data also showed that sealing the faired hub made no difference in the drag reductions. The lack of change with sealing may be due to model size effects in that the cracks and gaps in the fairings became smaller faster than the overall scale reduction, generating a sealing effect.

The redistribution of the drag reduction components in the GRMS model scale and the difference in sealing effects indicate that the hub/pylon interaction is very sensitive and that rotor head fairing development work should be carried out on a scale comparable to the full-size hardware.

Another interesting result from the GRMS testing is that the removal of the beanie decreases hub drag even further due to reduction of hub cross section. However, drag reduction is not the complete story; flight testing of a similar beanie on the YAH-64 indicated a marked reduction in tail vibration due to a reduction in turbulence.

In addition to these hub fairing modifications, several airframe modifications were evaluated in the tunnel. A modified nose gear box fairing, a rotation of the stationary torque link, and the ALQ 144 antenna were evaluated, as well as the modified doghouse and the boundary layer fences described previously.

The nose gear box fairing modification, shown in Figure 34, consisted of eliminating the bluff forward face formed by the engine nacelle and the nose gearbox. A fairing was wrapped around the nose gearbox and blended into the top and bottom of the engine nacelle. The intent was to eliminate the area of flow stagnation formed by the forward nacelle face.

The rotation of the stationary torque link involved aligning the torque link parallel to a buttline and even with the mast, as opposed to the basic configuration of approximately 45 degrees to a buttline at approximately 300 degrees azimuth.

Installation of the ALQ 144 radar antenna consisted of placing a cylinder (approximately 9 inches in diameter and 8 inches high, full scale) on the top centerline of the basic doghouse and downstream of the mast. The ALQ 144 is proposed equipment for the YAH-64, and this testing presented an opportunity to evaluate its impact on airframe drag.

The drag impact of the five airframe modifications is shown in Table 2 for both full- and reduced-scale model testing. The comparison is presented at zero fuselage angle and the highest tested speed for each model, 145 knots for the HPER models and 120 knots for the GRMS. The modified doghouse produces a small drag reduction in the GRMS but no effect in the HPER, while the fences are less effective in the GRMS model than in the HPER model.

60

Figure 34.   Nose Gearbox Fairing

TABLE 2. DRAG INCREMENTS DUE TO AIRFRAME MODIFICATIONS

Configuration	Drag[1], $\Delta D/q$. ft^2		
	HPER	GRMS	
		Basic Hub	Rotor Wake
Boundary Layer Fences	-0.74	-0.20	-0.20
Modified Doghouse	0	-0.15	-0.17
With Fences	0	-0.20	-0.26
ALQ 144 Antenna	1.96	0.50	0.35
Nose Gearbox Fairing	0	0	N/A
Torque Link Rotation	0.97	-0.4	N/A

NOTE:

[1]HPER data: V_T = 145 kn, α_f = 0 deg, Ω = 289 rpm, no airflow.

GRMS data: V_T = 120 kn, α_f = 0 deg, Ω = 770 rpm, exhaust airflow.

The ALQ 144 antenna adds less drag in the GRMS model configuration than in the HPER configuration. The rotated torque link shows a completely opposite trend in that, instead of a drag increase, the GRMS data shows a drag reduction.

It is felt that these differences are caused by the absence of engine airflow in the HPER testing. The YAH-64 draws air from around the mast. During the HPER testing the fans became inoperative, and testing continued without fan airflow and with the inlets sealed. (The HPER drag reduction data are referenced to a baseline without airflow.) The GRMS data were taken with full airflow simulation. The increased effectiveness of the torque link rotation indicates the sensitivity of the flow environment around the mast. Similarly, the reduced effectiveness of the boundary layer fences may

indicate that the engine exhaust provides some boundary layer control over the aft pylon, reducing the separation the fences were intended to control. All of this emphasizes the importance of airflow simulation in the evaluation of drag reduction studies.

The impact of the full main rotor wake is also shown in Table 2. The GRMS data were recorded with the basic YAH-64 hub for comparison with the HPER data, as well as with and without the GRMS rotor blades to determine the effect of the rotor wake. The results of the comparison for the YAH-64 model indicate that the inclusion of the main rotor wake supported the quali- tative evaluation of the hub-alone data and produced a small increment in drag. The largest quantitative change was in the ALQ 144 antenna, where including the main rotor wake reduced the drag of the antenna.

Another airframe interaction effect is the impact of the wing. The addition of the wing and the Hellfire missiles increases the total aircraft drag (inclu- ding all components) by 4.5 and 3.5 square feet at fuselage attitudes of -10 and 0 degrees respectively. When examined component by component, however, it can be shown that the lift of the wing creates a favorable inter- ference, causing a reduction in pylon drag (Figure 35). At a 10-degree nose down attitude, the pylon drag is unchanged by the wing. At a 0-degree fuselage attitude, the wing causes a reduction in pylon drag of 2.3 square feet. The reduction in pylon drag is offset by increases in fuselage drag caused by the addition of the wing and missiles.
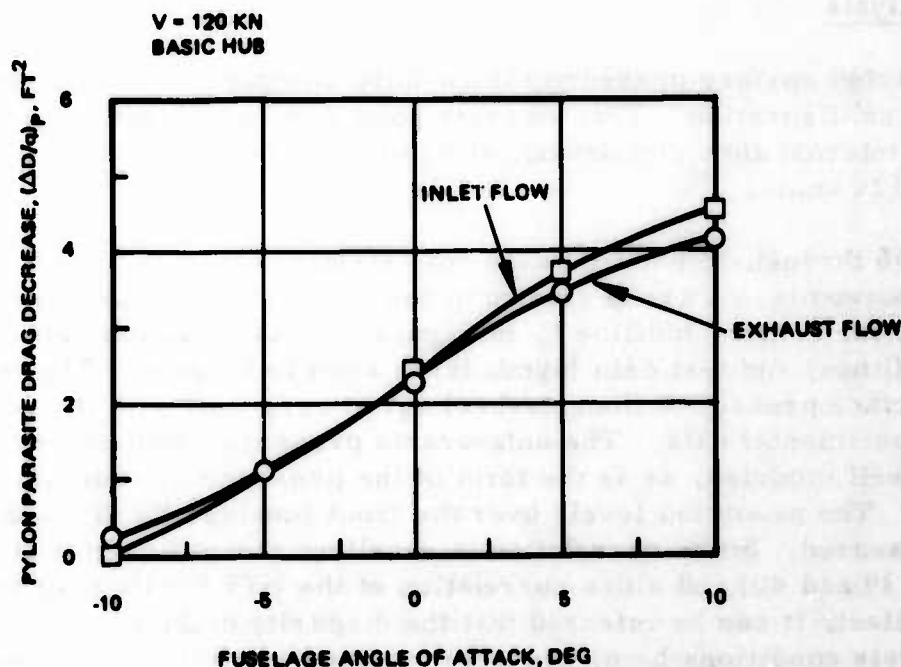
Figure 35. Effect of Wing and Rocket Pod on Pylon Drag.

63

This favorable interference indicates that as much of the aircraft as possible should be simulated during drag evaluation studies.

EXPERIMENTAL AND ANALYTICAL PRESSURES

Surface pressure data were taken at a number of locations on the model surface. Most of the locations were on the right-hand side, but a few were on the left, to provide checks of flow symmetry. For convenience the pressure data were recorded at points coinciding with the centers of the panels used to define the mathematical model.

During post-test processing the data were assembled into "strips" roughly corresponding to station, buttline, and waterline cuts on the analytic model. Half-bu was chosen for the mathematical model for both HPER and GRMS for convenience and to provide commonality. Calculated viscous effects were properly modeled using the appropriate Reynolds number. Unless otherwise specified, comparisons were made across configurations at a nominal 0-degree pitch and yaw, at a tunnel dynamic pressure of 48.6 pounds per square foot, and at a nominal 120 knots. Where the rotor is present, disc loading is set at 7 pounds per square foot, and the rotor trimmed to represent a cruise speed of 120 knots. Where a parameter is varied with a fixed configuration, such as over a pitch or yaw sweep, the point number is given in addition to the run number.

Test/Analysis

The predicted surface pressure values were compared with the test data for a matching configuration. This was test point 236, wings off, scale YAH-64 hub, full internal flow simulation, and 0-degree pitch or yaw at a tunnel speed of 120 knots.

Figures 36 through 38 show buttline cuts starting close to the centerline and working outwards. A cross section of the body is superimposed on the cut closest to the center, buttline 5, in Figure 36. Correlation between the analysis (lines) and test data (symbols) is seen to be good. The calculated upper surface pressures (long dashes) agree very well with the general trend of the experimental data. The unfavorable pressure gradient on the aft pylon is well modeled, as is the form of the pressure distribution on the front fuselage. The predicted levels over the front fuselage lie somewhat above those measured. Since correlation is excellent along the sides of the fuselage (Figures 39 and 40) and since correlation of the HPER data over this region was excellent, it can be inferred that the disparity must arise from the test and analysis conditions being properly matched in pitch. This conclusion is strengthened when the effect of model pitch (discussed below) is examined. At the other buttline cuts the correlation is also very good, the only

64

AERODYNAMIC DATA
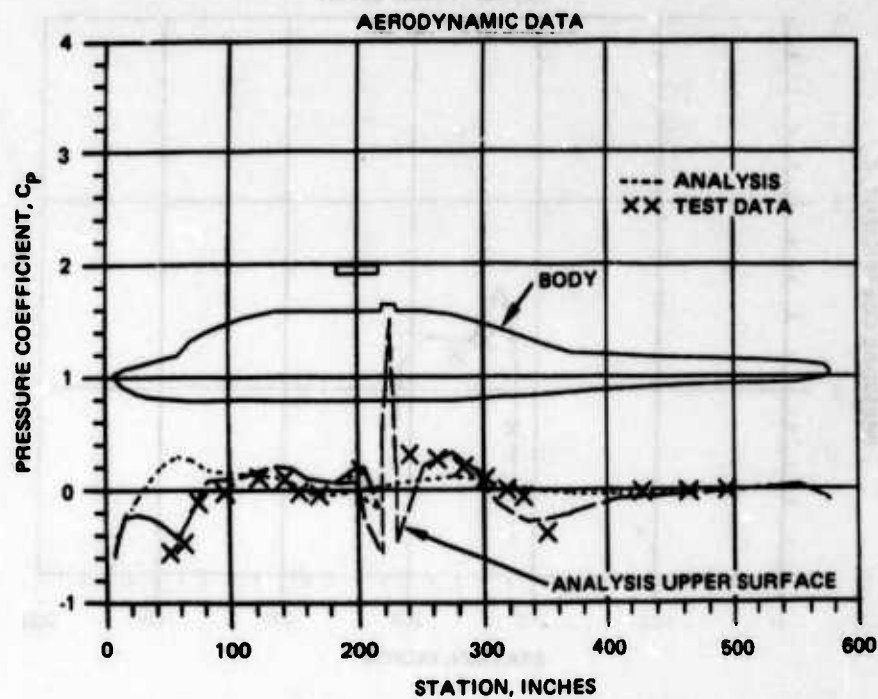
Figure 36. AH-64 GRMS Test/Analysis Comparison
at Buttline 5.

AERODYNAMIC DATA
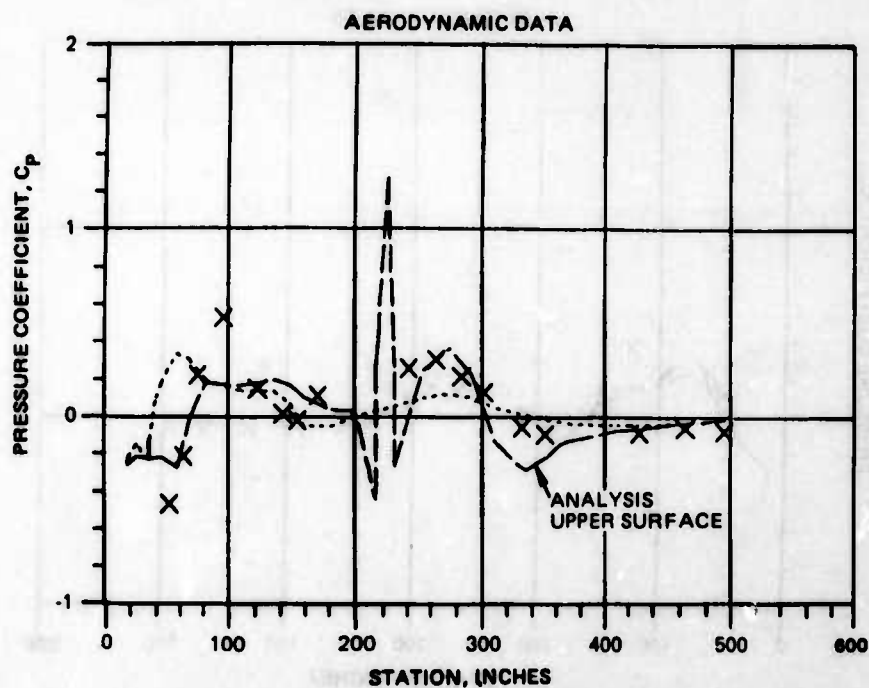
Figure 37. AH-64 GRMS Test/Analysis Comparison
at Buttline 12.

65
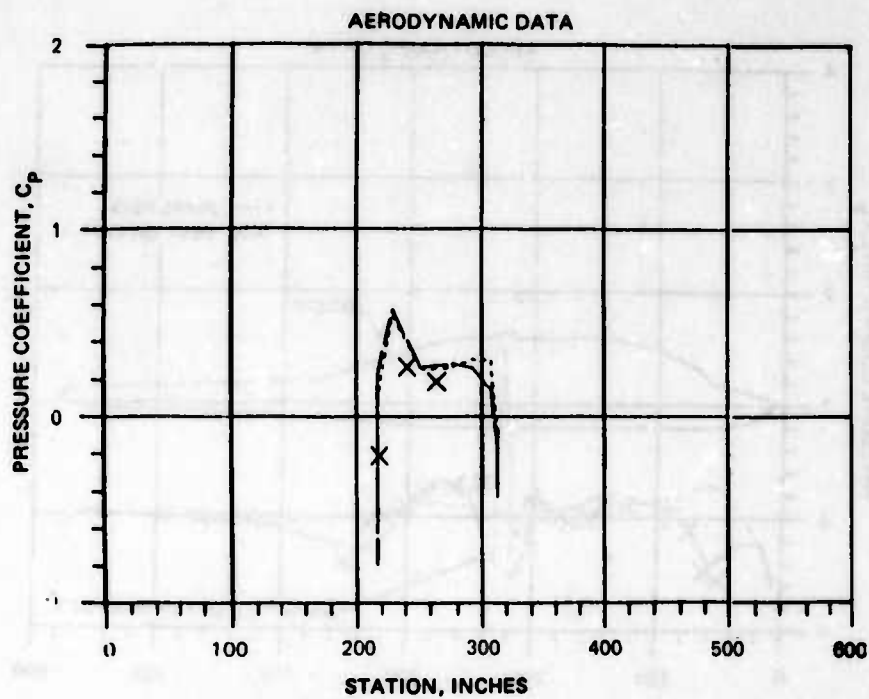
Figure 38. AH-64 GRMS Test/Analysis Comparison along Nacelle at Buttline 35.
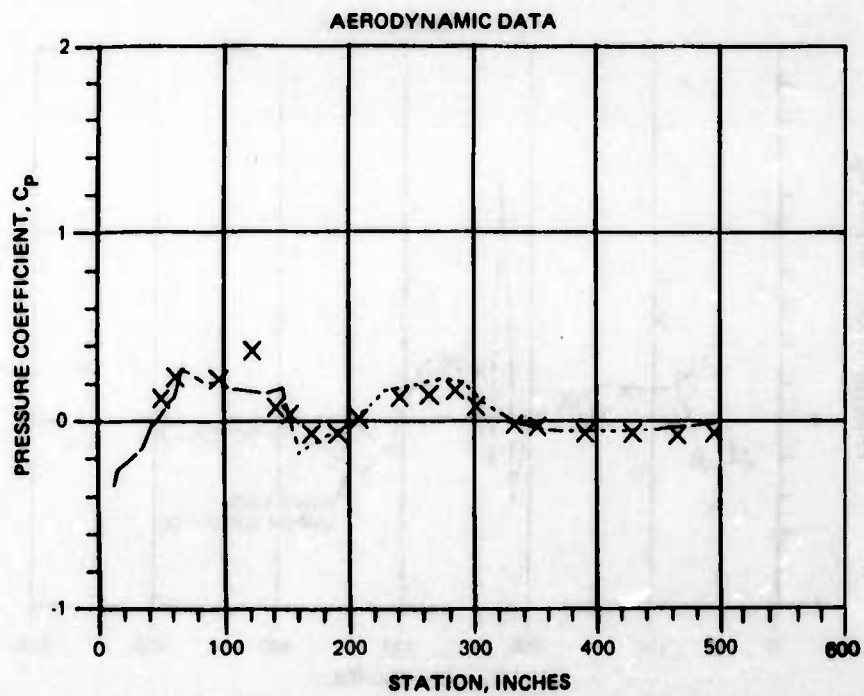
Figure 39. AH-64 GRMS Test/Analysis Comparison along Waterline 132.

66
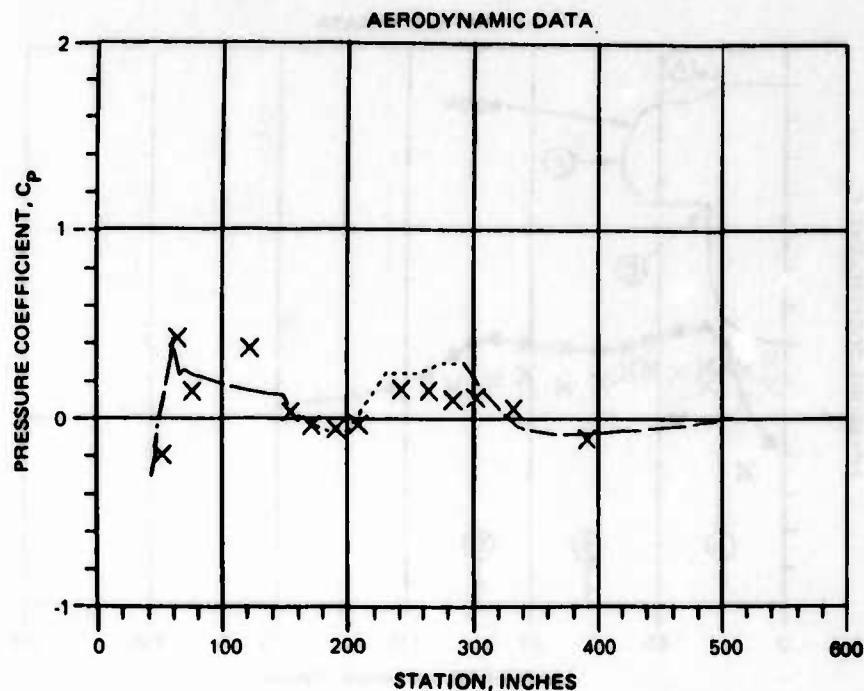
Figure 40. AH-64 GRMS Test/Analysis Comparison
along Waterline 142.

significant discrepancy being on the front fuselage at buttline 12 (Figure 37),
where at $X = 100.0$ the analytic model does not have the detail to pick up the
high suction peak around the edge of the canopy cut by the buttline at that
station. As with the earlier HPER data, nacelle pressures (Figure 38) are
well matched.

A comparison of pressures along the waterline cuts (Figures 39 and 40)
shows excellent correlation. The suction peak on the front fuselage is well
modeled, as is the influence on the engine nacelle between Stations 200 and
300. The single test data point at Station 120, which is not correlated, is
the result of a configuration feature not modeled by the analysis. The
correlation of the aft portions of the fuselage and the tailcone is particularly
good, providing confidence in the boundary layer model used in the viscous
calculation.

The data comparisons at the section cuts (Figures 41 through 45) also show
excellent correlation. At Station 241, just behind the rotor well collar, the
correlation is seen to be fair (Figure 41). The analysis is trending above the
test data but still within a scatter band, as defined by the left side/right side
variation in the test data. The correlation improves at stations further aft,

67
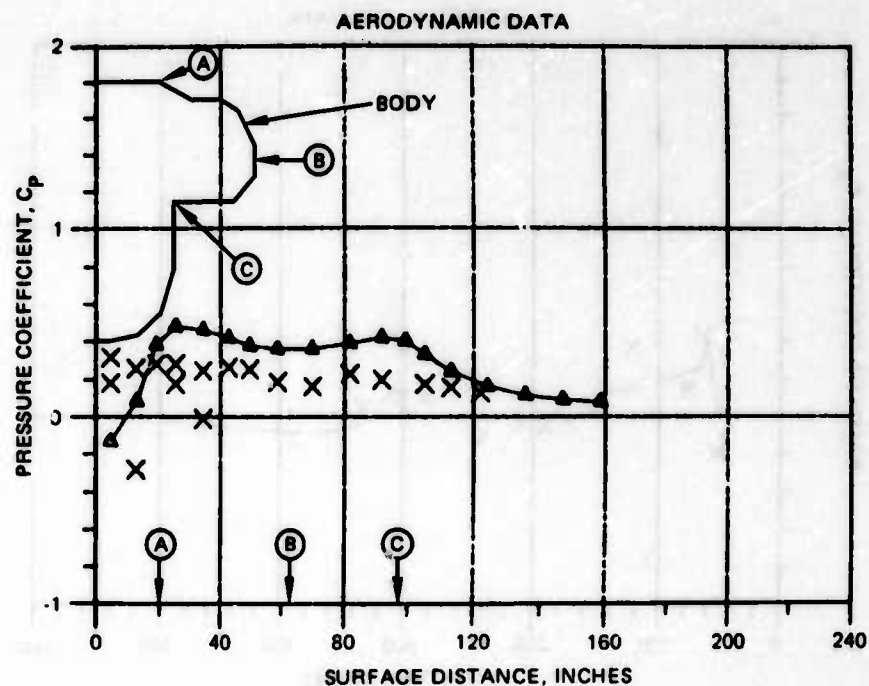
Figure 41. AH-64 GRMS Test/Analysis Comparison
at Station 241.
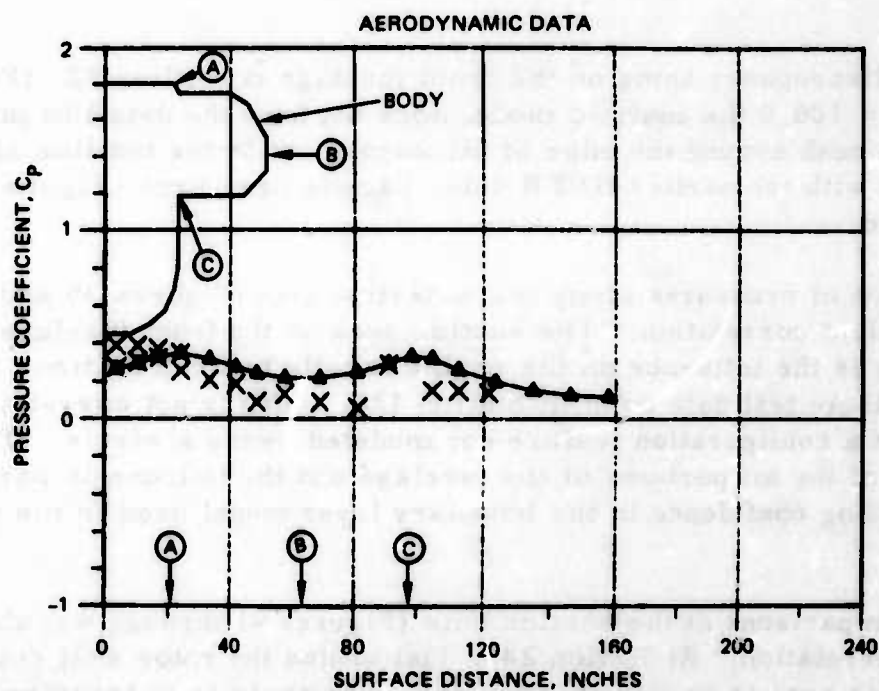
Figure 42. AH-64 GRMS Test/Analysis Comparison
at Station 264.
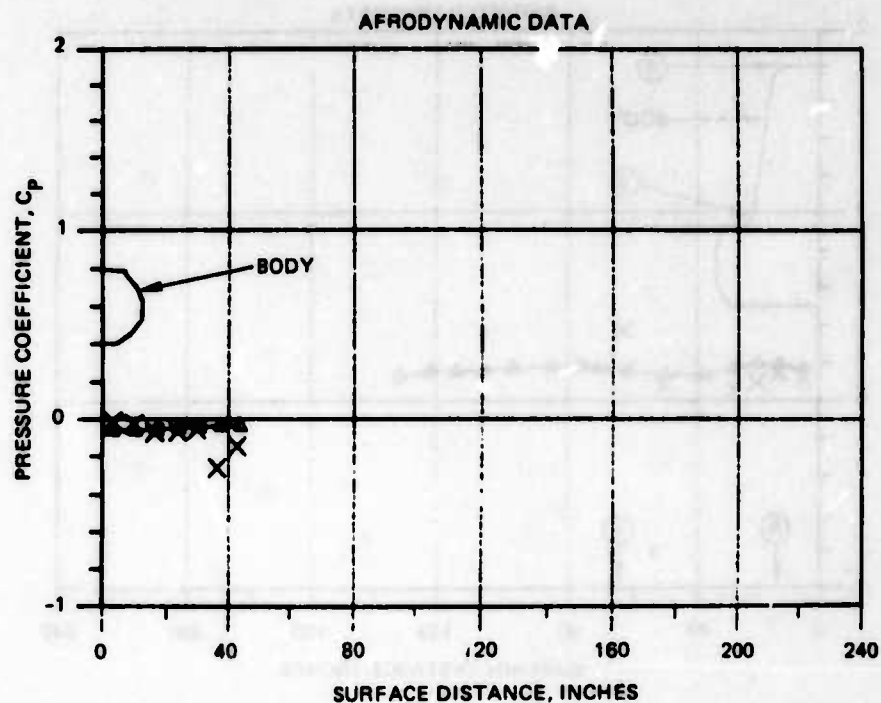
Figure 43. AH-64 GRMS Test/Analysis Comparison
at Station 430.
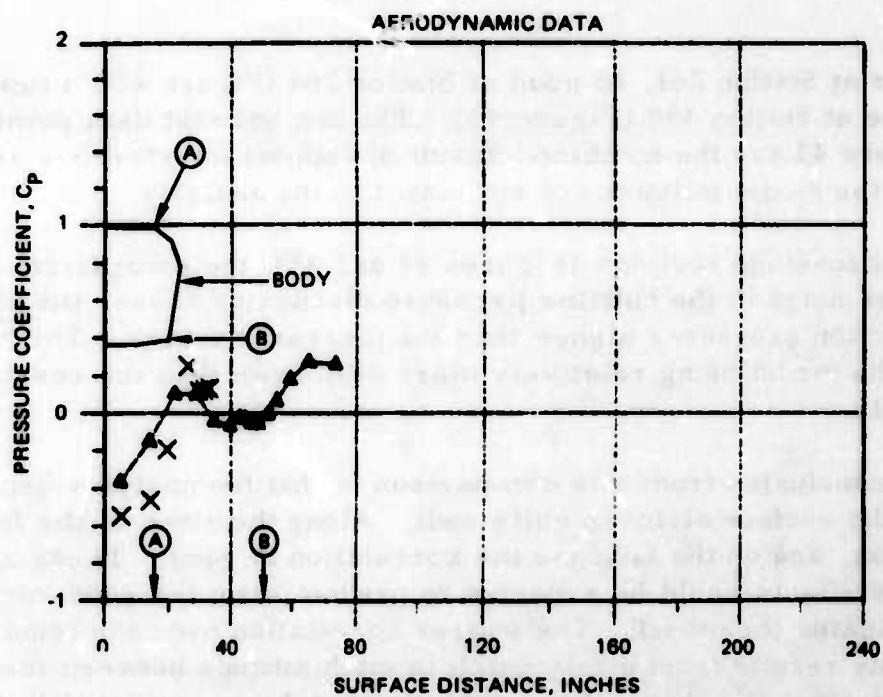
Figure 44. AH-64 GRMS Test/Analysis Comparison
at Station 51.

69

AERODYNAMIC DATA
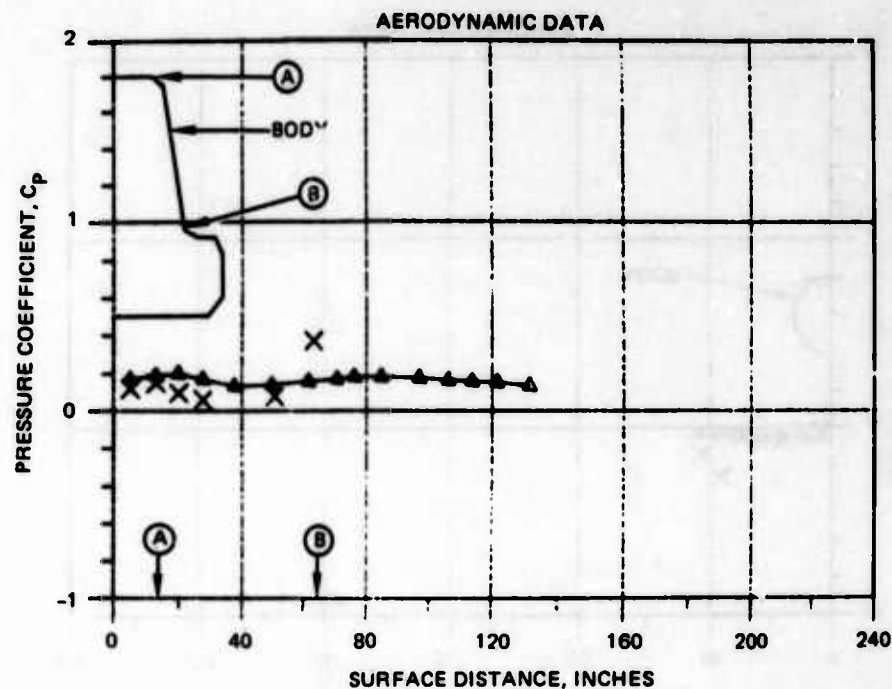
Figure 45. AH-64 GRMS Test/Analysis Comparison
at Station 122.

from only fair at Station 241, to good at Station 264 (Figure 42), to excellent
on the tailcone at Station 430 (Figure 43). The two odd test data points
shown in Figure 43 are the combined result of support interference and a
thickening of the model tailcone not simulated in the analysis.

Over the front fuselage sections (Figures 44 and 45), the comparison reflects
the differences noted in the buttline pressure discussion above, the analysis
predicting suction pressures higher than the measured values. This is con-
sistent with the model being relatively more nose down than the case analyzed
mathematically.

The general conclusion from this comparison is that the analysis generally
represented the surface airloads quite well. Along the sides of the fuselage,
on the aft pylon, and on the tailcone the correlation is good. These are areas
where viscous effects would be expected to predominate; the good correlation
therefore validates the model. The poorer correlation over the front of the
model probably results from a mismatch in pitch attitude between the two
configurations since the shape of the analytic model was validated in the
HPER study, where correlation was excellent over the front fuselage.

70

Rotor On/Rotor Off

The bulk of the data taken during the test were with the GRMS model rotor off and with various configuration options added. Similarly, the mathematical analysis of the aircraft did not include the effect of the rotor downwash analysis of the aircraft. Consequently, a comparison of the rotor on/rotor off pressure data is needed before observations based on the tunnel data can be related to what may happen on the aircraft. The cases compared are Run 82 (rotor on) and Run 158 (rotor off). In both cases the rotorhead was that from the basic GRMS model, so the comparisons show the effect solely of the rotor downwash. The fuselage angle of attack is nominally 0 degrees as is the yaw angle, and the wing is on.

The effects of rotor downwash appear to be limited to the front fuselage. This is highlighted in Figures 46 and 47, which are buttline cuts at 5 and 12 respectively. With the rotor on, suction over the front fuselage appears to be enhanced by an amount equivalent to an angle-of-attack change of about 5 degrees nose down (see the discussion of the effect of pitch change below). A similar effect is seen on the engine nacelle in Figure 48. In the Waterline 142 cut shown (Figure 49),a similar effect shows up with the suction pressure around the side of the nose showing increases. Although no strong
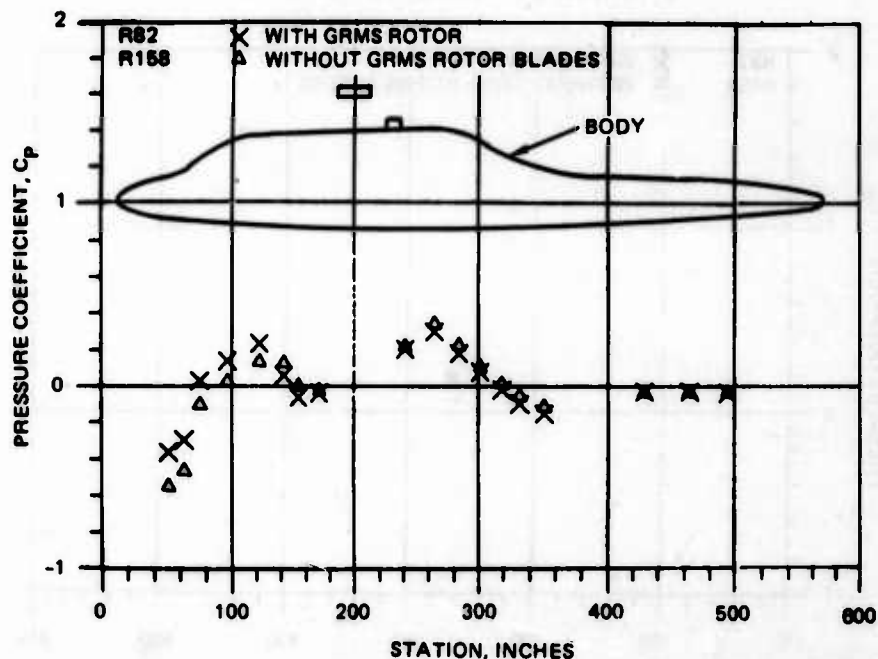
Figure 46. Effect of Main Rotor Wake on Surface
Pressures along Buttline 5.

71
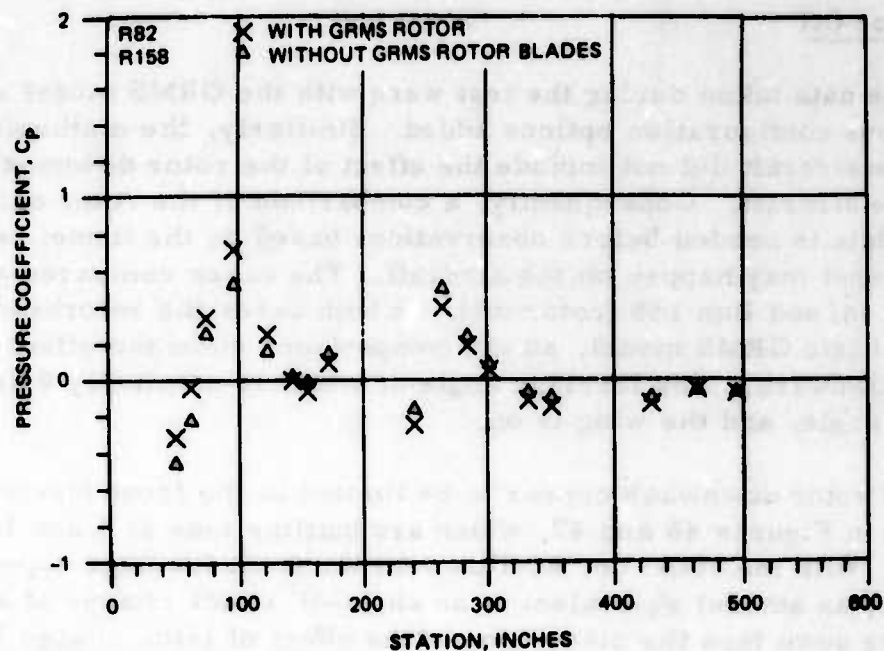
Figure 47.   Effect of Main Rotor Wake on Surface
Pressures along Buttline 12.
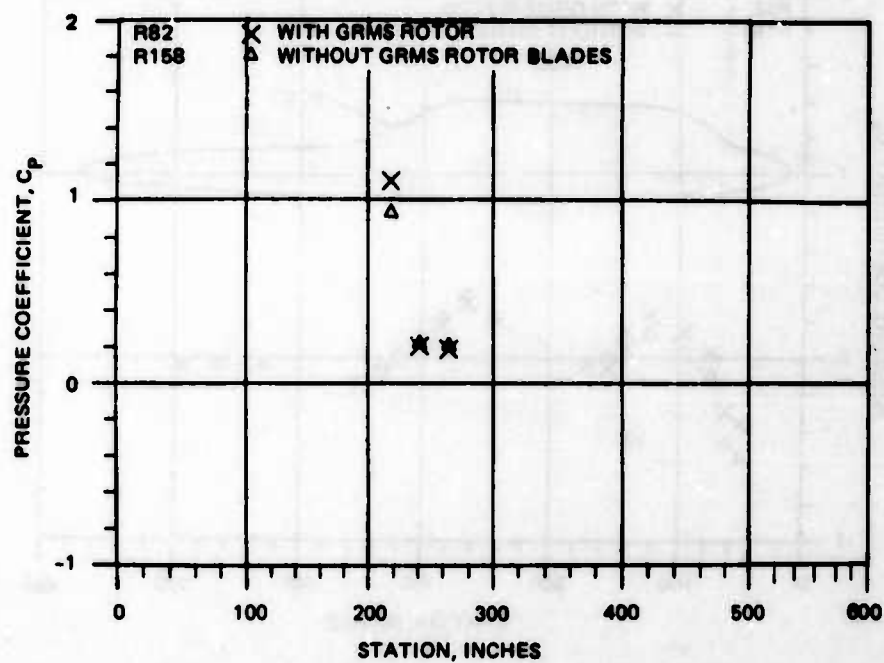
Figure 48.   Effect of Main Rotor Wake on Surface
Pressures along Nacelle at Buttline 35.

72
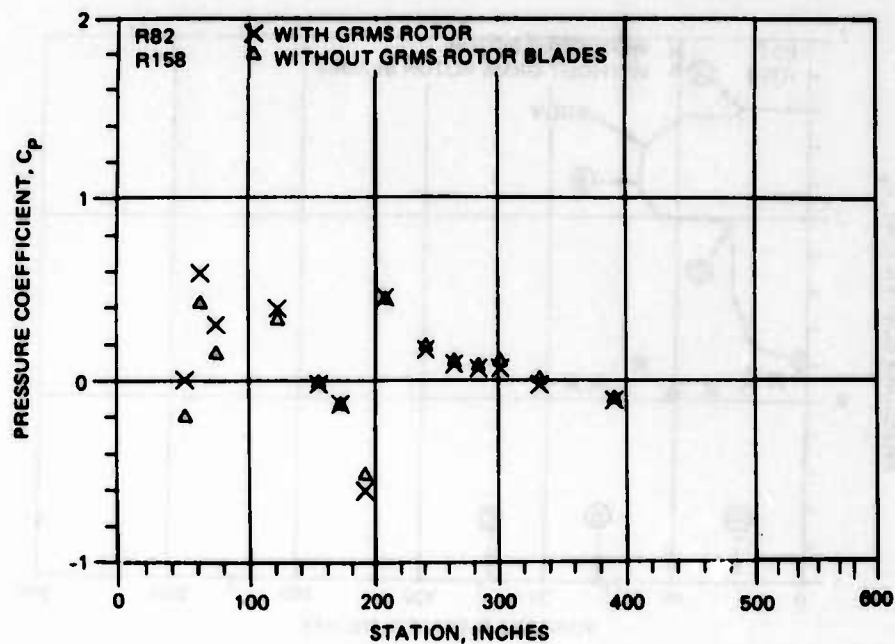
Figure 49. Effect of Main Rotor Wake on Surface Pressures along Waterline 142.

rotor on/rotor off trends are present on the aft fuselage, it is interesting to note changes in the left-side/right-side pressures plotted in Figure 50 at Station 270; in this figure the doublet values represent left- and right-side pressures. Although the differences between the two sides (not identified in the figure) appear to be random, the range is not affected by rotor downwash, although there does appear to be a reduction in the average value away from the centerline.

The general conclusion that emerges from this comparison is that, at least for the trimmed forward flight case examined, the influence of the rotor seems to be equivalent to flying the aircraft slightly nose down.

73
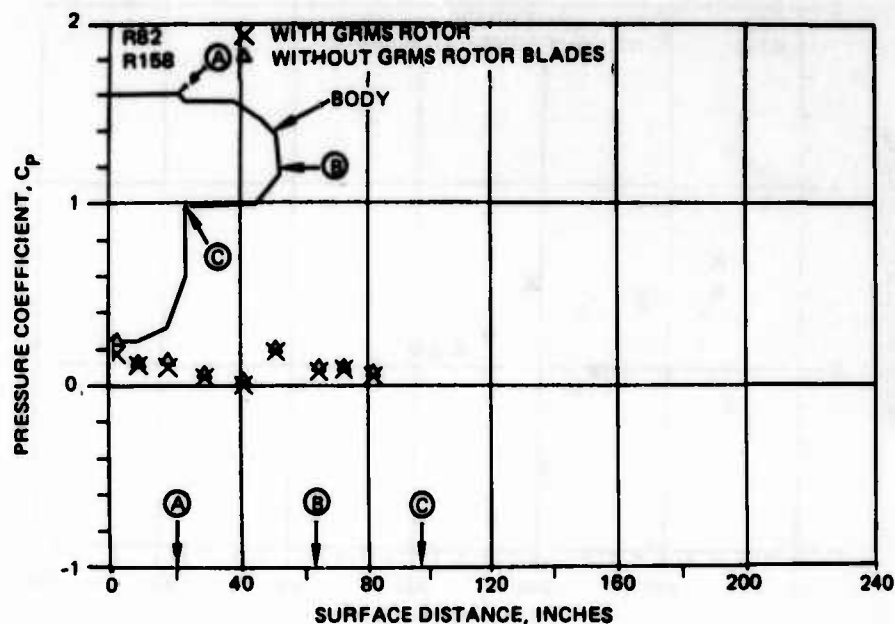
Figure 50.   Effect of Main Rotor Wake on Surface
Pressures at Station 264.

Test Rotor Hub/Scale Rotor Hub

Because of the dynamic requirements of the GRMS model, the rotor hub used
for the rotor-on tests was quite different from the representative, scaled
version used for the rest of the testing. Consequently, a review of the effect
of hub geometry change, aside from the rotor downwash influence, is in order.

Overall, the effect of changing from the GRMS hub to the representative,
scaled YAH-64 hub appears to be negligible for the cases examined. An
example is shown on the model centerline at a 0-degree angle of attack
(Figure 51), where the changes in hub geometry have a negligible effect. As
might be expected the change has its greatest effect on the aft pylon, but
even there the influence is very local.

Angle of Attack

As was noted in the discussion on the effect of the rotor, conditions on the aft
pylon and rear fuselage are insensitive to changes in flow angularity. This
appears to be independent of the means by which the flow angularity is induced.
In Figures 52 through 54 the influence of pitch attitude is studied. In Run 158

74
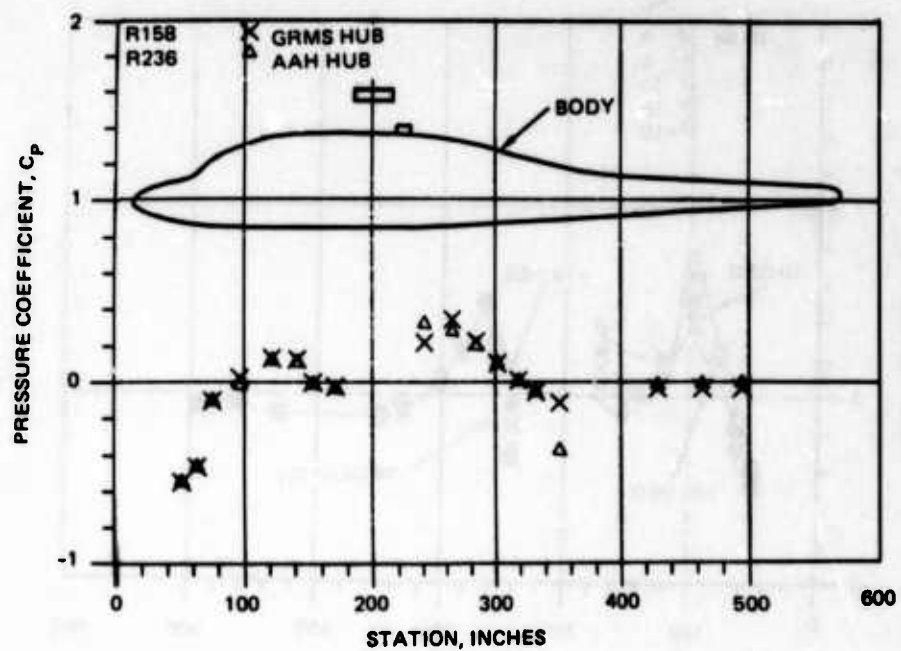
Figure 51. Effect of Hub Configuration along Body
Centerline at Buttline 5.
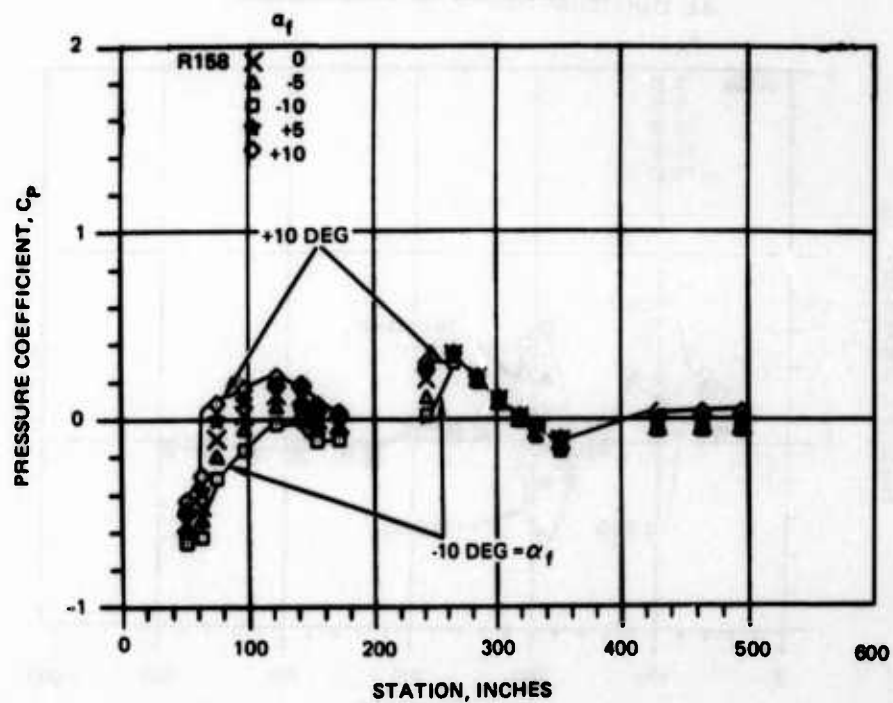
Figure 52. Effect of Angle of Attack on YAH-64 GRMS
at Buttline 5.

75
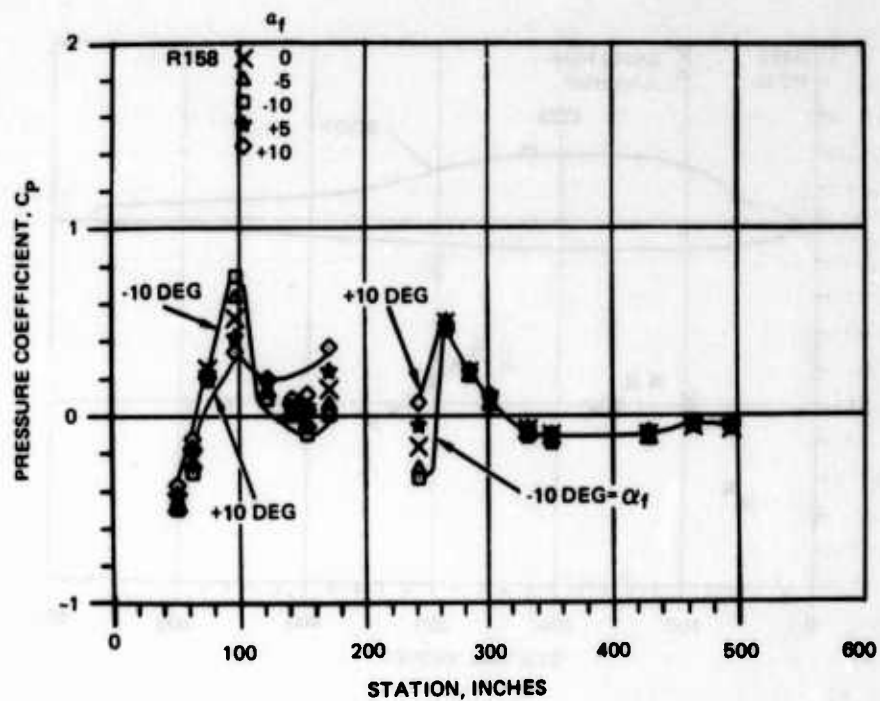
Figure 53. Effect of Angle of Attack on YAH-64 GRMS at Buttline 12.
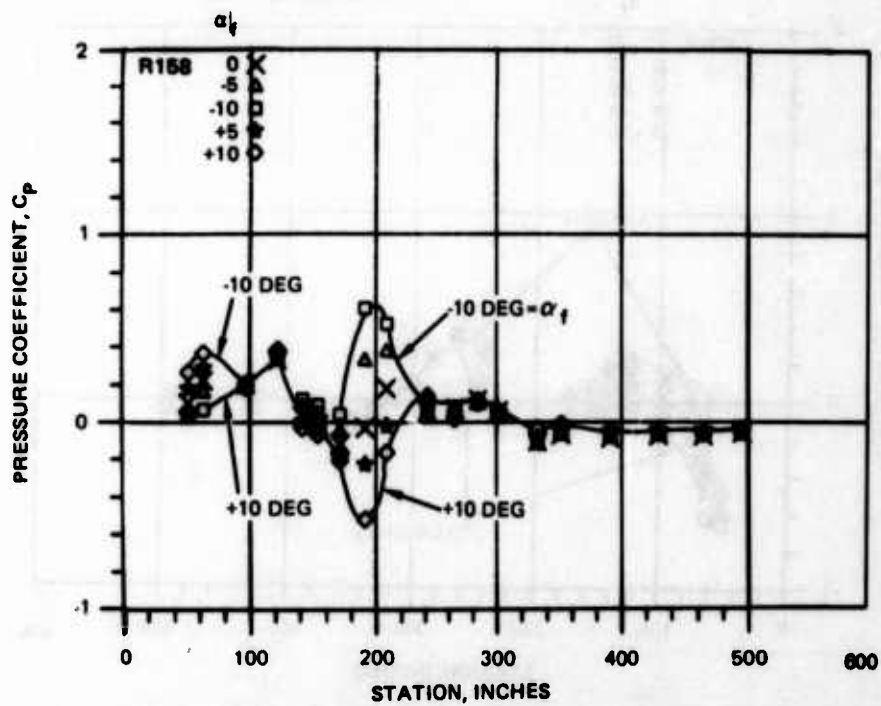
Figure 54. Effect of Angle of Attack on YAH-64 GRMS at Waterline 130.

76

the model was pitched through a range of angles from +10 degrees (nose up) to -10 degrees (nose down). Pressure variation close to the centerline (Buttline 5) is shown in Figure 52. Apart from one point in the lee of the rotor well collar, all the variation is restricted to the front fuselage. As would be expected, raising the nose increases suction pressures over the crown of the canopy (Station 120). In Figure 53, a buttline of 12 is plotted and here, forward of Station 100, the effect of pitch is softened as the points plotted are down on the side of the nose. This section cuts the corner between the cockpit side and the upper surface at Station 100 and, magnified by the edge, the effect of pitch is stronger. Aft of Station 100 the effect weakens until, at a station close to 180, it grows again, the trend reversed, driven by the flow stagnating, then spilling up around the transfer gear box fairing in front of the engine nacelle. Further aft there is again no variation with pitch. On the nacelle itself, the trend rights itself, and increased suction with increasing angle of attack is seen.

The cuts along Waterlines 130 and 142, plotted in Figures 54 and 55, lie just below and just above the plane of the wing. In these two cuts, the effect of pitch is most strongly present. Ahead of Station 100, the variation is due to the FABs installation which acts like a small winglet. The large excursion ahead of Station 200 is due to the wing, the flow decelerating pressure becoming more positive as the angle of attack is increased for the cut below the wing.
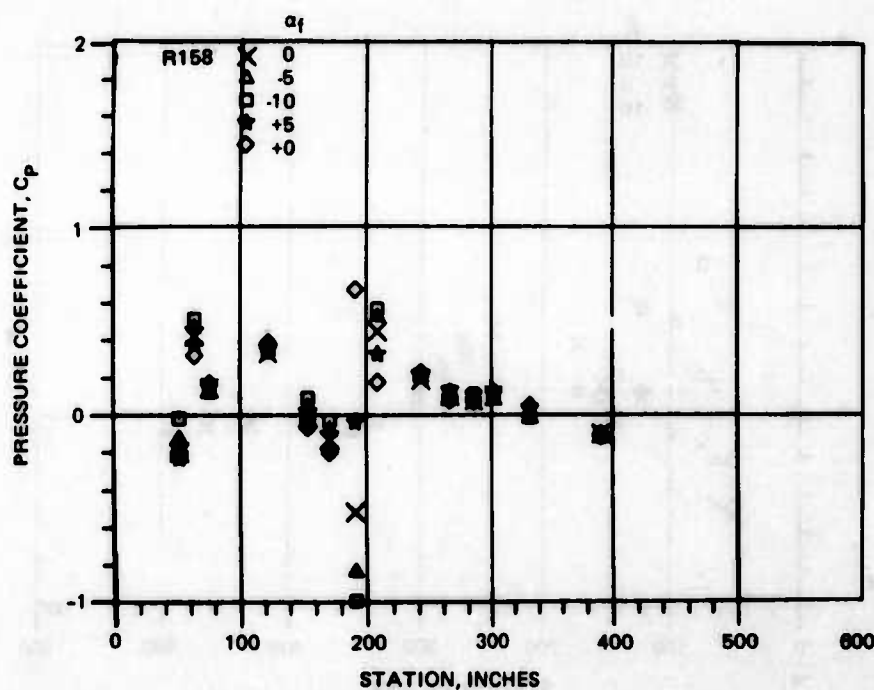
Figure 55. Effect of Angle of Attack on YAH-64 GRMS
at Waterline 142.

The trend reverses for the cut above the wing. It is interesting to note that aft of Station 200, in the space below the engine nacelle, the nacelle dominates even close to the wing trailing edge (Figure 55, the two points before and after Station 200). From these data it can be inferred that not only is the wing carrying lift, but that the nacelle is also contributing. This is confirmed by the data taken at stations cutting the nacelle.

The conclusions of the pitch sweep discussed here support the tentative conclusion that the flow on the aft pylon is insensitive to angle of attack. This must in large measure be due to the influence of the wing and, to a lesser degree, the engine nacelles, both of which contribute some induced downwash counter to the geometric angle of attack.

Yaw

As might be inferred, the effects of yaw, determined from the results of Run 261, were mostly confined to the front fuselage and to the sides of the rear fuselage and nacelles. A cut along Buttline 12 (Figure 56) illustrates the effect. Where the section is close to the corner between the upper surface and the side, there is considerable magnification. The suction is greater when the corner is facing upstream (the squares in Figure 56 at -10 degrees yaw). This effect also shows up in the waterline cuts (Figure 57).
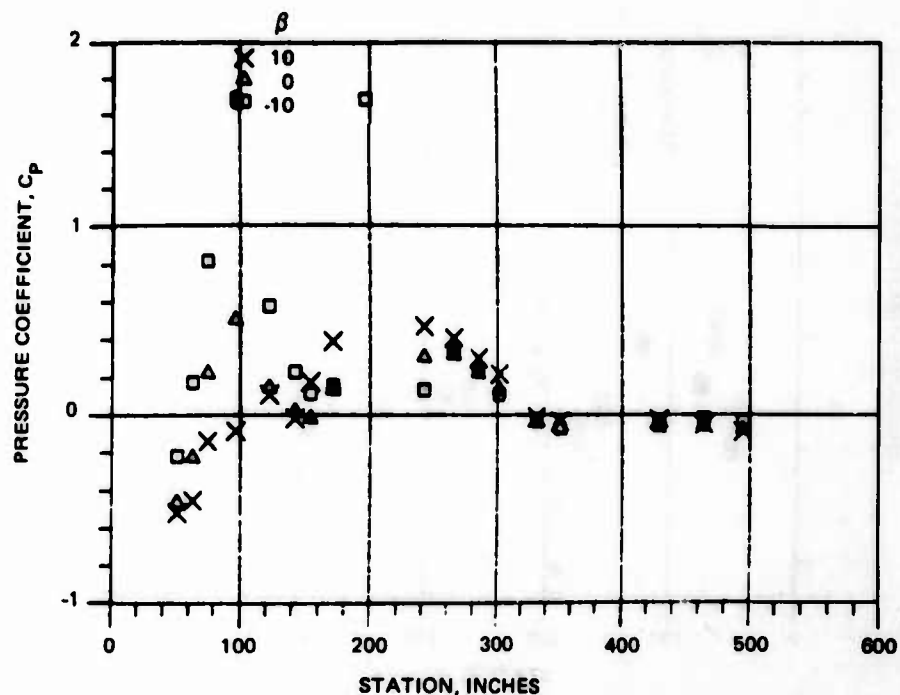
Figure 56. Effect of Yaw Angle on YAH-64 GRMS at Buttline 12.
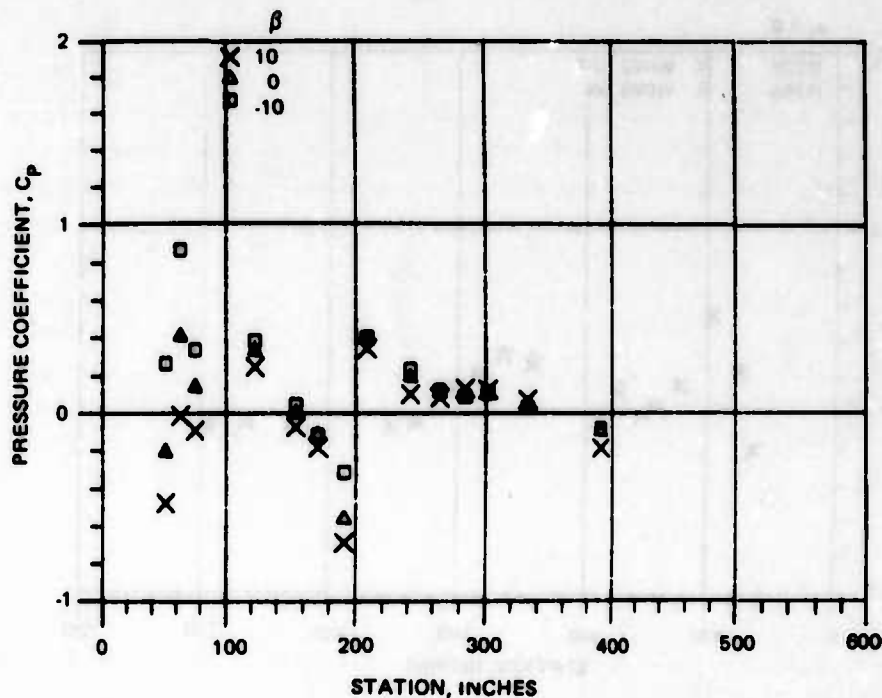
Figure 57. Effect of Yaw Angle on YAH-64 GRMS
at Waterline 142.

The effect noted close to Station 200 (also in Figure 57) is due to the influence
of the forward elements of the engine nacelle.

Wing On/Wing Off

Comparison of Runs 236 and 256, wing off and wing on respectively, allow
the influence of the wing to be defined at a low loading. Unfortunately,
pressures were not recorded during a pitch sweep, so no comparison at
higher wing lift levels is possible. On the buttlines close to the center
(Buttline 12 in Figure 58 is typical), the effect of the wing is negligible.
This comment is appropriate for most of the other strips with the exception
of the waterline cuts. The presence of the wing shows very clearly, however,
just above the wing upper surface (Figure 59). The deceleration of the flow
approaching the wing and the accelerated flow over its upper surface are
evident. Other than along these strips and around the front portions of the
nacelle, the wing has little effect on the fuselage airloads of low wing loading.
At higher fuselage pitch attitudes, the wing-induced effects must be consider-
able, but these are not available from a wing on/off test and must be inferred
from the results of the pitch sweep discussed above.

79
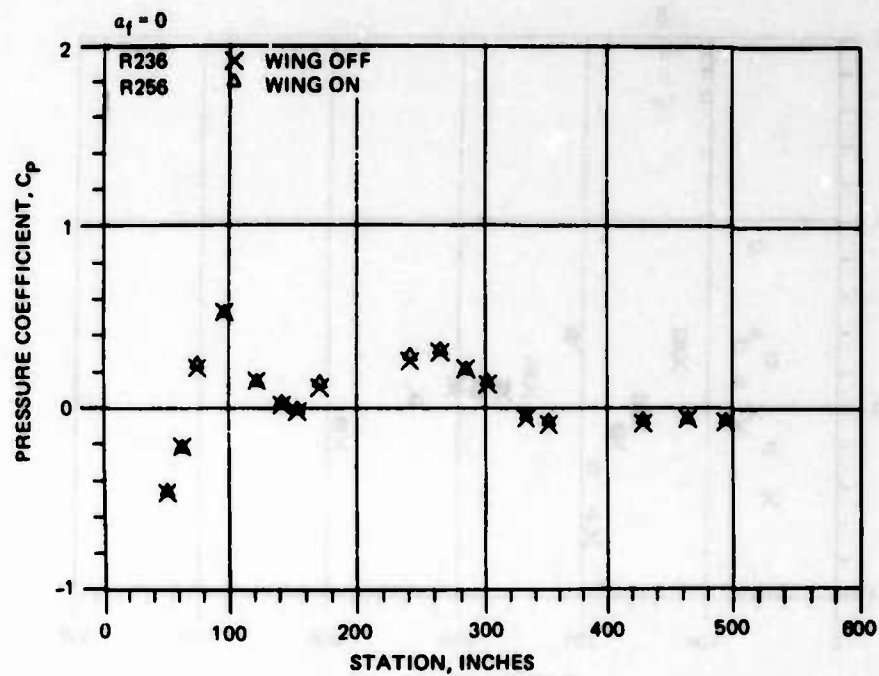
Figure 58. Effect of Wing on YAH-64 GRMS along Buttline 12.
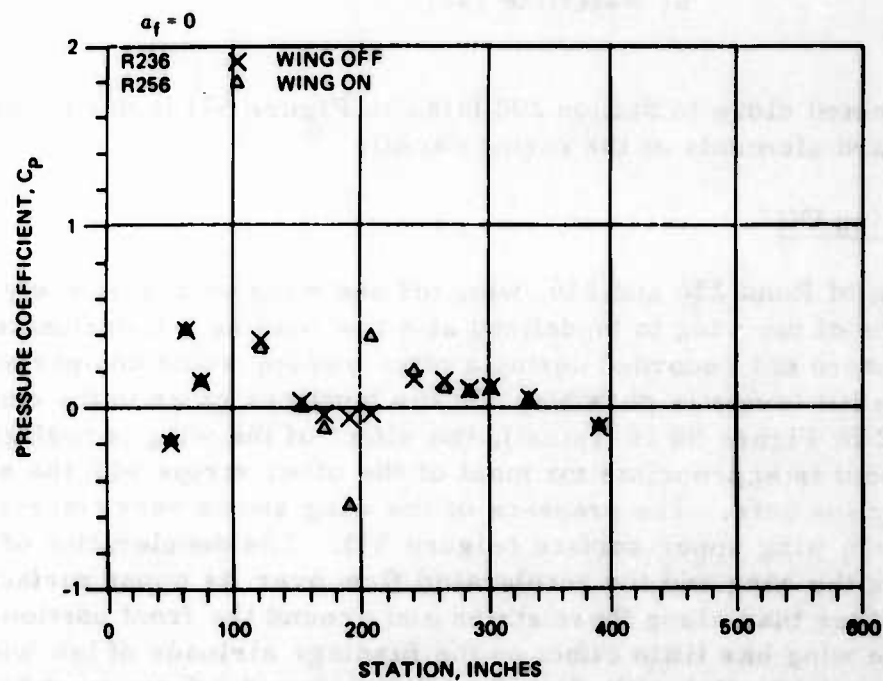
Figure 59. Effect of Wing on YAH-64 GRMS along Waterline 142.

Sealed Faired Hub/Unsealed Faired Hub

It has been shown that fairing a rotor hub alone is not sufficient to reduce drag and that for maximum effectiveness the fairing must also be sealed to prevent through-flow of air and drag covering momentum losses. A comparison of Runs 256 and 191 with and without sealing should prove whether the "hub on fuselage" interference drag is similarly affected. A close study of all the data from these cases showed no significant differences in surface pressures. Pressures along Station 241, a station cut downstream of the rotor hub, are presented in Figure 60. The agreement between the two cases, even to the matching of the left/right differences is remarkable and must rule out the existence of any significant hub/fuselage interference effect associated with hub fairing sealing, at least for this configuration at the flow conditions tested.

Nacelle Inflow/Exhaust Modeling

Because of the way in which nacelle flow was simulated it was not possible to accurately model both inlet and exhaust flows simultaneously. A series of runs was carried out to explore this effect: Run 236 with correct exhaust modeling and 237 with correct inlet modeling. Runs 236 and 237 were wings off. Except in the immediate vicinity of the inlet, the difference between
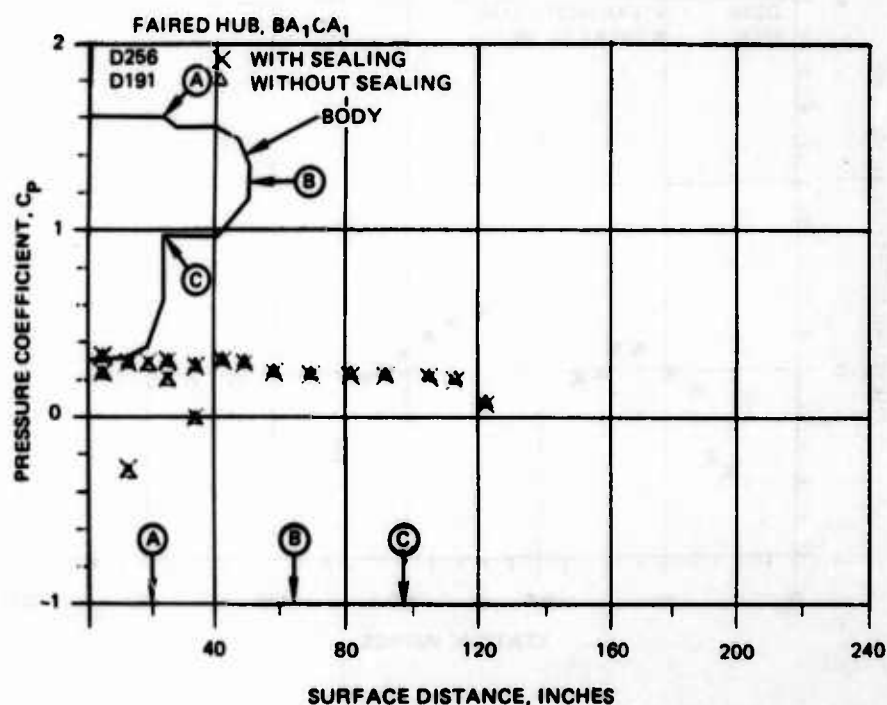
Figure 60. Effect of Sealing Faired Hub on YAH-64 GRMS at Station 241.

81

inlet and exhaust flow levels made no noticeable difference, as can be seen from the distributions presented in Figures 61 and 62. A similar effect was shown for wings-on configurations.

Only along Buttline 35, through the nacelle with a point close to the inlet lip, does any appreciable effect become apparent. These are plotted for wings-off and wings-on cases in Figures 63 and 64. With the triangles in each case representing correct inlet modeling, it can be seen that the wing has a controlling effect on the lip pressures. In one case (wings off) suction is enhanced, and in the other (wings on) suction is reduced. This large influence from a lightly loaded wing is an indication that the tap in question is located very close to the inlet lip stagnation point. It is also a clear warning that under certain conditions the pressure field around the wing could seriously distort the engine inlet flow field and impair engine efficiency.

There was no evidence in any of the test pressure distributions of changes in surface pressure that could be attributed to an improperly modeled exhaust flow. It should be noted that the correct exhaust velocity is very close to the free-stream value at the 120-knot test condition and, consequently, any mismatch effects, if present, would be weak. The same cannot be said for the inlet, however, since even small variations in inlet mass flow can cause
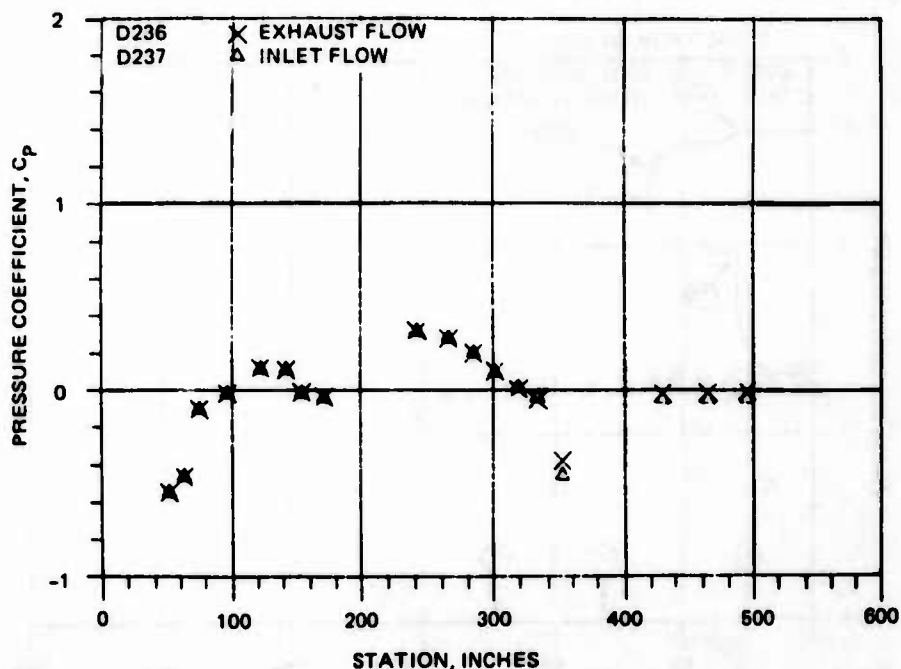
Figure 61. Effect of Airflow Modeling on YAH-64 GRMS along Buttline 5.

82
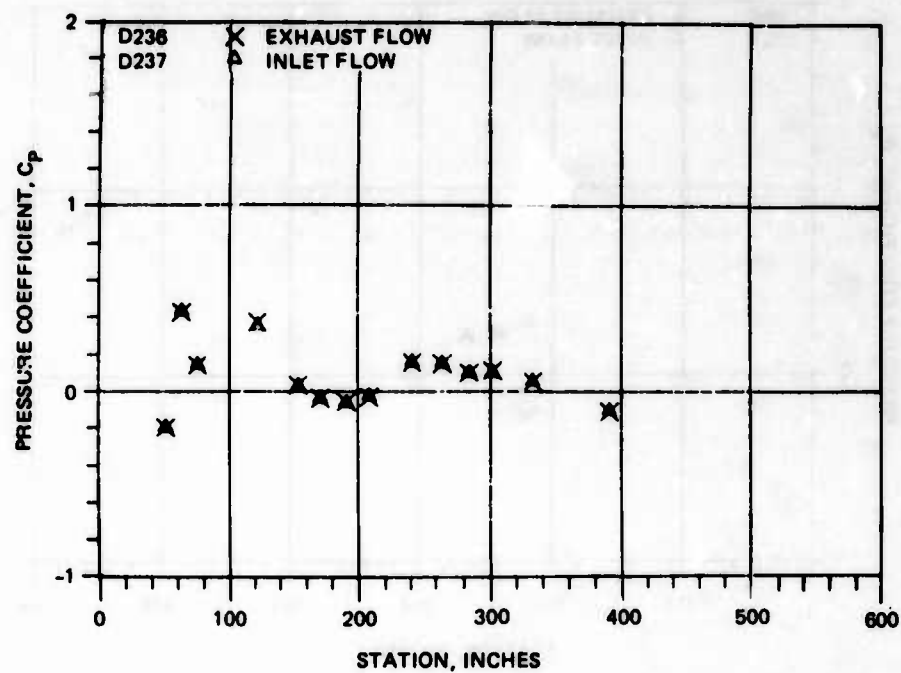
Figure 62. Effect of Airflow Modeling on YAH-64 GRMS along Waterline 142.
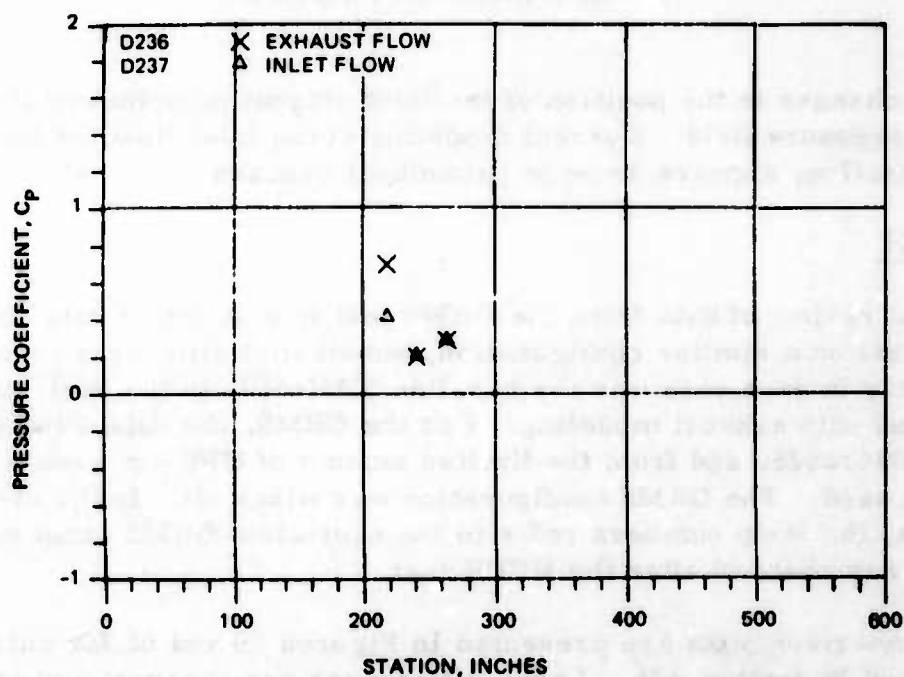
Figure 63. Effect of Airflow Modeling on YAH-64 GRMS along Nacelle at Buttline 35, Wings Off

83
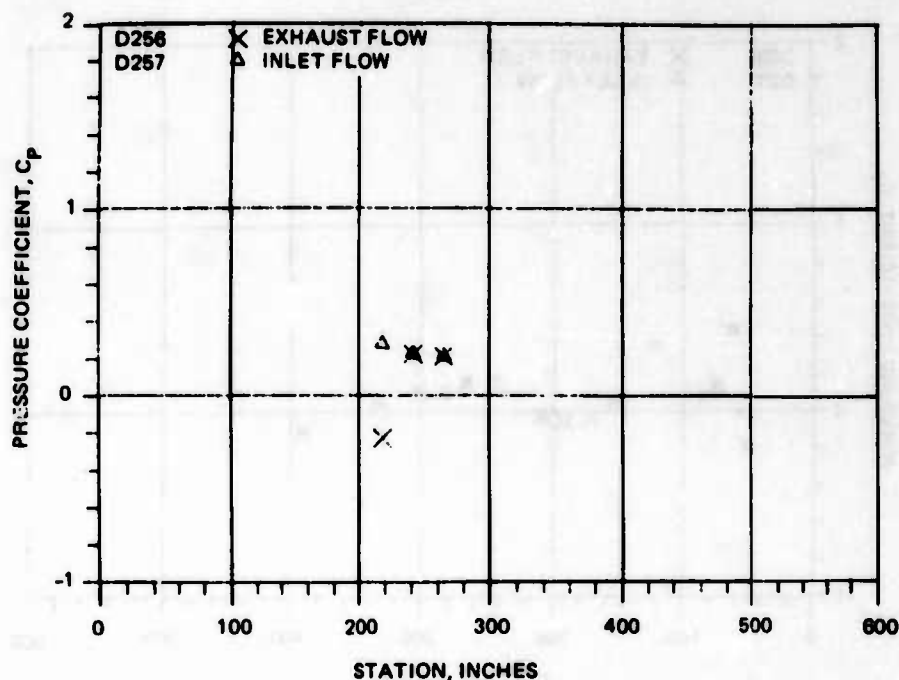
Figure 64. Effect of Airflow Modeling on
YAH-64 GRMS along Nacelle
at Buttline 35, Wings On.

substantial changes in the position of the inlet stagnation point and its
associated pressure field. Correct modeling of the inlet flow, at least for
this configuration, appears to be of paramount concern.

GRMS/HPER

In the initial review of data from the GRMS test in relation to data taken in
the HPER test on a similar configuration, substantial differences were found.
The geometry in each case was the baseline YAH-64 with the basic hub,
rotating, and with exhaust modeling. For the GRMS, the data was taken from
Run/Point 236/2525, and from the limited amount of HPER pressure data
30/106 was used. The GRMS configuration was wings off. In the discussion
that follows, the strip numbers refer to the equivalent GRMS strip since the
numbering was changed after the HPER test.

Typical comparison plots are presented in Figures 65 and 66 for cuts at
Buttline 5 and Waterline 126. Large differences are apparent and are the
result of three principal effects: the tunnel blockage effect, the pre-
sence of an unnatural ground plane position, and possible tunnel flow align-
ment differences between the two cases. Differences due to the fore-and-aft

84
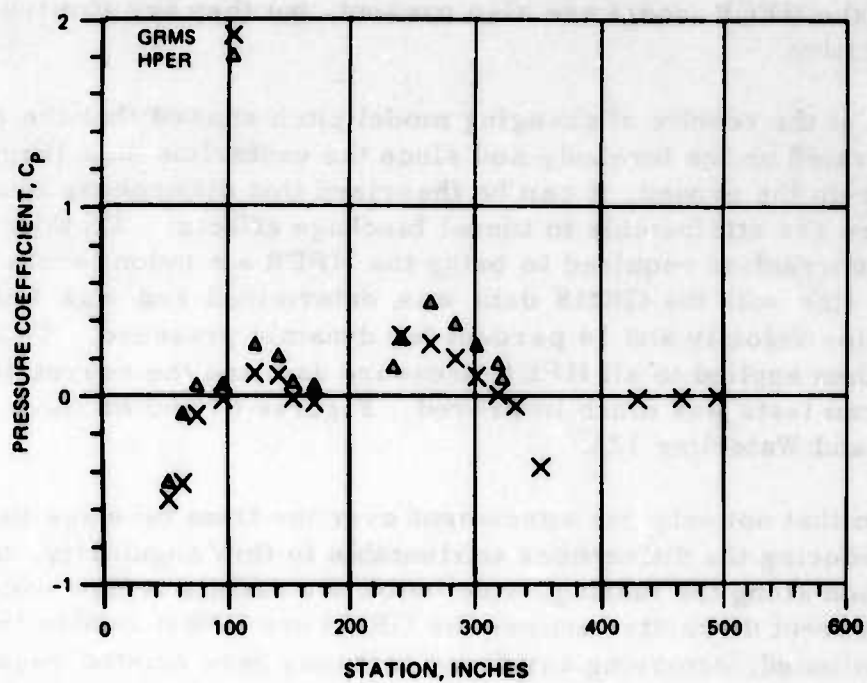
Figure 65. Comparison of YAH-64 GRMS/HPER
Pressures along Buttline 5.
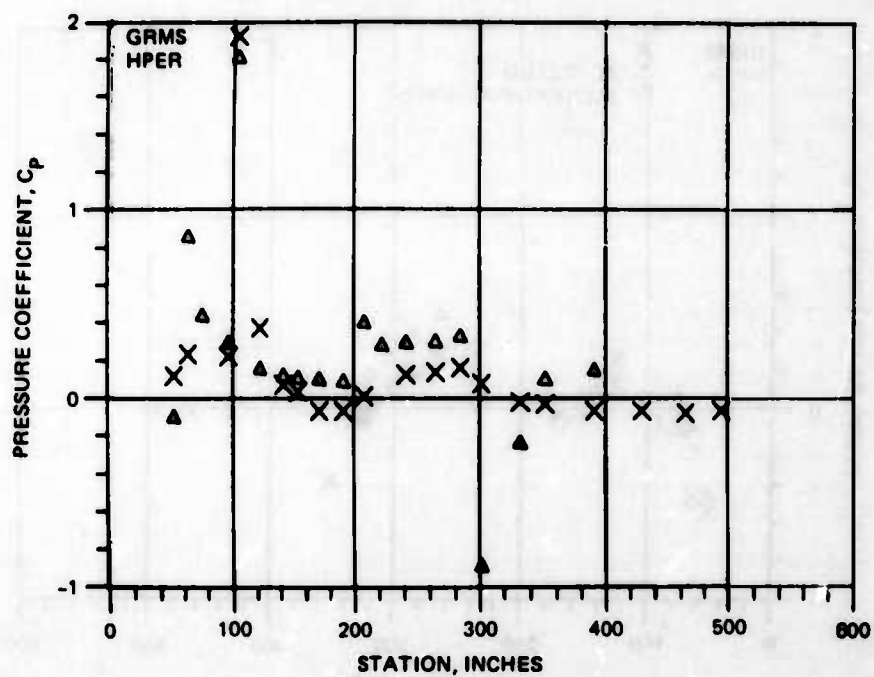
Figure 66. Comparison of YAH-64 GRMS/HPER
Pressures along Waterline 132.

85

truncation of the HPER model are also present, but they are limited to the model extremities.

Since a study of the results of changing model pitch showed that the effects were concentrated on the forebody and since the centerline data (Figure 65) are remote from the ground, it can be theorized that differences in aft pylon pressure are attributable to tunnel blockage effects. On this basis the blockage correction required to bring the HPER aft pylon levels and gradient into line with the GRMS data was determined and was found to be 7 percent for velocity and 14 percent for dynamic pressure. This correction was then applied to all HPER pressure data and the correlation between the two tests was much improved. Figures 67 and 68 show the effect at Buttline 5 and Waterline 126.

It can be seen that not only has agreement over the front fuselage been much improved, reducing the differences attributable to flow angularity, but also that correlation along the fuselage side below the nacelle is now excellent. The large apparent disparity between the GRMS and HPER data in this region has been eliminated, removing any fears that may have existed regarding the ability of the HPER model, with its gross truncation, to represent the flow around the aircraft. The remaining disagreements that exist, most obvious along Waterline 130 (Figure 68), can be attributed to configuration differences resulting from the truncation of the HPER model.
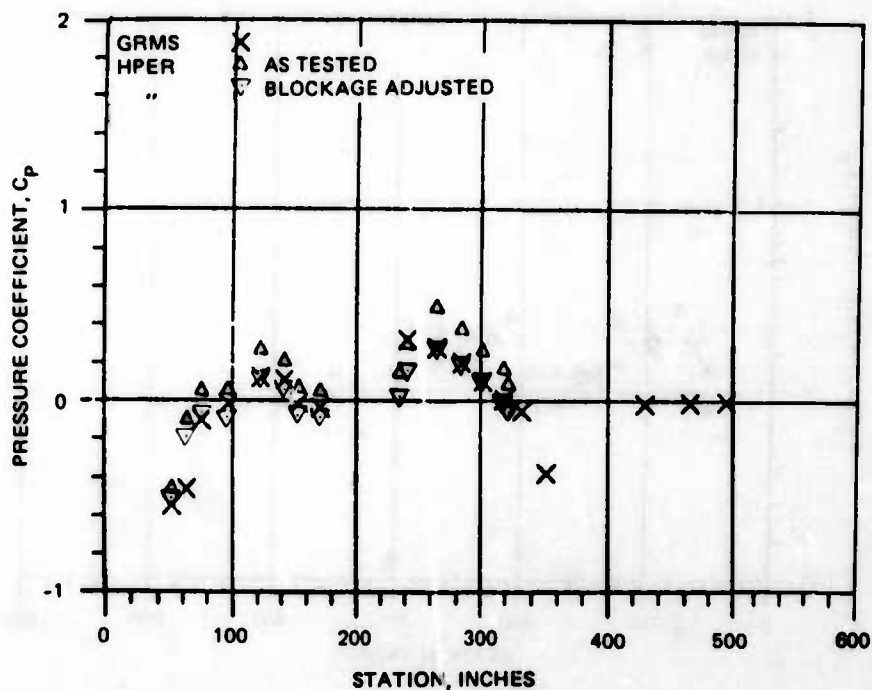
Figure 67. Effect of HPER Blockage Correction on YAH-64 GRMS/HPER Pressure along Buttline 5.

86
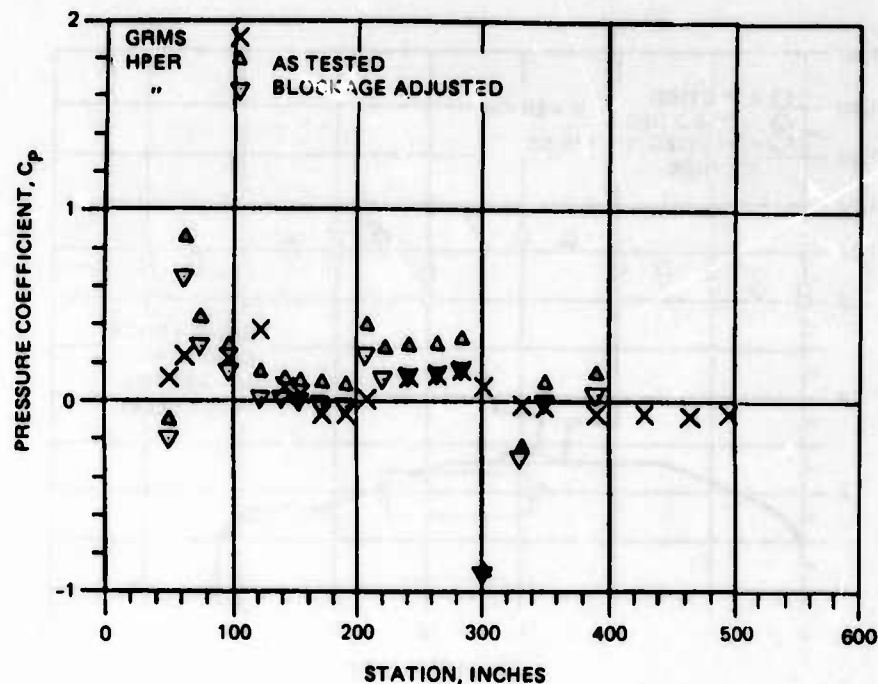
Figure 68. Effect of HPER Blockage Correction on
YAH-64 GRMS/HPER Pressure along
Waterline 130.

The analytical correction to the tunnel dynamic pressure was compared with
HPER static pressure measurements along the tunnel ceiling and was shown
to correlate well (Figure 69). The dynamic pressure increase varied from
approximately 5 percent over the model nose to 14 percent over the aft pylon
area behind the mast.

From the above argument, it is plain that large corrections in the tunnel
blockage allowance must be made to achieve correlation of the data from the
two tests. Unfortunately, this probably masks some other effects, most
notably differences in model setting and flow angularity. It is improbable
that the applied blockage factor is uniform, as applied, and consequently it
must be acknowledged that if it is reduced towards the front of the fuselage,
the correlation over the nose will be degraded. This reinforces the probabil-
ity that differences in flow angularity exist. A resolution of this question is
not possible with the data available and must await further testing and/or
numerical analysis.

87
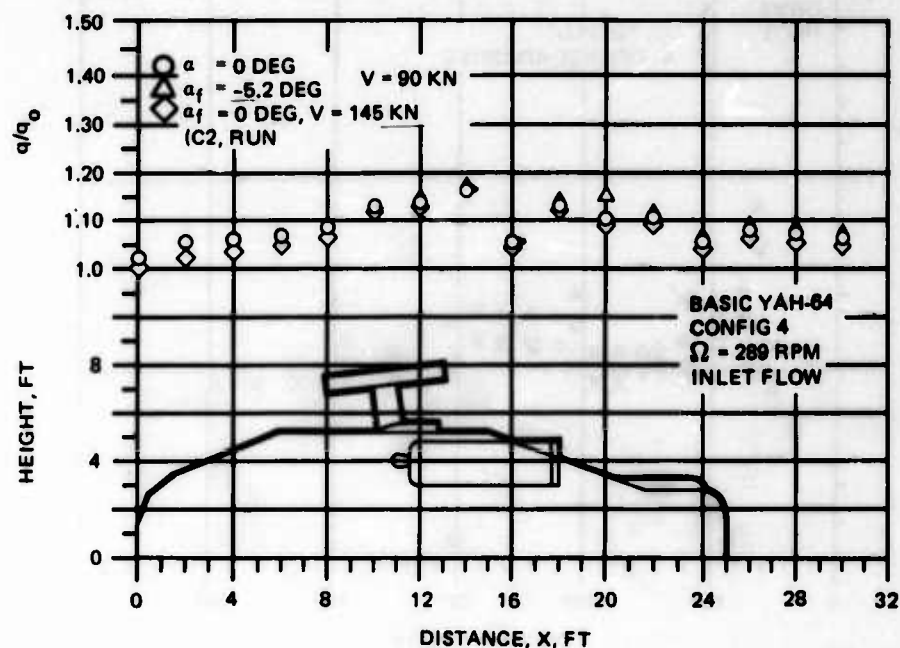
Figure 69. Measured Tunnel Blockage on
YAH-64 HPER.

EMPENNAGE TESTING

One of the parameters that is most important to a stabilator design effort is
the schedule of incidence required as a function of forward speed, especially
at low speeds. For the YAH-64, a maximum incidence of 45 degrees had
been selected during the preliminary design, based on the values Boeing
Vertol and Sikorsky had used in the UH-60A development program. There
was some question, however, as to whether the YAH-64 configuration was
similar enough to the other two helicopters to justify this decision. Testing
was conducted using the powered YAH-64 model to verify the maximum angle
and to determine the required incidence schedule.

Test Equipment

The model consisted of a YAH-64 body shell (30 percent of full scale) mounted
on the NASA/Army GRMS hardware. The rotor on this model had a diameter
of 10.3 feet, which is only 21 percent of the actual YAH-64 diameter. The
model scale was thus a hybrid: 0.30 for the airframe but only 0.21 for the
rotor. This situation required two different setups for the stabilator evalua-
tion: one corresponding to the 0.21 scale for low forward speeds where the

88

rotor wake is expected to dominate the stabilator flow field, and one corresponding to the 0.30 scale for high forward speeds where the wing and fuselage wakes are expected to dominate. The geometry of these two configurations is shown in Figure 70. The model had fans in the nacelles so that realistic mass flows in the inlet and exhaust systems could be simulated.

All wake surveys were done with a gimbal-mounted probe, which pointed into the local flow. The probe mount was attached to the model support sting so that downwash and sidewash angles were measured with respect to the body axis system of the model. The probe measured local velocity with a small, calibrated wind turbine, and for these tests it was mounted on a traversing mechanism with a travel of two feet. The probe was initially placed to survey along the horizontal lines representing the quarter-chord position of either the 0.21-scale or the 0.30-scale stabilator. Subsequent remounting of the probe allowed surveys to be made over most of the empennage region at three heights above the 0.30-stabilator quarter-chord.

The 14- by 20-foot V/STOL test section can be run either as a closed section or as an open section with the side walls and ceiling removed. In either case the rotor is approximately one diameter above the floor, high enough to minimize ground effects. For these flow surveys the open test section was used for low speeds between 25 and 60 knots and the closed section for the 40- to 120-knot range.

Following the flow surveys made with the stabilators off, stabilator-on runs were made to determine the stabilator lift in the combined flowfields of the rotor and airframe. The 0.21-scale stabilator was mounted above the tail boom, as shown in Figure 70. The 0.30-scale stabilator was mounted on the empennage balance system of the GRMS model.

Test Conditions

Five types of tests were conducted:

- Flow surveys along the stabilator quarter-chord with the rotor on and empennage off

- Flow surveys in the empennage region with the rotor on and empennage off

- Flow surveys in the empennage region with the rotor off and empennage off

- Low-speed trim measurements with the rotor on and 0.21-scale stabilator on

89
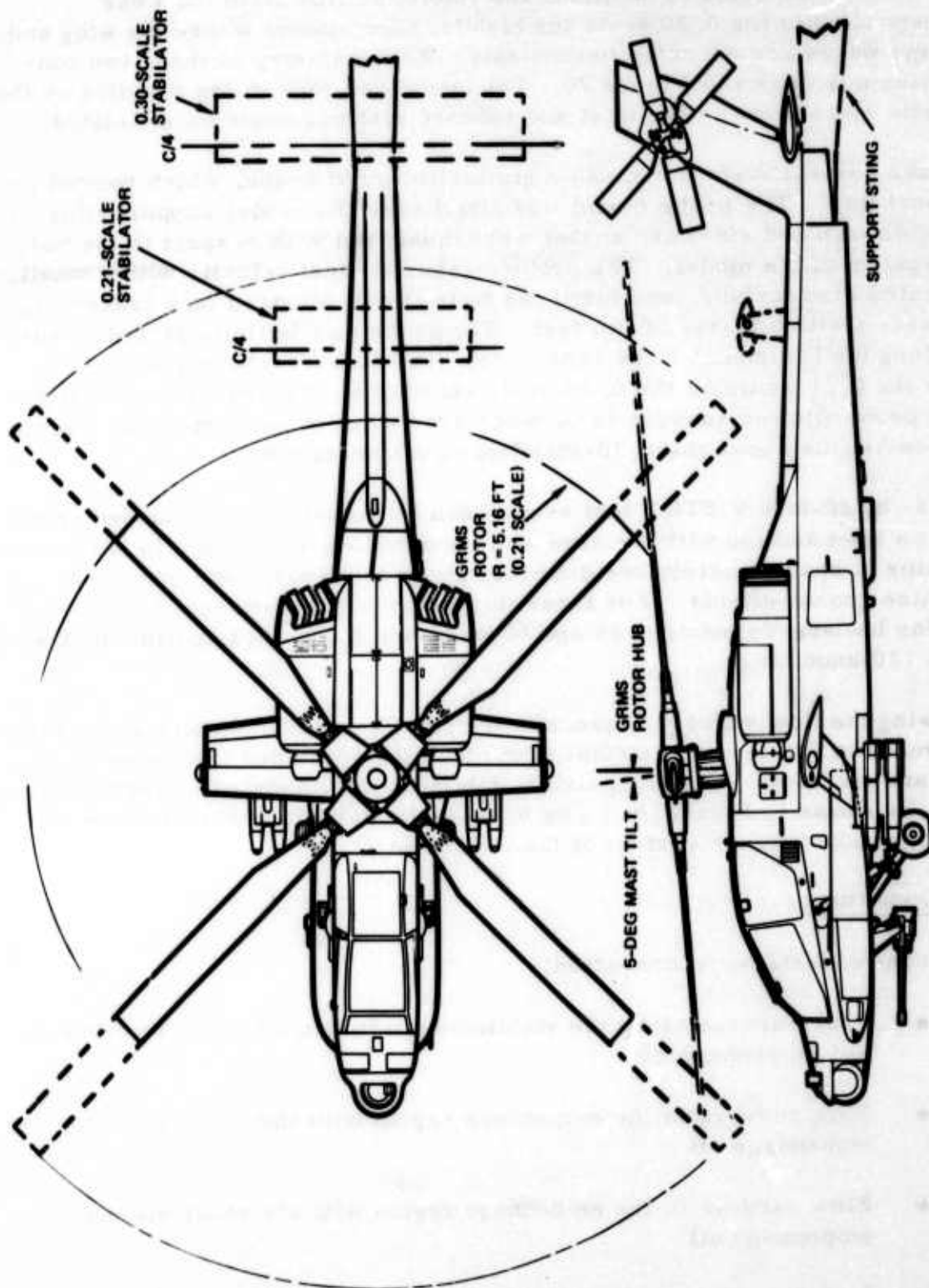
Figure 70. Model Configuration.

0.30-SCALE STABILATOR

C/4

0.21-SCALE STABILATOR

C/4

GRMS ROTOR
R = 5.16 FT
(0.21 SCALE)

GRMS ROTOR HUB

5-DEG MAST TILT

SUPPORT STING

- High-speed stability measurements with the rotor on and 0.30-scale stabilator on

The test conditions were different for each.

Flow surveys along stabilator quarter-chord. These surveys were made with full-scale tip speeds but with a slightly low rotor disc loading of 7 pounds per square foot, which corresponds to a gross weight of about 12,700 pounds. The maximum disc loading for these tests was limited by the capability of the rotor balance system, which had originally been designed for a smaller rotor. Collective pitch was used to maintain a constant rotor thrust, and cyclic pitch was used to trim the rotor tip path plane perpendicular to the rotor shaft, which is a good representation of the actual flight condition of the YAH-64.

The mounting of the flow survey probe limited the test points to model buttlines between -10 and +14 inches, or between -33.3 and +46.7 inches full scale. This compares to semi-spans of 64 and 84 inches for the proposed 33- and 42-square foot stabilators respectively.

Data were taken at tunnel speeds from 25 to 120 knots and fuselage pitch angles from 0 to 10 degrees. (A 5-degree forward tilt of the rotor shaft made the shaft pitch angle range from -5 to +5 degrees.) The actual angle of attack of the model was corrected for wind tunnel wall effects. The closed test section caused the angles of attack to be higher than the pitch attitude, but the open test section caused them to be lower. The test conditions for the flow surveys made at the stabilator positions are listed in Table 3.

Flow survey at empennage: rotor on. For these tests the flow survey rig was located at the same fuselage station as the 0.30-scale stabilator quarter-chord, but at three waterlines above it going up to waterline 62.2 (which compares to 72.6 for the top of the vertical stabilator). Again, the model buttline spread was from -10 to +14 inches or from -33.3 to +46.7 inches full scale. This survey was done for only one test condition, 120 knots and a 0-degree pitch attitude.

Flow survey at empennage: rotor off. The GRMS rotor blades were removed, but the GRMS rotor hub was left on and rotated at the normal rotor speed. The test conditions and the region of the survey were the same as with the rotor blades on.

TABLE 3. TEST CONDITIONS FOR FLOW SURVEYS AT STABILATOR POSITION

Run No.	Tunnel Configuration	Stabilator Position	Fuselage Pitch Attitude, deg	Tunnel Speed, kn
55	Closed	0.21	0	40
56	Closed	0.21	0	50
57	Closed	0.21	0	60
58	Closed	0.21	0	80
60	Open	0.21	0	30
61	Open	0.21	0	25
62	Open	0.21	0	40
63	Open	0.21	0	50
64	Open	0.21	0	60
65	Open	0.21	10	25
66	Open	0.21	10	30
67	Open	0.21	10	40
68	Open	0.21	10	50
69	Open	0.21	10	60
70	Closed	0.30	0	40
71	Closed	0.30	0	50
72	Closed	0.30	0	60
73	Closed	0.30	0	80
74	Closed	0.30	0	100
75	Closed	0.30	0	120
76	Closed	0.30	5	80
77	Closed	0.30	5	100
78	Closed	0.30	5	120

Low-speed trim measurements. The 0.21-scale stabilator was installed on the tailboom, as shown in Figure 70. Runs were made with stabilator incidences of 30, 40, and 45 degrees at 30, 40, and 50 knots. For these tests, the fuselage pitch attitude was 0 degrees.

High-speed stability measurements. The 0.30-scale stabilator was mounted on the GRMS empennage balance. The tunnel speed was 120 knots, and the initial fuselage pitch attitude was 6.5 degrees. With the rotor trimmed for a disc loading of 7 pounds per square foot and no flapping with respect to the shaft, the pitch attitude was reduced while loading collective and cyclic pitch fixed at the initial values. This procedure was followed with the stabilator incidence set at both plus and minus 2.5 degrees. The procedure was repeated with only the right-hand stabilator panel installed, and then with no stabilator at all.

Results

Flow surveys along stabilator quarter-chord. The downwash and sidewash angles and the dynamic pressure ratios are plotted as functions of buttline position for the five basic test conditions (Figures 71 to 75). These results substantiated the design decision, which made 45 degrees the maximum stabilator incidence since no downwash values significantly higher were measured. Taken as a group, these plots show the strong asymmetrical characteristics of the rotor wake. It has been known for some time that at high speeds the downwash behind the advancing side of the rotor is greater than that behind the retreating side. The usual explanation is that the reverse flow region, which is producing a downward lift, reduces the downwash behind it. At low speeds the reverse flow region is hidden in the hub region, so it is surprising to see that this same trend is so prominent at low speeds. The explanation appears to be that the rotor wake is being shifted to the right by swirl traceable to induced effects from the tip and root votices and to the parasite drag torque of the hub itself. Evidence of this rightward shift is shown in wind tunnel tests done at Ohio State University and reported in Reference 9. The asymmetry in sidewash angle shown in Figures 71 to 75 indicates that at the stabilator position the flow is directed outward toward the edges of the rotor wake caused by rolling up the tip vortices.

9. Velkoff and Horak, ROTOR WAKE MEASUREMENTS AT VERY LOW ADVANCE RATIOS, Proceedings of the 35th Forum of the American Helicopter Society, 1979.

SYMB	RUN	TUNNEL SPEED, KN	α_f, DEG
O	55	40	2.5
□	56	50	1.8
△	57	60	1.4
▽	58	80	1.1

WAKE DOWNWASH ANGLE, DEG

WAKE SIDEWASH ANGLE, DEG

FLOW FROM RT

FLOW FROM LT

$\frac{q_{WAKE}}{q_{TUNNEL}}$

MODEL BUTTLINE POSITION, IN.
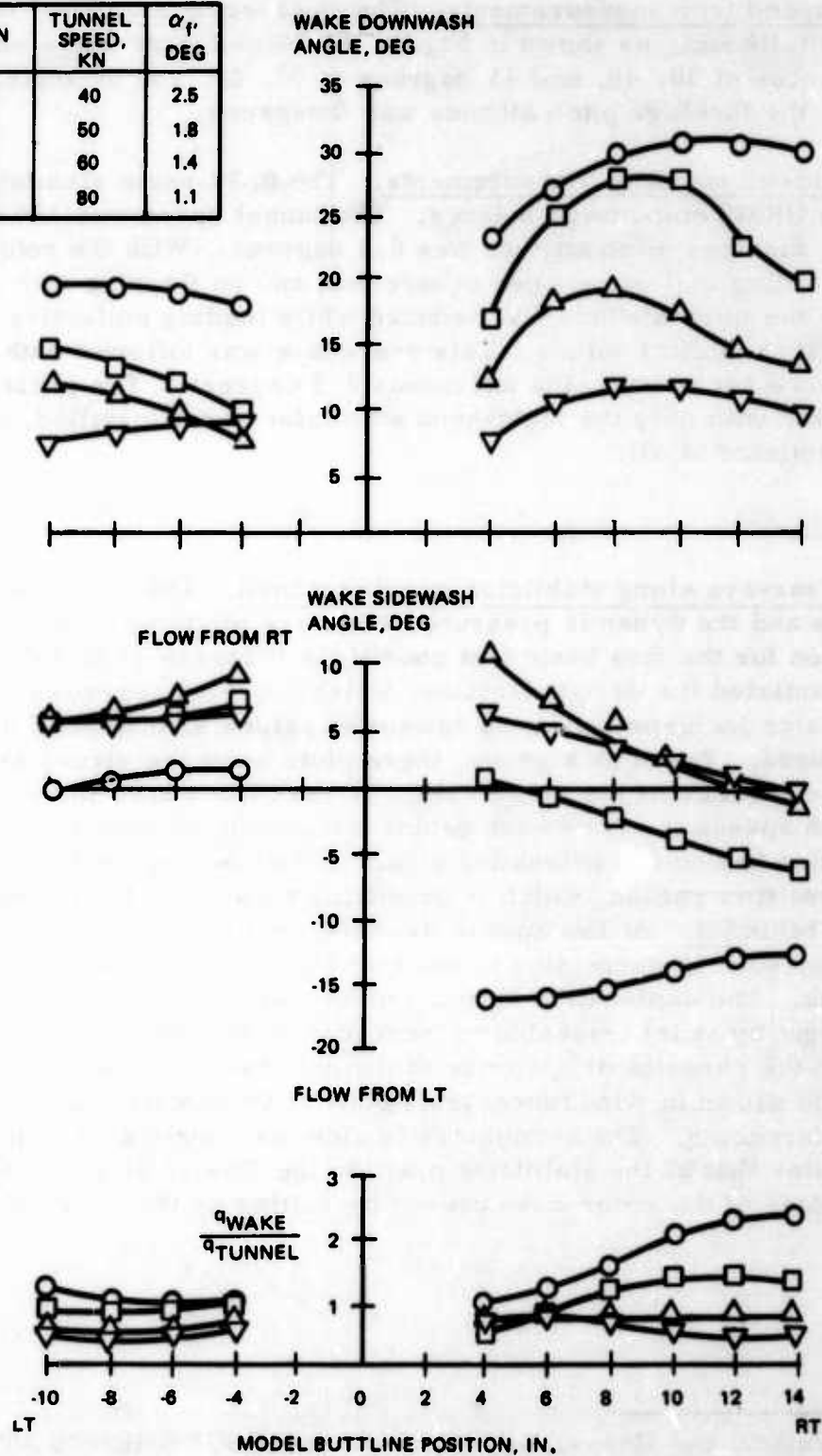
Figure 71. Flow Conditions: 0.21-scale Stabilator, Closed Test Section, 0-degree Pitch Attitude.

94

Figure 72. Flow Conditions: 0.21-scale Stabilator, Open Test Section, 0-degree Pitch Attitude.
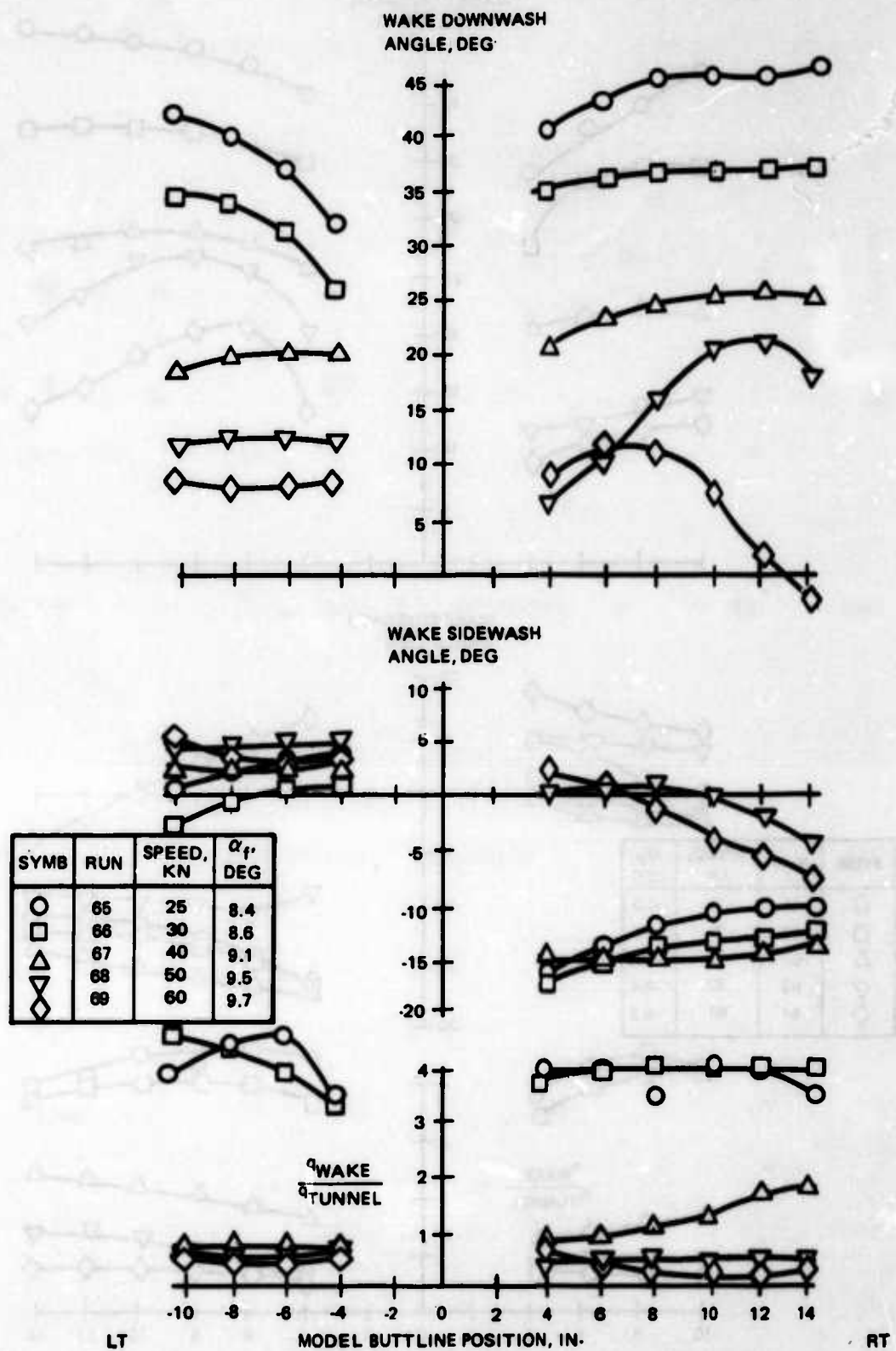
Figure 73. Flow Conditions: 0.21-scale Stabilator, Open Test Section, 10-degree Pitch Attitude.

SYMB	RUN	TUNNEL SPEED, KN	α_f, DEG
○	70	40	2.5
□	71	50	1.9
△	72	60	1.1
▽	73	80	0.6
◇	74	100	0.5
◇	75	120	0.4

WAKE DOWNWASH ANGLE, DEG

WAKE SIDEWASH ANGLE, DEG

$\dfrac{q_{WAKE}}{q_{TUNNEL}}$

LT

MODEL BUTTLINE POSITION, IN:

RT
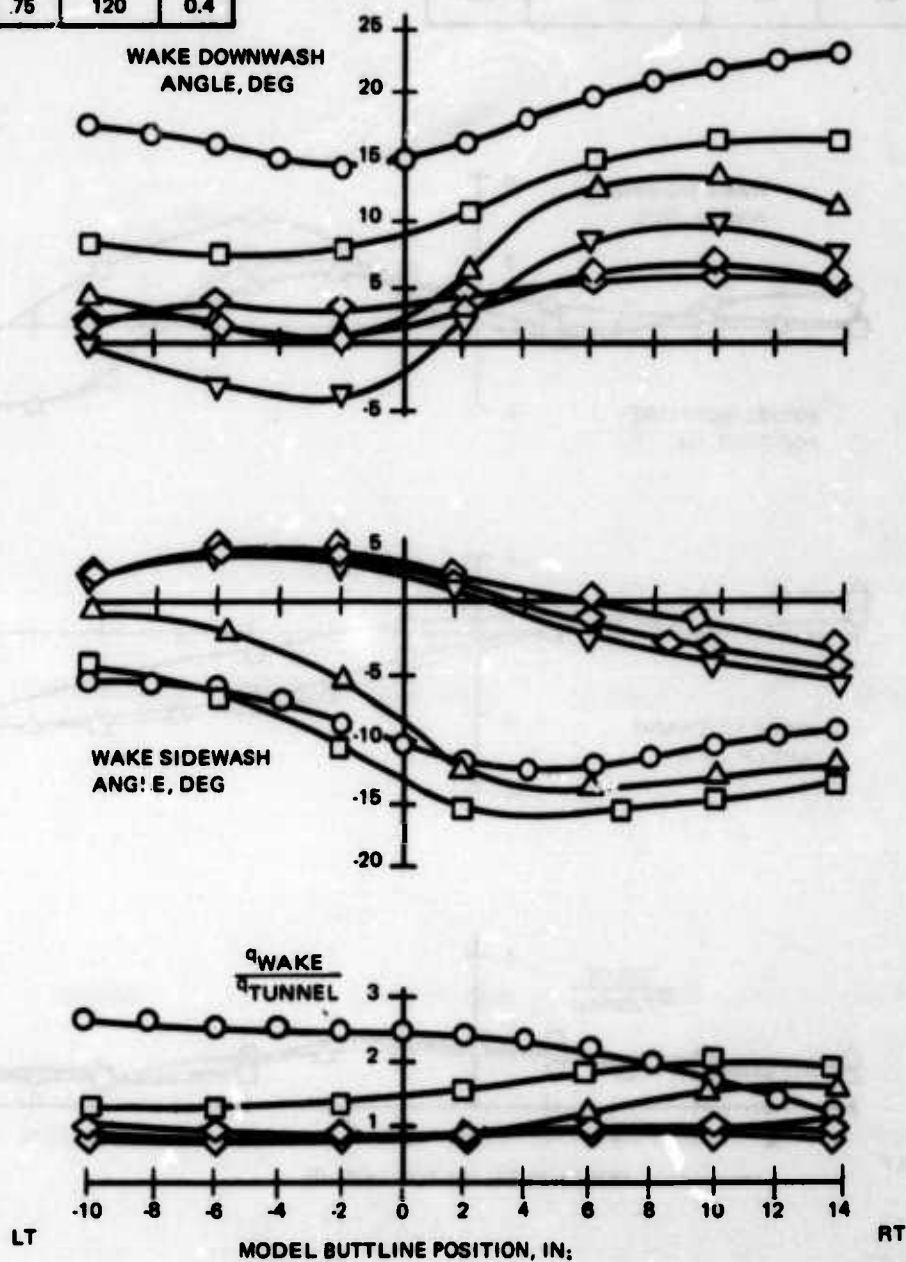
Figure 74. Flow Conditions: 0.30-scale Stabilator, Closed Test Section, 0-degree Pitch Attitude.

97

SYMB	RUN	TUNNEL SPEED, KN	α_f, DEG
○	76	80	6.0
□	77	100	5.8
△	78	120	5.2

WAKE DOWNWASH ANGLE, DEG

MODEL BUTTLINE POSITION, IN.

WAKE SIDEWASH ANGLE, DEG

$\dfrac{q_{WAKE}}{q_{TUNNEL}}$

LT   MODEL BUTTLINE POSITION, IN.   RT
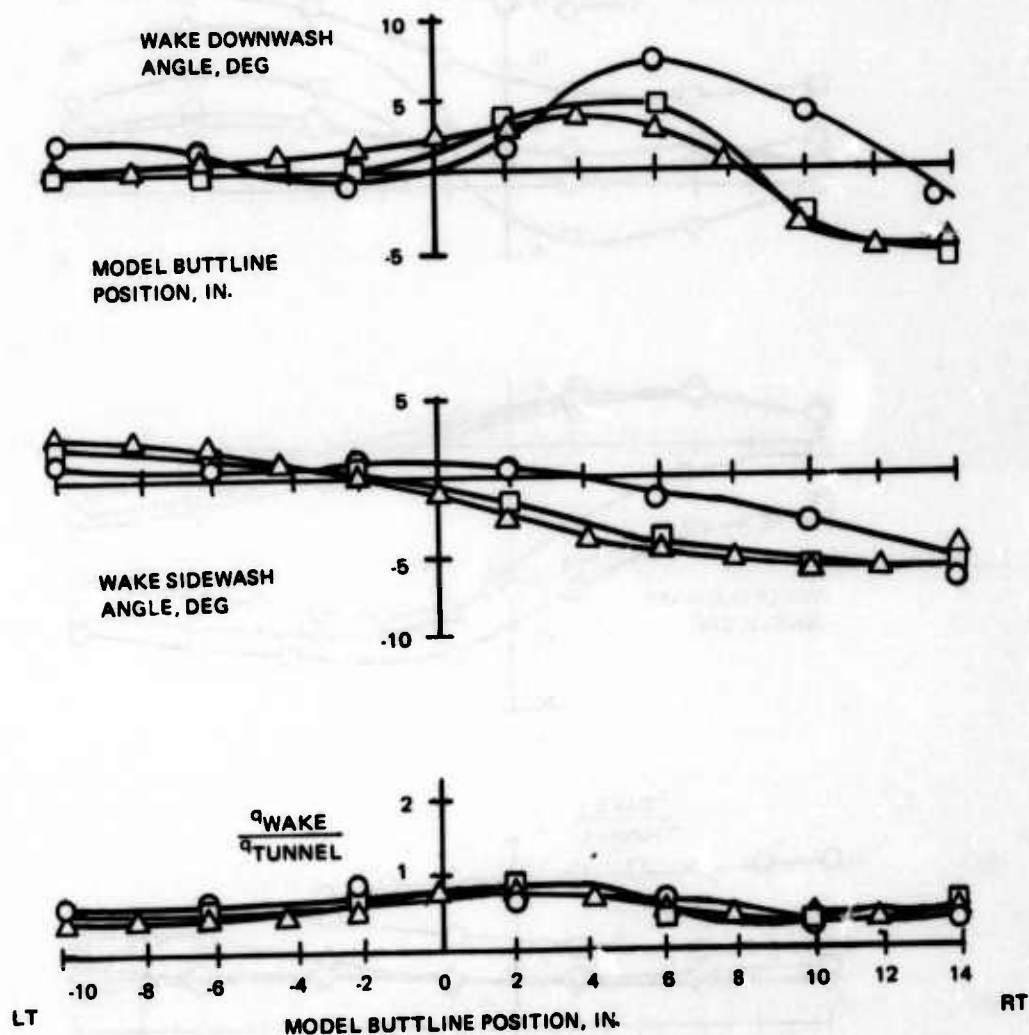
Figure 75.   Flow Conditions: 0.30-scale Stabilator, Closed Test Section, 5-degree Pitch Attitude.

98

The open test section is more representative of actual flight but is usable only up to about 60 knots due to an unstable flow condition that develops at higher speeds, where the closed section must be used. The comparison of downwash angles measured with the two different test section configurations (Figure 76) shows that there is no significant difference with respect to flow conditions at speeds as low as 40 knots.

The 0.21-scale stabilator position was chosen to be in the correct geometric relationship with the main rotor for low-speed testing. The 0.30-scale stabilator position was lower and further aft. Figure 77 shows that the down- wash angle at this position is somewhat less than at the 0.21-scale position for the same test conditions. Figure 78 presents another comparison from which the conclusion may be drawn that at low speeds (25 and 30 knots) the wake is big enough that different fuselage angles do not significantly affect the results. At higher speeds the proximity of the wake to the stabilator is evidently a function of fuselage angle, with higher angles passing the wake further above the stabilator position and thus having less effect on the down- wash at that location.

At very low speeds the wake effects should be expected to be similar to those in hover, where the dynamic pressure in the fully developed wake is equal to the rotor disc loading. This is illustrated in Figure 79, which shows this relationship to be essentially true for the measurements made at 25 knots and helps to explain the very high ratios with respect to tunnel dynamic pressure shown for 25 and 30 knots in Figure 72. At higher speeds the dynamic pres- sure ratio is affected both by the tunnel dynamic pressure and by momentum losses due to drag.

It has been generally accepted that the velocity induced by the rotor wake is parallel to the rotor thrust vector and is, therefore, essentially vertical. An analysis of the present data shows that in some conditions, however, the wake also induces an appreciable horizontal velocity. The results of the analysis of the flow conditions at the 0.21-scale stabilator position are pre- sented in Figure 80 for measurements made at Buttlines 14 and -10, which were chosen because they should be subjected to the smallest fuselage inter- ference effects. The analysis shows that the vertical component of induced velocity is one to two times the momentum value of the induced velocity at the rotor. These values are consistent with measurements made by other investi- gators. At low speeds the rotor is also inducing an appreciable aft horizontal velocity, which has not been previously reported. At speeds above about 50 knots, the apparent horizontally induced velocity reverses and becomes pointed forward. This is primarily the result of momentum losses due to the drag of airframe components ahead of the survey location. There is an indica- tion, however, in the very low measured dynamic pressure ratios at 60 knots shown in Figure 73, that for some conditions the rotor wake induces an appreciable counterflow, which adds to the momentum loss effect.

99
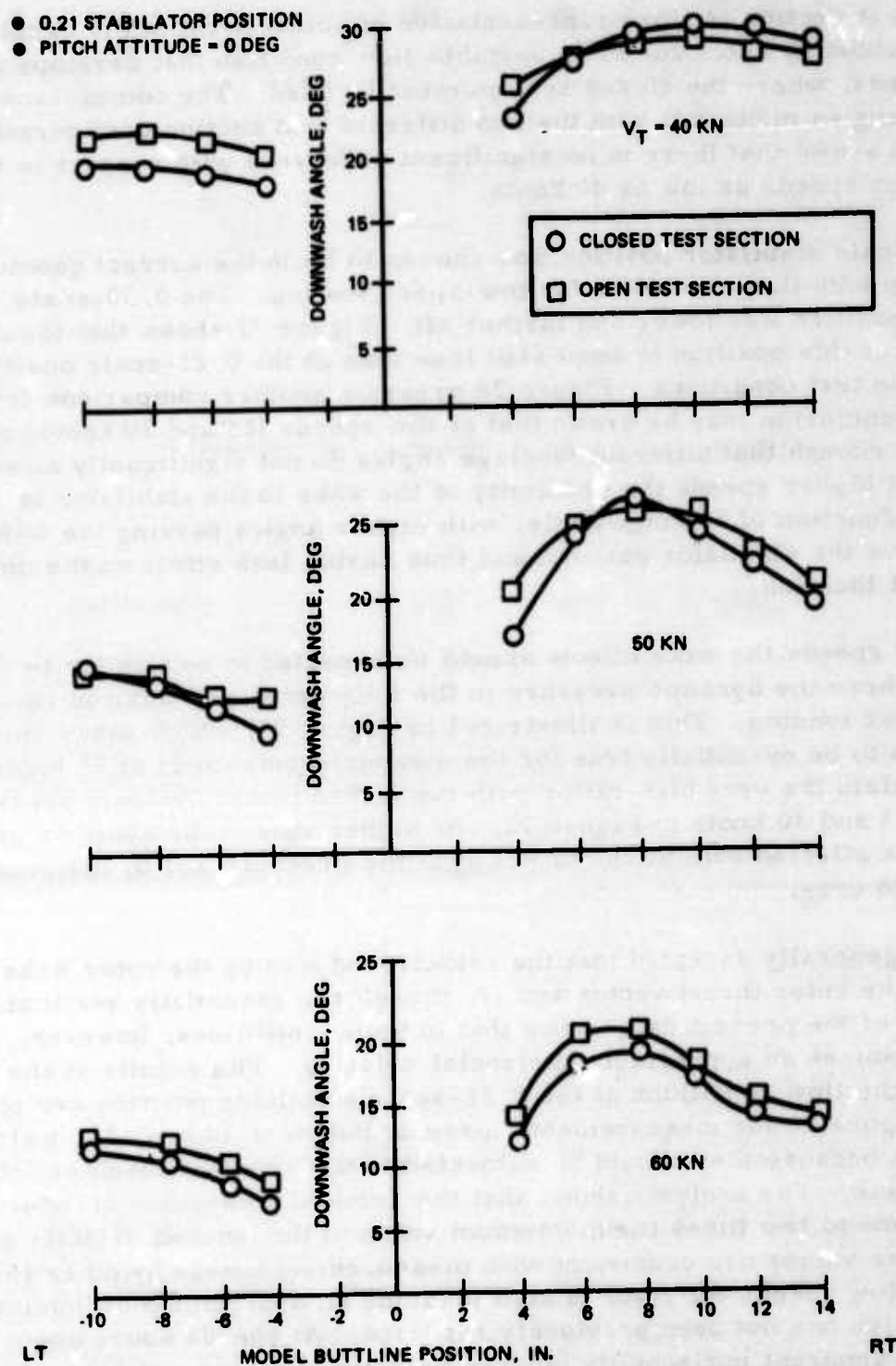
Figure 76. Effect of Test Section Configuration
on Downwash Angle.
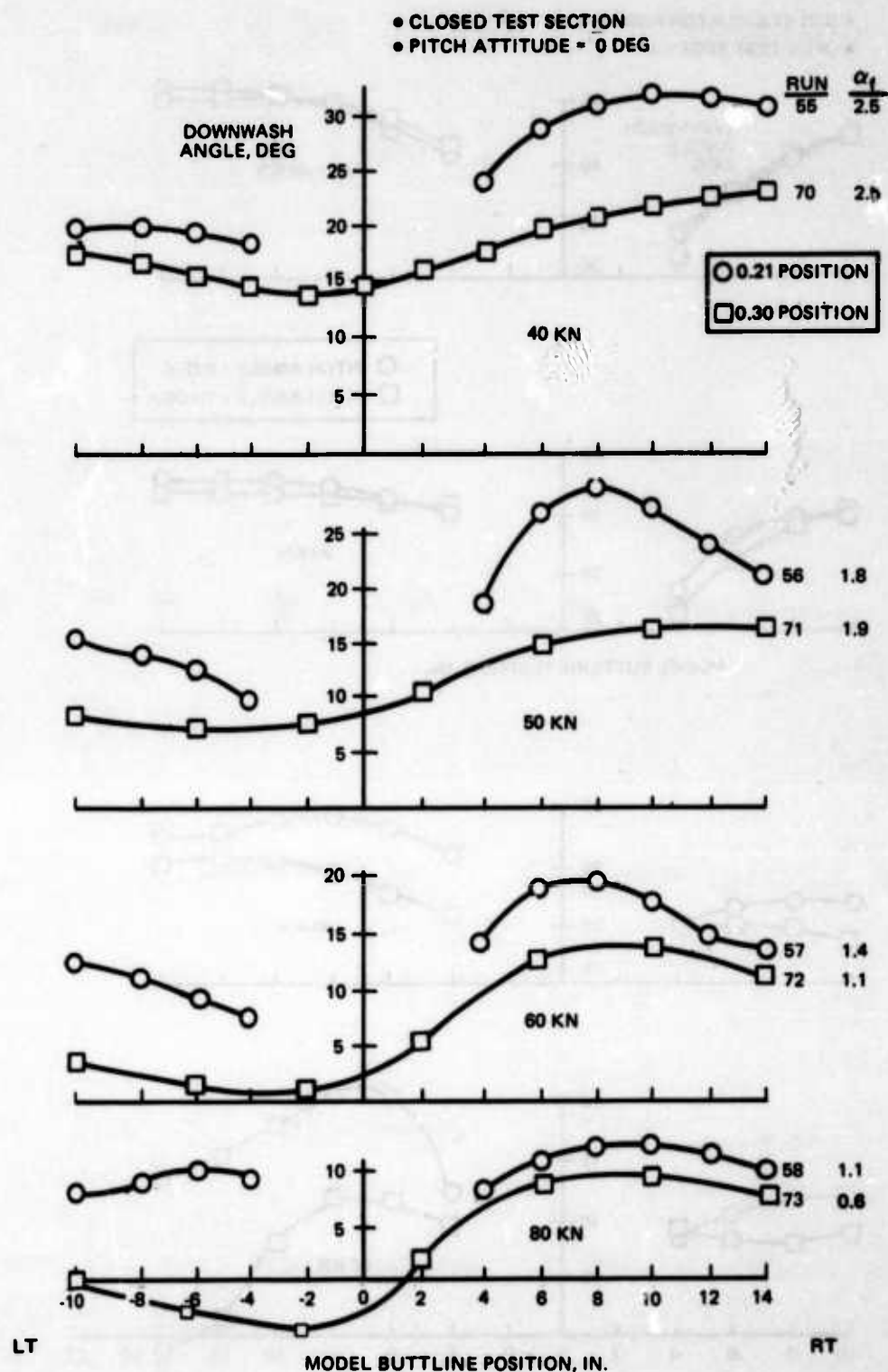
Figure 77.   Effect of Stabilator Position on
Downwash Angle.

101
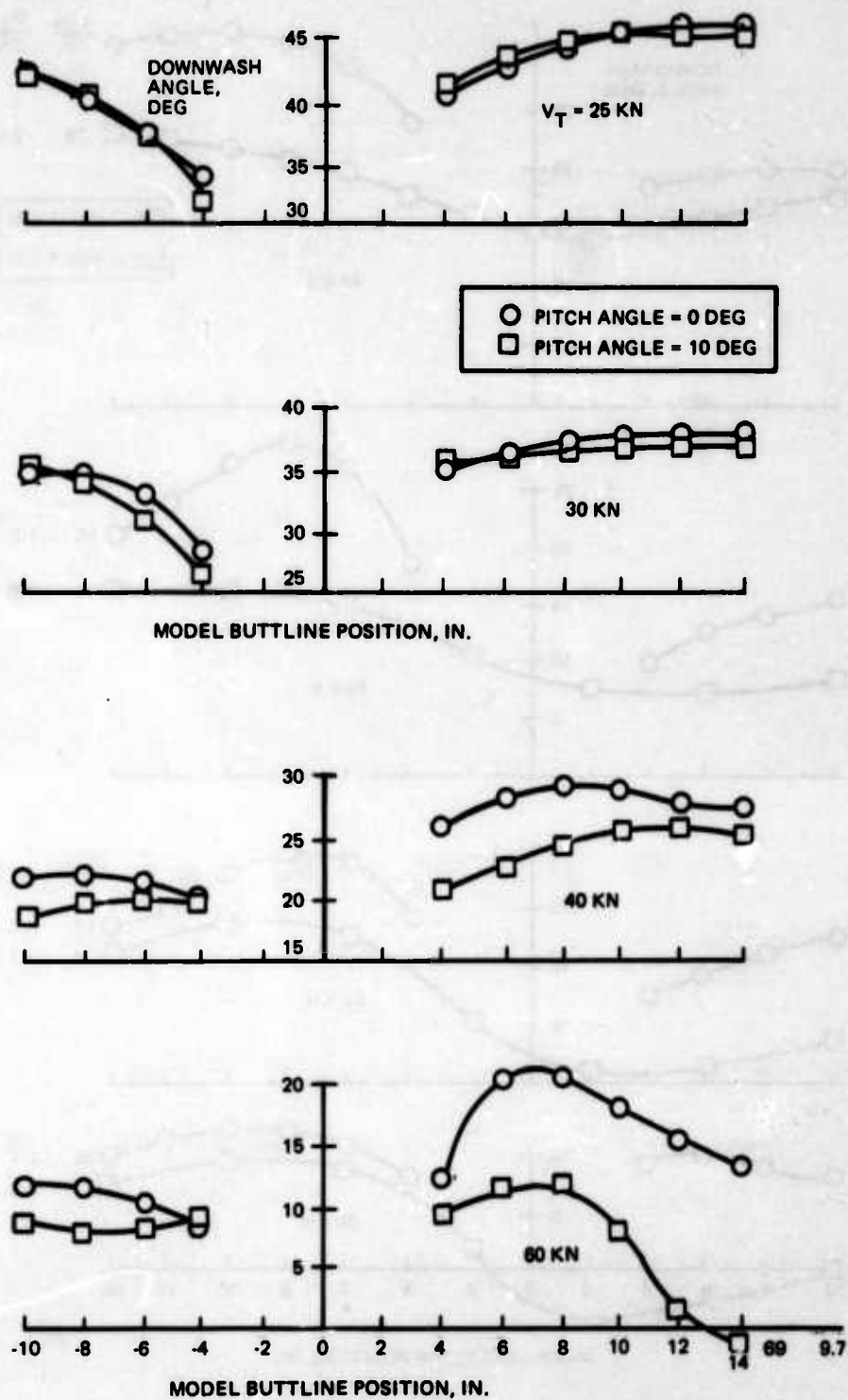
Figure 78. Effect of Fuselage Pitch Angle
on Downwash Angle.

102
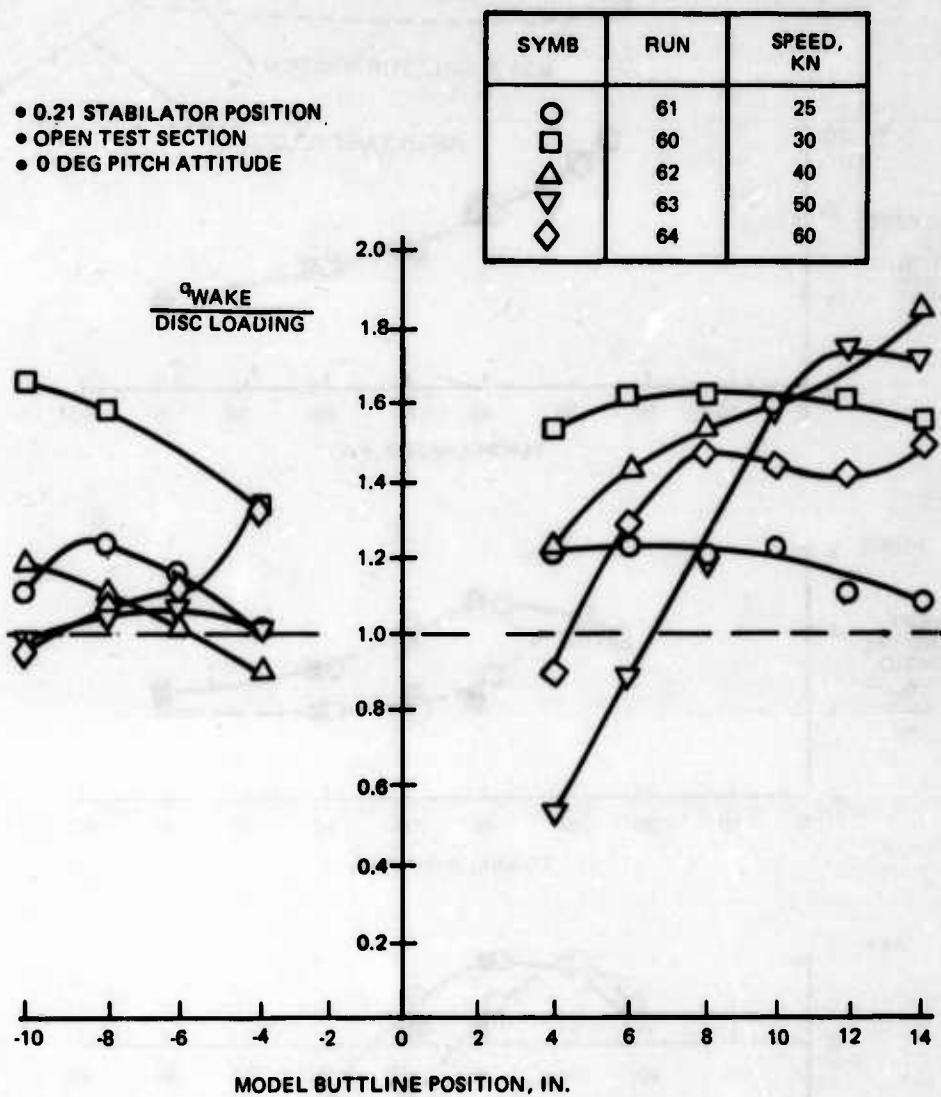
Figure 79. Ratio of Dynamic Pressure
in Wake to Disc Loading.

103
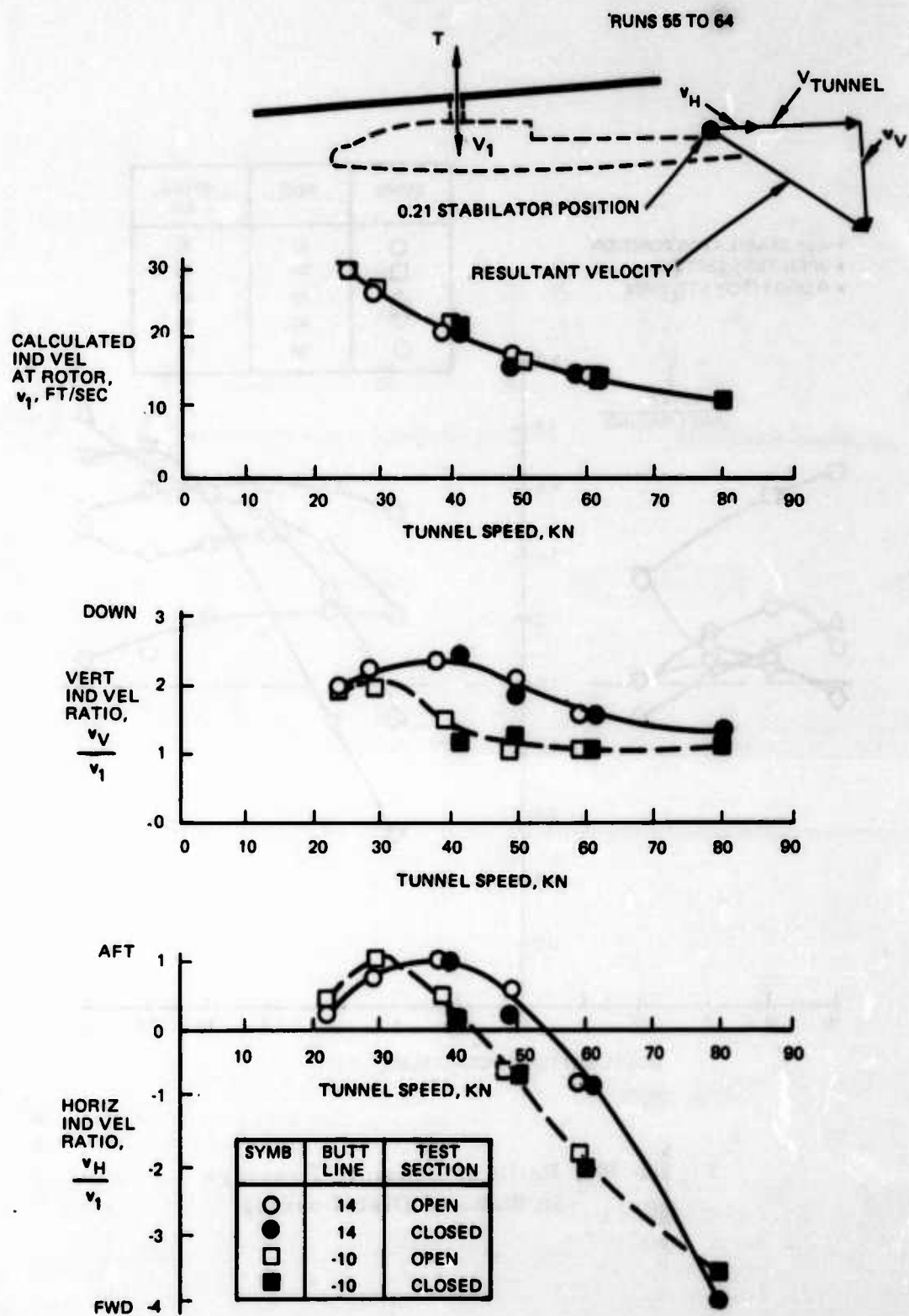
Figure 80. Vertical and Horizontal Induced Velocities.

Flow surveys above the 0.30-scale stabilator position. Following surveys along the 0.30-scale stabilator position, a series of 120-knot, rotor-on runs at higher locations was made (Figure 81). It may be seen that for the four locations surveyed, the downwash and sidewash on the right side were about the same, but on the left side there was considerable variation. Evidence that this is not just data scatter is presented in Figure 82, which shows Runs 75 and 107, done under identical test conditions. An alternate presentation of the data is given in Figures 83 through 85 as three views of the vector field in the survey region. Figure 82 again illustrates the higher downwash on the right side than the left. Figure 84 indicates the source of a possible directional stability problem. The diverging streamlines at the lowest survey location will reduce the effectiveness of any vertical surface or tail rotor located in this region since yaw displacements will not be accompanied by the expected favorable change in angle of attack. The converging streamlines at the upper survey location, however, should result in enhanced effectiveness for any stabilizing device operating there.

Figure 85 is the rear view of the vector field, illustrating the conclusions drawn from the other two views. Although no attempt was made to measure the unsteady characteristics of the flow, it is not hard to conclude that if the steady components appear so chaotic, the unsteady components must be even more so. Taken together, the diverging streamlines in the lower part of the wake (Figure 84) and the large gradients of direction change (Figure 85) probably explain why most helicopters exhibit a slight heading wander in cruise flight. It also may explain why the Dutch Roll mode is usually less well damped than a theory based on straight flow assumptions would predict. The stabilizing convergent streamlines in the upper part of the wake probably explain why large tip plates on the T-tail of the YAH-64 improved the Dutch Roll stability by a much larger degree than could be predicted by analysis.

Figure 86 shows the rear view of the flowfield survey made with the wings removed to represent helicopters more conventional than the YAH-64. Compared to Figure 85, it may be concluded that the effect of the wings is small.

Flow survey without rotor blades. Figures 87 and 88 show the flow survey results with the GRMS blades off but with the GRMS hub on and rotating at full rotor speed. Although the overall vertical induced velocities are much decreased, as would be expected, there is still essentially as much lateral velocity as is shown in Figures 81 and 85. The conclusion is that it is the rotation of the rotor hub that produces the swirl in the wake. Unfortunately, no surveys were made with the hub nonrotating to verify this conclusion.

105
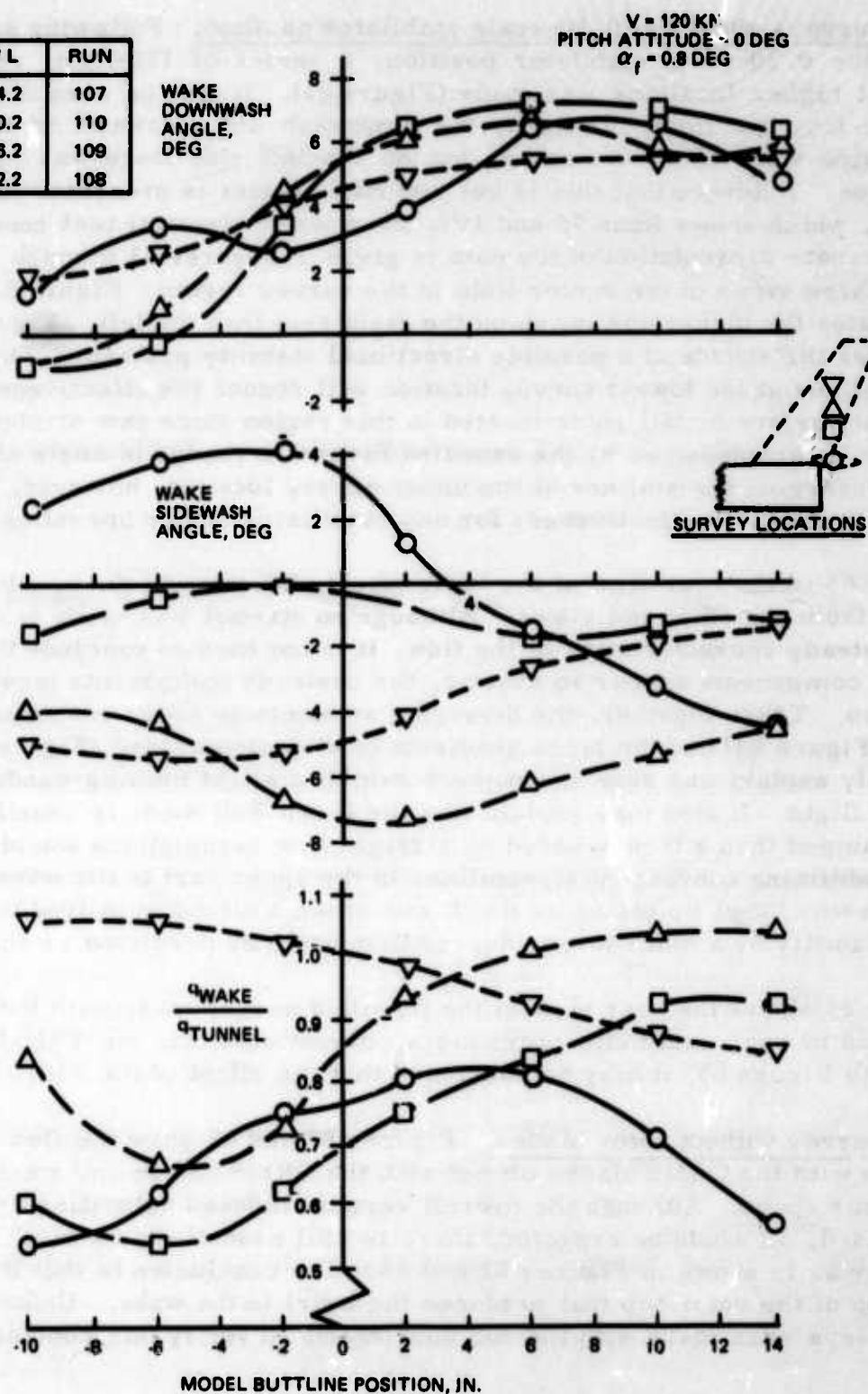
Figure 81. Flow Survey at Empennage, Rotor On,
Closed Test Section.

106
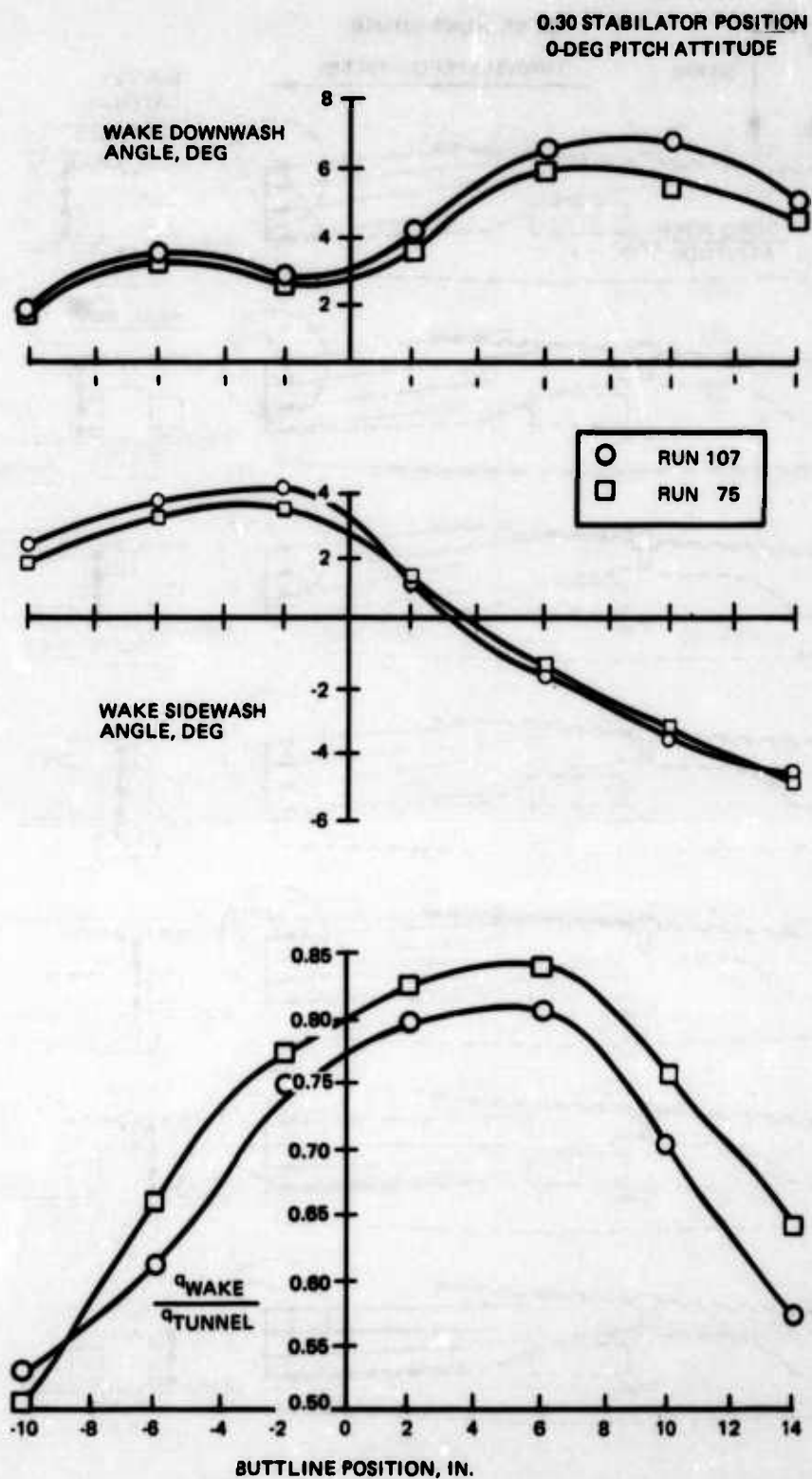
Figure 82. Repeatability Study at 120 Knots.
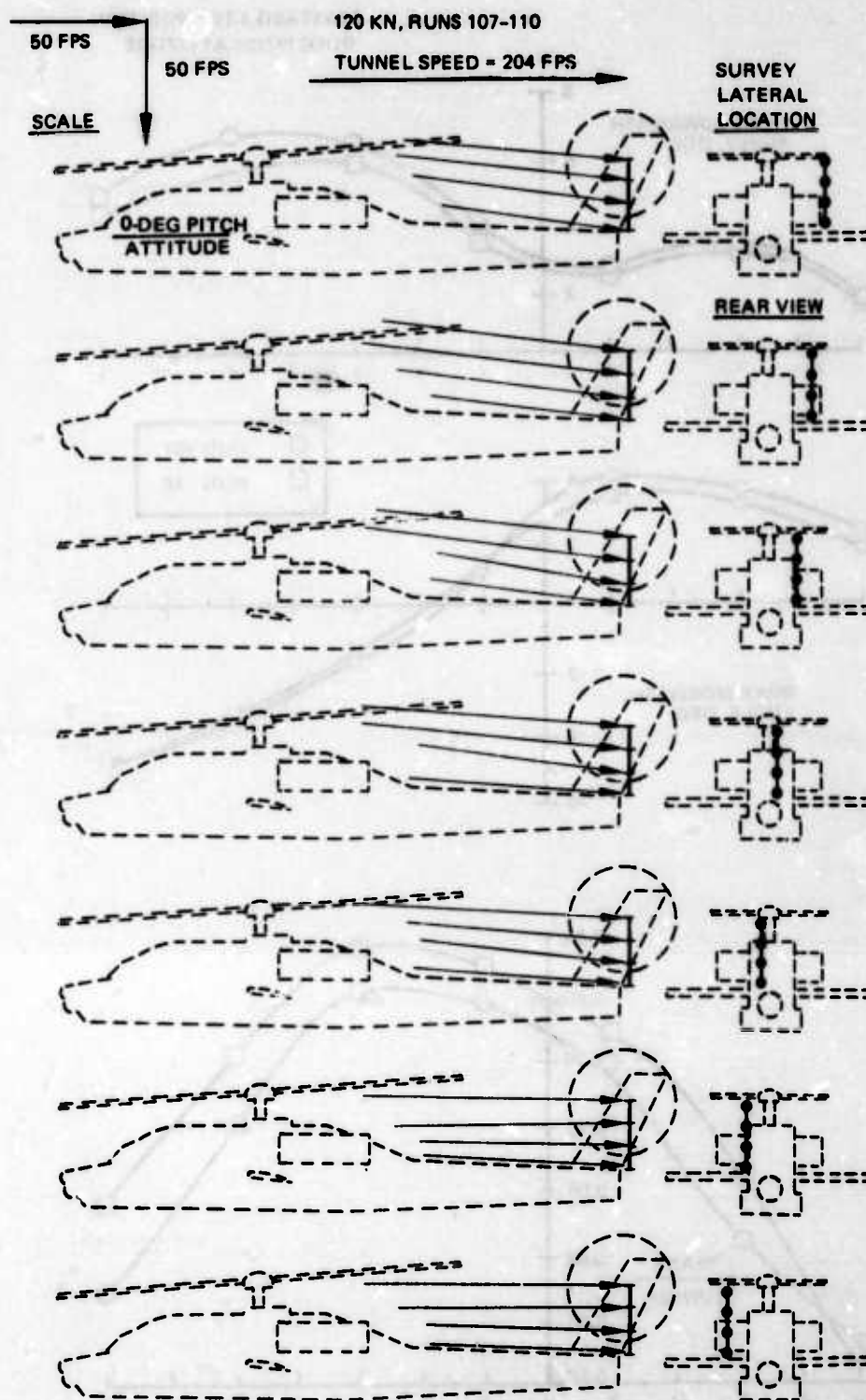
Figure 83. Side Views of Velocity Vectors.
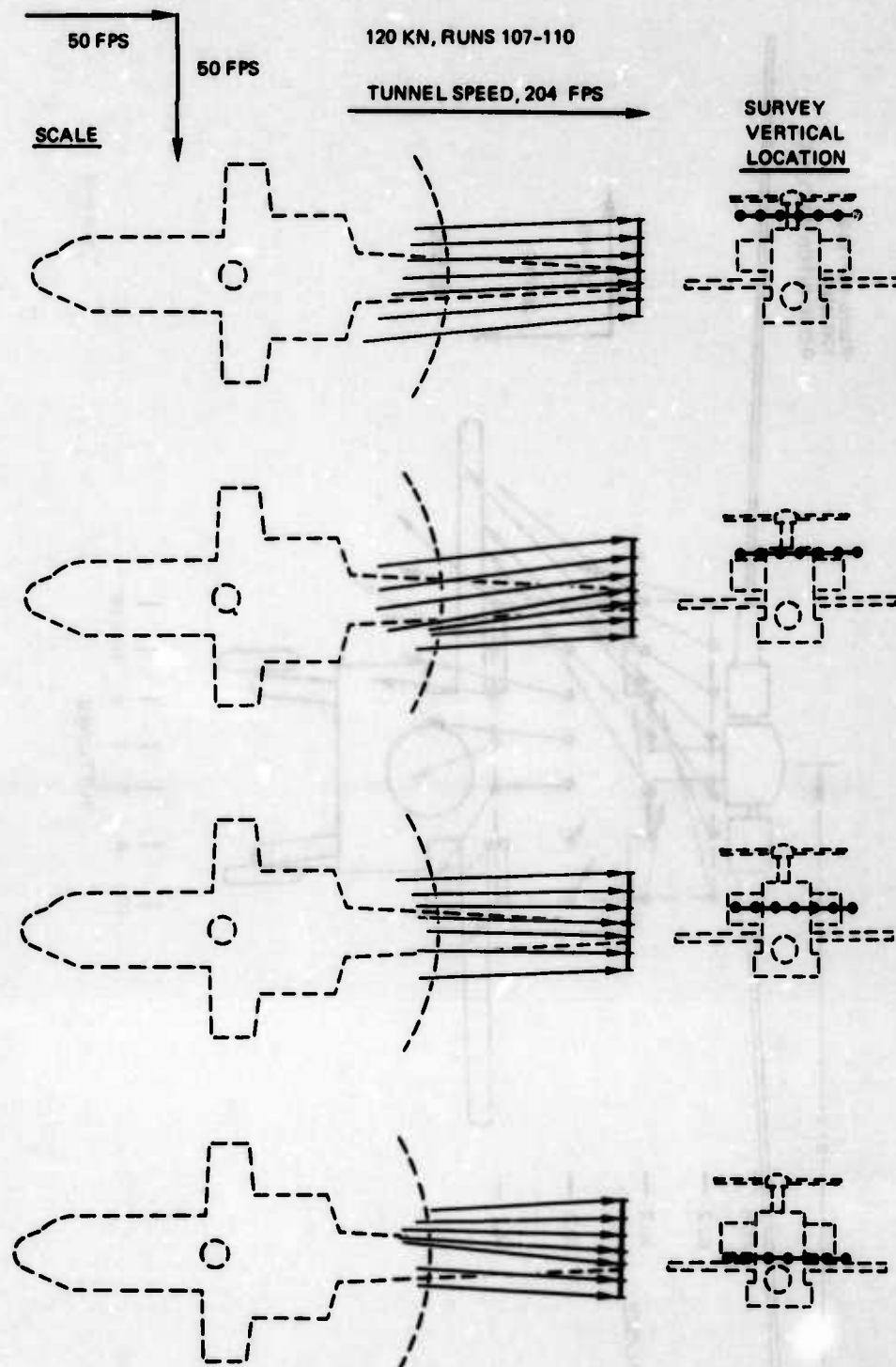
Figure 84. Top Views of Velocity Vectors.
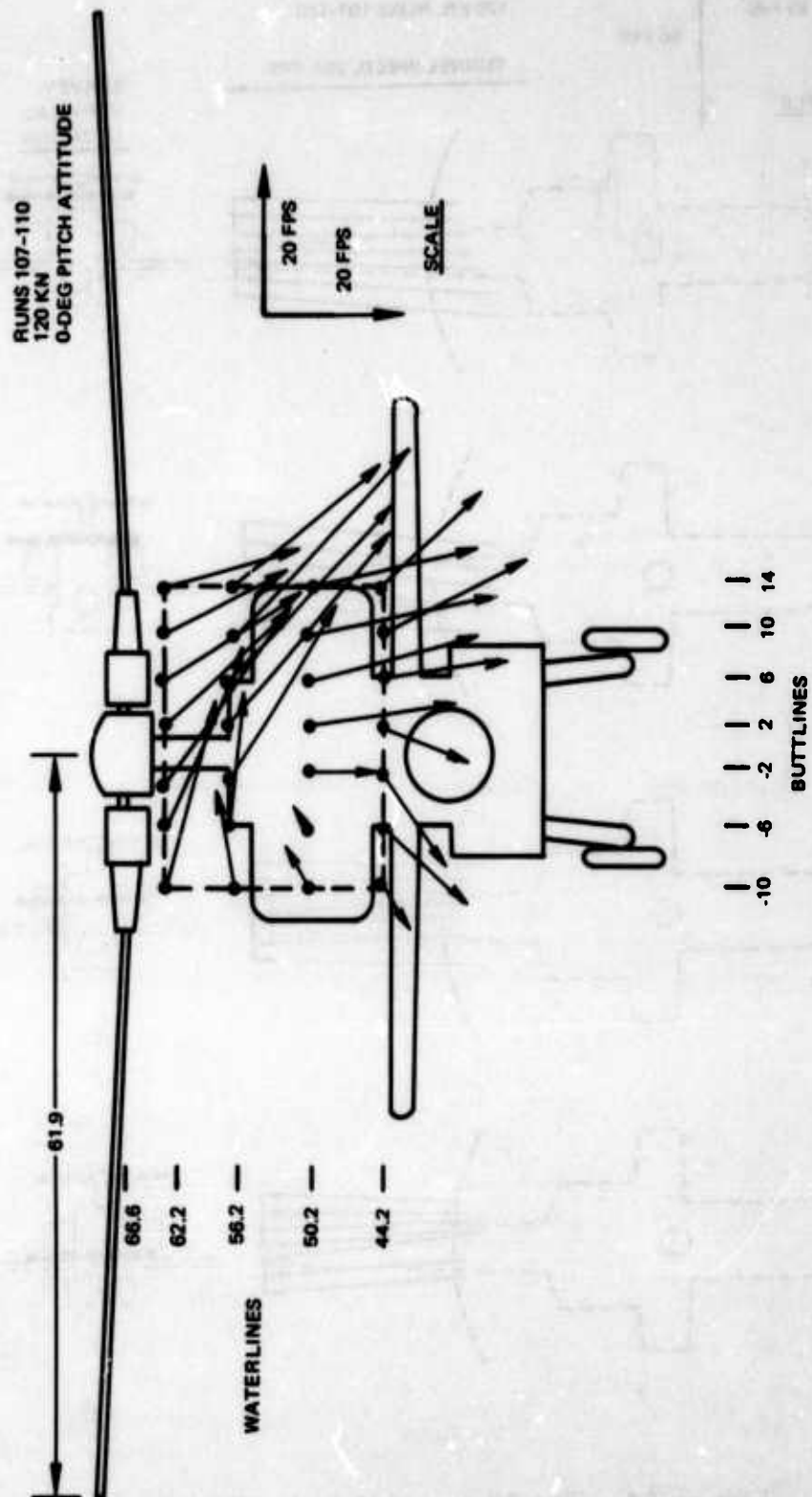
Figure 85. Rear View of Velocity Vectors, Rotor Blades and Wings On.

RUNS 114-117
120 KN
0-DEG PITCH ATTITUDE

20 FPS

20 FPS

SCALE
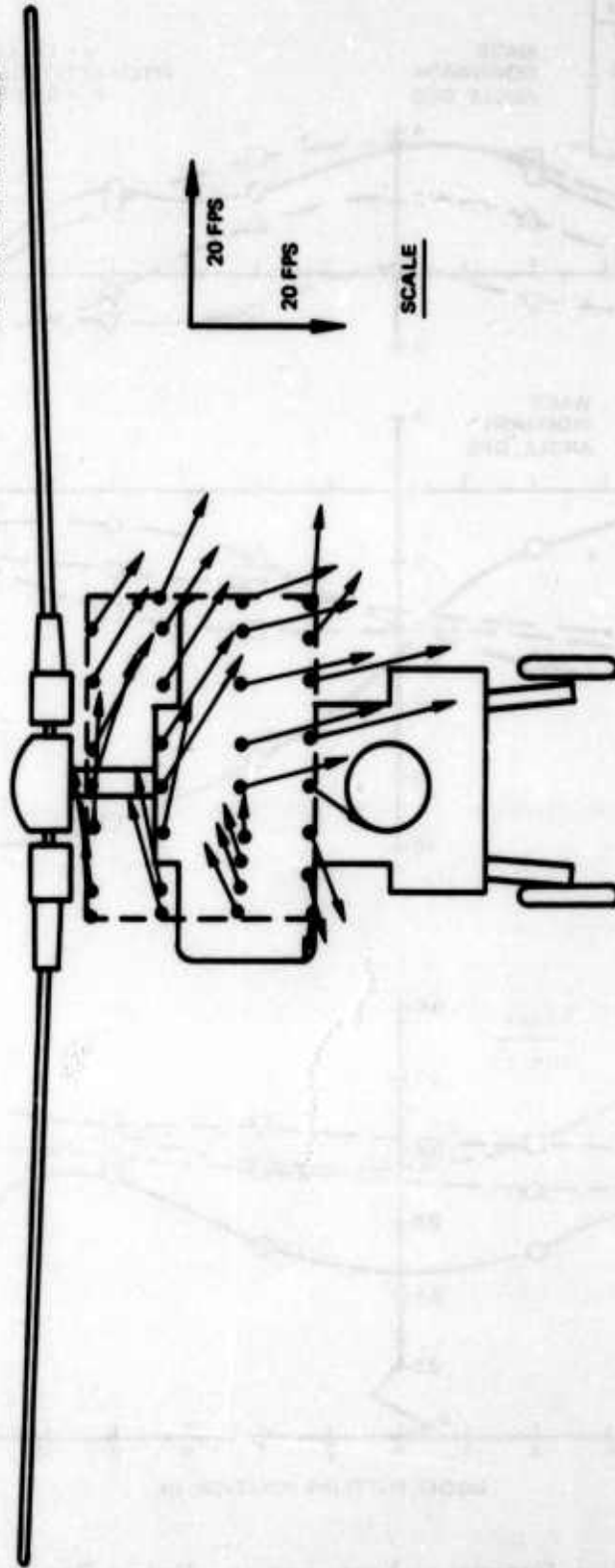
Figure 86. Rear View of Velocity Vectors, Wings Off.

111
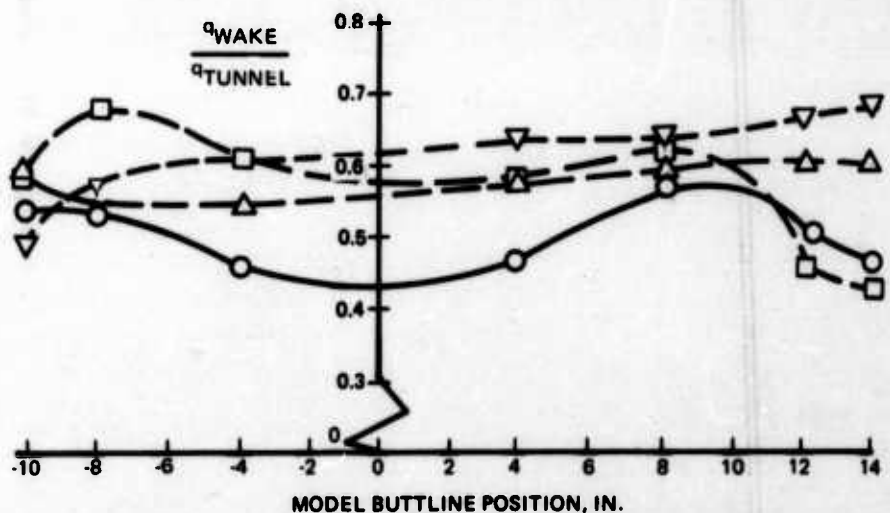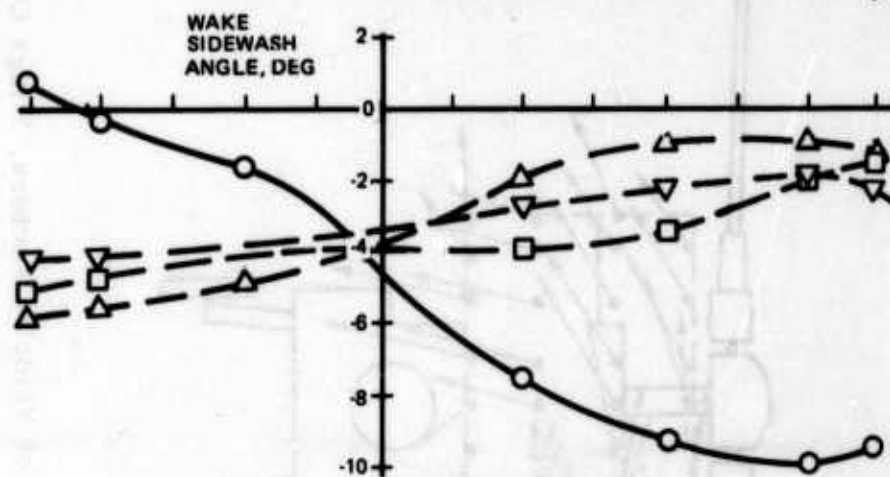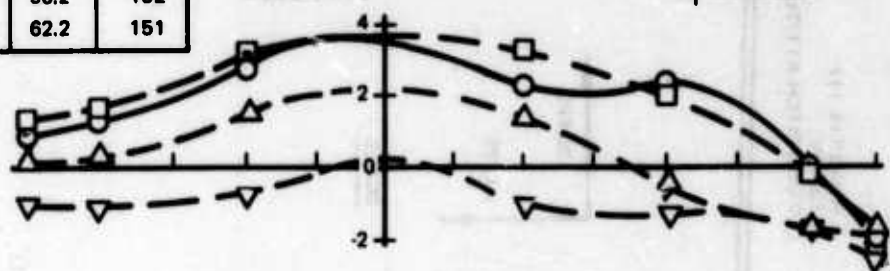
Figure 87.   Flow Survey at Empennage, Rotor Blades Off,
GRMS Rotor Hub Rotating at Normal Speed.

20 FPS

20 FPS
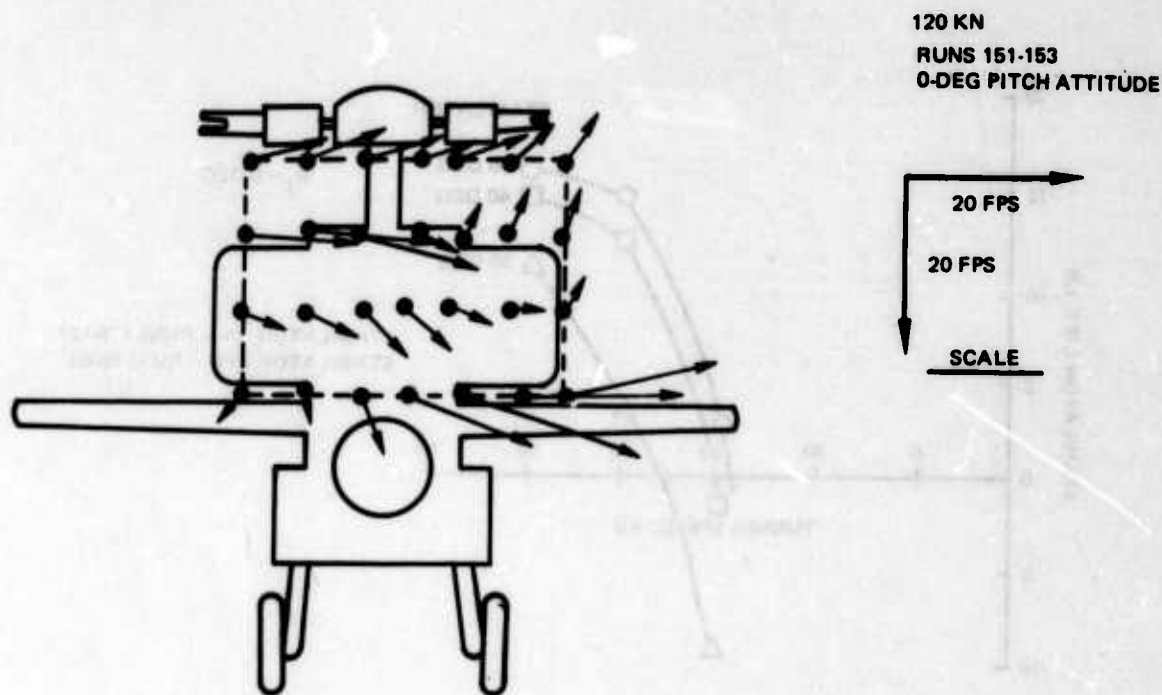
SCALE

Figure 88. Rear View of Velocity Vectors,
Rotor Blades Off, GRMS Hub
Rotating at Normal Speed.

Low-speed trim measurements. Low-speed tests with the 0.21-scale stabil-
ator at three (high) incidence angles yielded the results plotted in Figure 89.
The intersection of the test lines with zero stabilator lift is a first approxi-
mation of the required incidence schedule at low speeds.

High-speed stability measurements. Runs at 120 knots were made with the
0.30-scale stabilator in order to measure its effect on stability. Two values
of incidence and three combinations of right and left panels on and off were
used. The results in terms of stabilator lift and induced downwash angle are
shown in Figure 90. One of the objectives of this series of runs was to
establish whether the two stabilator panels differed in effectiveness because
of the different flow conditions on them as measured during the flow surveys.
The results show that the two panels have nearly the same effectiveness
since the slope with both panels is slightly greater than twice the slope with
the right panel only. The small variation from exactly twice the ratio can
be attributed to the decrease in effective aspect ratio when testing with one
panel.

113
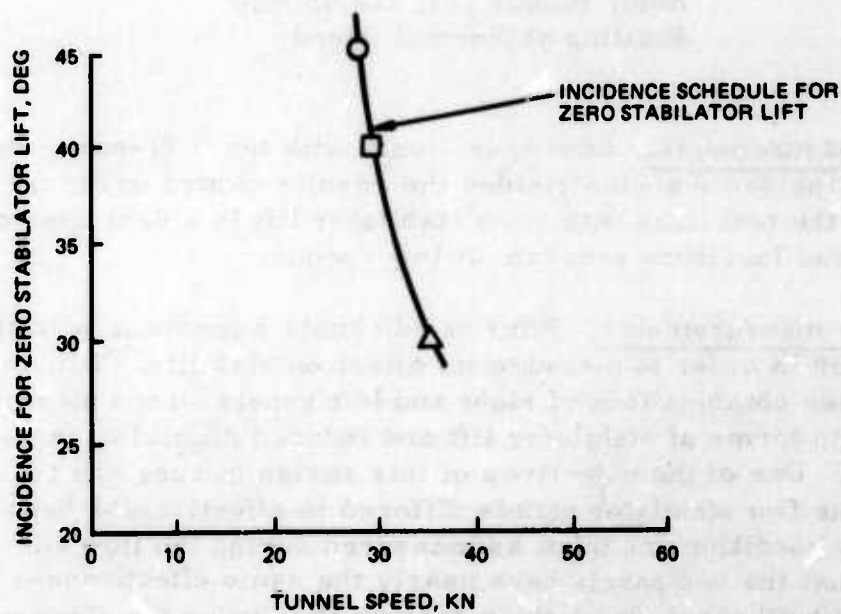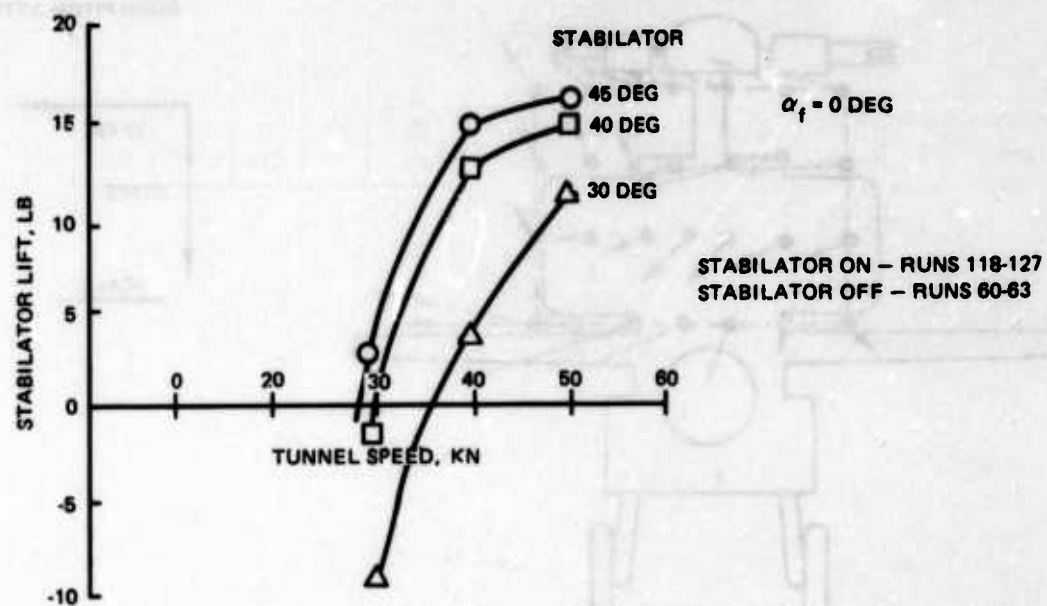
Figure 89. Lift of 0.21-scale Stabilator at Low Speed.
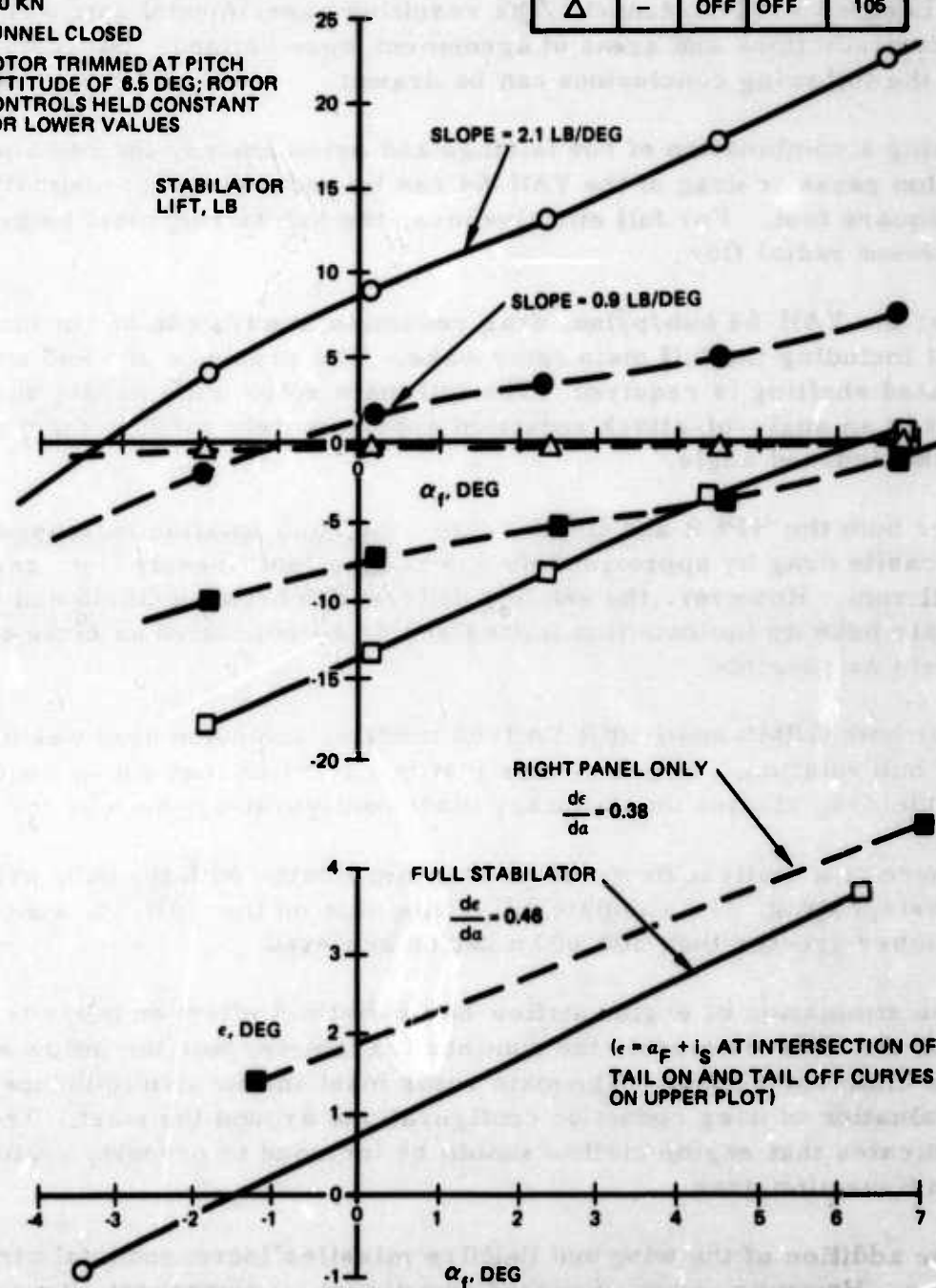
Figure 90. Stabilator Lift and Downwash Characteristics.

CONCLUSIONS

A study has been conducted using a viscous wing/body computer program (DRAG) to analyze low-drag concepts of a current helicopter. Based on this analysis, full-scale wind tunnel models were fabricated and tested in the NASA/Langley V/STOL tunnel. The resulting experimental data were compared to predictions and areas of agreement were defined. Based on the study, the following conclusions can be drawn:

- Using a combination of hub fairings and pylon fences, the combined hub/pylon parasite drag of the YAH-64 can be reduced by approximately 1 square foot. For full effectiveness, the hub fairing must be sealed to prevent radial flow.

- For the YAH-64 hub/pylon, drag reduction studies can be conducted without including the full main rotor wake. The presence of a hub and associated shafting is required. The full main rotor wake impact on airframe lift is an angle-of-attack reduction approximately equal to the momentum wake-induced angle.

- For both the HPER and GRMS scale hubs, hub rotation increased hub parasite drag by approximately 0.5 square foot linearly from zero to full rpm. However, the existing differences between GRMS and HPER scale hubs do indicate that testing should be conducted as close to full scale as possible.

- For both GRMS and HPER YAH-64 models, the pylon drag was unchanged by hub rotation. This indicates that hub rotation may not be required for pylon drag studies on stationary mast configurations such as the YAH-64.

- There is a critical Reynolds number associated with the hub, pylon, and fuselage drag. To simulate full-scale data on the YAH-64, a Reynolds number greater than 300,000 must be achieved.

- The simulation of engine airflow has a distinct effect on parasite drag. For the YAH-64 model, the dominant parameter was the inflow around the main rotor mast. The main rotor mast inflow also influenced the evaluation of drag reduction configurations around the mast. This indicates that engine airflow should be included to properly evaluate the configuration drag.

- The addition of the wing and Hellfire missiles increased total aircraft drag. However, when examined component by component, it was shown that the presence of the YAH-64 wing created a favorable interference on the engine nacelle, reducing the pylon component drag.

- The flow over the aft pylon of the YAH-64 is insensitive to angle of attack. For a rotor-off case, no changes in pressure distribution were measured over an angle-of-attack range of ±10 degrees.

- The HPER test data requires a tunnel blockage correction larger than that predicted by either generally accepted wind tunnel blockage methods or advanced analytical techniques. A correction to tunnel dynamic pressure of approximately 14 percent is required.

- Using the corrected HPER dynamic pressure, the surface pressure distributions measured on the large-scale HPER and small-scale GRMS models agree with those predicted by Program DRAG. On this basis, the analysis is judged acceptable for application to the design of higher levels of modification.

As part of the larger wind tunnel test program, a series of runs was made to determine aerodynamic conditions at the empennage position of a powered model of the YAH-64. The significant conclusions are:

- At the lowest speed tested, 25 knots, downwash angles at the stabilator quarter-chord did not exceed 47 degrees.

- The right- and left-hand stabilator panels are equally effective in producing longitudinal angle-of-attack stability.

- Even at low speeds, there is a substantial asymmetric characteristic of the flow pattern in the rotor wake, with higher wake velocities and down-wash angles behind the advancing side of the disc than behind the retreating side.

- There is a predominant sidewash to the right, apparently due to the swirl effect induced by the rotor hub.

- At low speeds the rotor wake produces a significant aft component of horizontal induced velocity as well as the expected vertical component.

- The vertical and horizontal components of steady flow in the neighborhood of the empennage indicate large changes in flow direction over relatively small distances.

- In some portions of the rotor wake, the dynamic pressure is significantly higher than that corresponding to tunnel velocity.

117

- At low positions in the rotor wake, the flow is diverging laterally, which decreases the stabilizing effect of the vertical surfaces and tail rotors located in this region. Conversely, high in the wake the flow is converging, which increases the effectiveness of high-mounted stabilizing devices. This change in the character of the flow is due to rolling up the rotor tip vortices.

RECOMMENDATIONS

Based on the results of this effort, it is recommended that:

- The UH-60A model be tested at both HPER and GRMS scales. During the GRMS testing, the internal fan installation should be altered so that pylon parasite drag can be measured with the fans in a metric and nonmetric condition.

- Advanced hub/pylon concepts be developed with the sole objective of minimum drag, that these concepts be tested, and that a cost/benefit evaluation be conducted.

- The UH-60A be tested with hub rotation to determine the effects on a configuration where the main rotor mast rotates.

- Further effort be expended on refining analytical methods for determining tunnel blockage.

- The YAH-64 HPER model be tested in a wind tunnel where the model-to-tunnel relative size is the same as that of the YAH-64 GRMS in the V/STOL tunnel.

- The YAH-64 GRMS model be tested with a larger main rotor to determine the effect on airframe surface pressures. In addition, tail rotor simulation should be included.

REFERENCES

1. Special report presented to the American Helicopter Society, 31st Annual National Forum by the Ad Hoc Committee on Rotorcraft Drag, Washington D.C., 21 May 1975.

2. Wilson, John C., A GENERAL ROTOR MODEL SYSTEM FOR WIND TUNNEL INVESTIGATION OF ROTORCRAFT AERODYNAMICS AND ACOUSTICS, Journal of Aircraft, Vol. 6, 1974.

3. Pope, Allen, and Harper, John J., LOW-SPEED WIND TUNNEL TESTING, John Wiley and Sons, Inc., New York, 1966.

4. Hess, John L., CALCULATIONS OF POTENTIAL FLOW ABOUT ARBITRARY THREE-DIMENSIONAL LIFTING BODIES, Report No. J5679-01, McDonnell Douglas Corp., October 1972.

5. Dvorak, F., Maskew, B., and Woodward, F., INVESTIGATION OF THREE-DIMENSIONAL FLOW SEPARATION ON FUSELAGE CONFIGURATIONS, Analytical Methods, Inc.; USAAMRDL-TR-77-4, Eustis Directorate, U.S. Army Air Mobility Research and Development Laboratory, Fort Eustis, VA, March 1977, AD A039382.

6. Clark, D., Dvorak, F., Maskew, B., Summa, J., and Woodward, F., HELICOPTER FLOW FIELD ANALYSIS, Analytical Methods, Inc.; USARTL-TR-79-4, Applied Technology Labora ory, U.S. Army Research and Technology Laboratories, Fort Eustis, VA, April 1979, AD A069542.

7. Woodward, F., Dvorak, F., and Geller, E., A COMPUTER PROGRAM FOR THREE-DIMENSIONAL LIFTING BODIES IN SUBSONIC INVISCID FLOW, Flow Research, Inc.; USAAMRDL-TR-74-18, Eustis Directorate, U.S. Army Air Mobility Research and Development Laboratory, Fort Eustis, VA, April 1974, AD 782202.

8. Sheehy, T.W., and Clark, D.R., A METHOD FOR PREDICTING HELICOPTER HUB DRAG, Sikorsky Aircraft Div., United Technologies Corp.; USAAMRDL-TR-75-48, Eustis Directorate, U.S. Army Air Mobility Research and Development Laboratory, Fort Eustis, VA, January 1976, AD A021201.

9. Velkoff and Horak, ROTOR WAKE MEASUREMENTS AT VERY LOW ADVANCE RATIOS, Proceedings of the 35th Forum of the American Helicopter Society, 1979.

APPENDIX A

WIND TUNNEL TEST DATA

Run logs and test configurations from all wind tunnel testing of the YAH-64 performed under this effort are presented in this appendix.

The total collection of analytical and experimental data recorded during the program was far too extensive and bulky to be included in this report. This data, in whole or in part, is available from the Applied Technology Laboratory to qualified users for research purposes.

MODEL CONFIGURATION CODE

AN	ALQ-144 antenna
BA_1	YAH-64 hub fairing
CA_1	YAH-64 cuff fairings
DA_B	YAH-64 basic doghouse
DA_1	YAH-64 first alternate doghouse
DF_1	YAH-64 aft pylon fences
FA_B	YAH-64 basic fuselage
HA_B	YAH-64 basic hub
HG_B	GRMS basic hub
MA_B	YAH-64 mast only (no hub)
PA_B	YAH-64 basic pylon
RG	GRMS rotor system
RP_1	YAH-64 missile pod
SC	Scoops added to alternate doghouse
TA_B	YAH-64 tail empennage
WA_1	YAH-64 wing

TABLE A-1. YAH-64 HPER MODEL TEST CONFIGURATION SEQUENCE

Configuration	Hub Nonrotating	Hub Rotating	Hub rpm Sweep	Hub Fairing Sealed	Rotate Torque Link Assembly	Engine Inlet	Engine Exhaust
1. $FA_B PA_B DA_B HA_B CA_1 BA_1$	X	X		X		X	X
2. $FA_B PA_B DA_B HA_B CA_1 BA_1 DA_1$	X	X	X	X			
3. $FA_B PA_B DA_B HA_B CA_1$	X	X		X			
4. $FA_B PA_B DA_B HA_B$	X	X	X		X	X	X
5. $FA_B PA_B DA_B MA_B$							
6. $FA_B PA_B DA_B$							
7. $FA_B PA_B DA_B DA_1$							
8. $FA_B PA_B$							

122

TABLE A-2. YAH-64 GRMS MODEL TEST CONFIGURATION SEQUENCES

Configuration	Hub Rotation	Hub Fairing Sealed	Rotate Torque Link	Engine Inlet/ Exhaust Runs	Basic Test Sequence	Wake Survey
1. FA_B PA_B DA_B TA_B WA_1 RP_1 RG				✓	✓	✓
1A. FA_B PA_B DA_B TA_B WA_1 RP_1 RG AN				✓	✓	
2. FA_B PA_B DA_B TA_B WA_1 RP_1 RG DF_1				✓	✓	
3. FA_B PA_B DA_B TA_B WA_1 RP_1 RG DF_1 DA_1					✓	
4. FA_B PA_B DA_B TA_B WA_1 RP_1 RG DA_1					✓	
5. FA_B PA_B DA_B TA_B RG DA_1					✓	✓
6. FA_B PA_B DA_B TA_B WA_1 RP_1 HG_B DA_1					✓	
7. FA_B PA_B DA_B TA_B WA_1 RP_1 HG_B DF_1 DA_1					✓	
8. FA_B PA_B DA_B TA_B WA_1 RP_1 HG_B DF_1					✓	
9. FA_B PA_B DA_B TA_B WA_1 RP_1 HG_B	✓				✓	✓
10. FA_B PA_B DA_B TA_B WA_1 RP_1 HA_B	✓		✓	✓	✓	✓
10A. FA_B PA_B DA_B TA_B WA_1 RP_1 HA_B AN					✓	
11. FA_B PA_B DA_B TA_B HA_B					✓	
12. FA_B PA_B DA_B TA_B WA_1 RP_1 HA_B DA_1					✓	
12A. FA_B PA_B DA_B TA_B WA_1 RP_1 HA_B DA_1 SC					✓	
13. FA_B PA_B DA_B TA_B WA_1 RP_1 HA_B DA_1 DF_1					✓	
14. FA_B PA_B DA_B TA_B WA_1 RP_1 HA_B DF_1					✓	
15. FA_B PA_B DA_B TA_B WA_1 RP_1 BA_1 CA_1 DF_1				✓	✓	
16. FA_B PA_B DA_B TA_B WA_1 RP_1 BA_1 CA_1	✓	✓	✓	✓	✓	✓
17. FA_B PA_B DA_B TA_B WA_1 RP_1 CA_1		✓			✓	
18. FA_B PA_B DA_B TA_B WA_1 RP_1 MA_B					✓	
19. FA_B PA_B DA_B TA_B WA_1 RP_1					✓	

TABLE A-3. YAH-64 HPER RUN LOG

Conf	Run No.	Vel, kn	α_1	Hub rpm	Hub Sealed	Rotate Torque Link	Engine Mass Flow	Comments
1	50	0	Sweep	0	Yes	No	Sweep	Fan static tare
	51	90	Sweep	289	No		E[1]	
	52	90	Sweep	0				
	53	145	Sweep	0				
	54	145	Sweep	289	No			
	46	90	Sweep	0	Yes			
	47	90	Sweep	289				
	48	145	Sweep	0				
1	49	145	Sweep	289	Yes			
2	34	60	Sweep	289	No			
	35	60	-5	Sweep				
		90	Sweep	0				
	36	30	Sweep	289				
	37	90	Sweep	289				
	38	120	Sweep	289				
	39	145	Sweep	289				
	40	145	Sweep	0	No			
	41	145	Sweep	289	Yes			
	42	145	Sweep	0				
	43	90	Sweep	0				
	44	90	Sweep	289	Yes		E	
2	45	0	Sweep	0	No		0	Weight tare
3	55	90	Sweep	0			E	
	56	90	Sweep	289				
	57	145	Sweep	289				
3	58	145	Sweep	0	No		E	
4	14, 15	80	Sweep	0	N/A		I	Pylon and fuselage gaps sealed
	16	60	0	Sweep				Pylon and fuselage gaps sealed
	17	60	0	Sweep				
	18	90	Sweep	0				
	19	30	Sweep	289				
	20	90	Sweep	289				
	21	120	Sweep	289				
	22	145	Sweep	289				
4	23	145	Sweep	0	N/A	No	I	

NOTE:[1] E denotes engine exhaust dynamic pressure matched. I denotes engine mast inlet dynamic pressure matched.

124

TABLE A-3. YAH-64 HPER RUN LOG (Continued)

Conf	Run No.	Vel, kn	α_l	Hub rpm	Hub Sealed	Rotate Torque Link	Engine Mass Flow	Comments
4	24	159	-5	0	N/A	No	I [1]	
	25	60	Sweep	289			I	
	26	30	Sweep	289			E	
	27	60	Sweep	289				
	28	90	Sweep	0				
	29	90	Sweep	289				
	30	120	Sweep	289				
	31	145	Sweep	289				
	32	145	Sweep	0			E	
	33	90	0, -5	289			Sweep	With various levels of airflow: inlets sealed, fans windmilling, exhaust flow, and inlet flow
	59	60	-5	Sweep		No	E	
	60	90	0	0		Yes	E	
	61	90	0	289		Yes	E	
	62	90	0	0		No	Sealed	Fans inoperative; mast and nacelle fan inlets sealed
		90	0	289				
		145	0	289				
		145	0	0				
	63	90	0	0				
		90	0	289				
		145	0	289				
		145	0	0				Fans inoperative; mast and nacelle fan inlets sealed
	63	90	0	0				Nose gearbox fairing
		90	0	289				
		145	0	289				
		145	0	0				Nose gearbox fairing
	64	90	0	0				With beanie
		90	0	289				
		145	0	289				
		145	0	0				With beanie
	65	90	0	0				With beanie sealed
		90	0	289				
		145	0	289				
4		145	0	0	N/A	No	Sealed	With beanie sealed

NOTE: [1] E denotes engine exhaust dynamic pressure matched. I denotes engine mast inlet dynamic pressure matched.

Conf	Run No.	Vel, kn	α_f	Hub rpm	Hub Sealed	Rotate Torque Link	Engine Mass Flow	Comments
4	65	90	0	0	N/A	No	Sealed	With fences
↑		90	0	289	↑	↑	↑	
		145	0	289				
		145	0	0				With fences
	67	90	0	0				With fences and alternate doghouse
		90	0	289				↕
		145	0	289				
		145	0	0				With fences and alternate doghouse
	68	90	0	0				With ALQ 144 antenna
		90	0	289				↕
		145	0	289	↓	↓	↓	
4		145	0	0				With ALQ 144 antenna
5	69	90	0	0				
5		120	0	0				
5		145	0	0				
6	70	90	0	0				
6		120	0	0				
6		145	0	0				
7	71	90	0	0				
7		120	0	0				
7		145	0	0				
8	72	90	0	0				
↑		120	0	0				
		145	0	0				
	73	90	0	0				Sealed mast opening
		120	0	0	↓	↓	↓	
8		145	0	0	N/A	No	Sealed	

TABLE A-4. YAH-64 GRMS MODEL RUN LOG – GRMS ROTOR ON

HH Conf No.	LaRC Run No.	Hub Sealed	Hub rpm	Rotate Torque Link	in, $\left(\frac{lbm}{sec}\right)$	Vel, kn	α, deg	β, deg	Comments
1	79	NA	1340	NA	E	40	Sweep	0	
	80					60			
	81					80			
	82					120	Sweep	0	
	83					80	0	Sweep	
	87				E	120		Sweep	
	84				1	80		0	
	85				1	120			
	106				E				Wake survey, stabilator position
	107								Stabilator position
	110								Stabilator + 6 inches
	109								Stabilator + 12 inches
	108					120			Stabilator + 18 inches
1A	88					Sweep	0		
2	89					40	Sweep		
	90					60			
	91					80			
	92					120			
3	93					40			
	94					60	Sweep		
	94					80	0		
	94					120	0		
	95					120	0		
4	96					Sweep	0		
5	97					40	Sweep		
	98					60	Sweep		
	99					80	Sweep	0	
	100					80	0	Sweep	
	117					120		0	Wake survey, stabilator position
	114								Stabilator + 6 inches
	115								Stabilator + 12 inches
	116				E	120	0	0	Stabilator + 18 inches
1	111				0	40	Sweep		Engines open. No drive pressure.
	112				0	80	Sweep		
	113	NA	1340	NA	0	120	Sweep		

127

TABLE A-5. YAH-64 GRMS MODEL RUN LOG — GRMS HUB ONLY

HH Conf No.	LaRC Run No.	Hub Sealed	Hub rpm	Rotate Torque Link	$\dot{m}, \left(\dfrac{lbm}{sec}\right)$	Vel, kn	α, deg	β, deg	Comments
6	167	NA	1340	NA	E	Sweep	0	0	
7	168	↑	↑	↑	↑	40	Sweep	↑	
	169					60			
	170					80			
	171					120			
8	172					40			
	173					60			
	174					80			
	175					120			
9	145					20			
	154					40			
	146					40			
	155					60			
	147					60			
	156					80			
	148					80			
	149					100	↓	↓	
	158					120	Sweep	0	
	160					80	0	Sweep	
	150		1340			120	0	Sweep	
	162		Sweep			80	Sweep	0	
	163		Sweep			80	↑	↑	
	166		770			30			
	165		770			60			
	164		770			120			
9	151		1340				↓	↓	Wake survey, stabilator position
	153		↑						Stabilator + 6 inches
	152	↓	↓	↓	↓	↓	Sweep	↓	Stabilator + 12 inches
	151	NA	1340	NA	E	120	0	0	Stabilator + 18 inches

TABLE A-6. YAH-64 GRMS MODEL RUN LOG — YAH-64 HUB

HH Conf No.	LaRC Run No.	Hub Sealed	Hub rpm	Rotate Torque Link	$\dot{m}$, $\left(\dfrac{lbm}{sec}\right)$	Vel, kn	α, deg	β, deg	Comments
10	253	NA	770	No	E	30	Sweep	0	
	254					40			
	255					80			
	256					120	Sweep	0	
	260					80	0	Sweep	
	261				F	120	0	Sweep	
	259				1	40	Sweep	0	
	258				1	80			
	257			No	1	120			
	262			Yes	E	80			
	263		770	Yes		120			
	255		Sweep	No		80	Sweep		
	242		770			120	0		Wake survey stabilator position
	243					120			
	244					120			
	246					120			Stabilator + 6 inches
	247					120			Stabilator + 12 inches
	248				F	120			Stabilator + 18 inches
	227				Sweep	0	0		
	228				Ram	80	Sweep		No fan drive pressure, Mast and nacelle inlets open
	229				Ram	120			
	230				Sealed	80			Mast and nacelle inlets sealed
	231				Sealed	120			
10A	232				E	80			
	233					120			
11	234					40			
	235					80			
	236				E	120			
	239				I	40			
	238				I	80			
	237				I	120	Sweep		
	241				E	120	0		Wake survey, stabilator position
	251					120			Stabilator + 6 inches
	250					120			Stabilator + 12 inches
	249					120	0		Stabilator + 18 inches
12	225					80	Sweep		
	226	NA	770	No	E	120	Sweep	0	

129

HH Conf No.	LaRC Run No.	Hub Sealed	Hub rpm	Rotate Torque Link	$\dot{m}$, $\left(\dfrac{lbm}{sec}\right)$	Vel, kn	α, deg	β, deg	Comments
13	222	NA	770	No	E	40	Sweep	0	
	223	NA				80			
	224	NA				120			
14	218	No				40			
	217					80			
	216					120	Sweep	0	
	219					80	0	Sweep	
	220					80	0	Sweep	
	221				E	120	0	Sweep	
	213				I	40	Sweep	0	
	214				I	80			
	215				I	120			
15	208				E	80			
	209				E	120			
	210				I	40			
	211				I	80			
	212	No			I	120			
16	188	Sealed			E	80			Beanie unsealed, cuffs sealed
	189					120			
	190					80			
	191					120	Sweep	0	Beanie and cuffs sealed
	197				E	80	0	Sweep	
	192				I	80	Sweep	0	
	193		770		I	120			
	194		Sweep		E	80			
	195		770		I	30			
	196			No		80			
	198			Yes		80			
	199					120	Sweep		
	200						0, -5		Wake survey, stabilator + 6 inches
	201			Yes					Wake survey, stabilator + 6 inches
	202			No					Stabilator + 6 inches
	203								Stabilator + 6 inches
	204								Stabilator + 12 inches
	205								Stabilator + 12 inches
	206								Stabilator + 18 inches
	207	Sealed	770	No	E	120	0, -5	0	Stabilator + 18 inches

TABLE A-6. YAH-64 GRMS MODEL RUN LOG — YAH-64 HUB (Continued)

HH Conf No.	LaRC Run No.	Hub Sealed	Hub rpm	Rotate Torque Link	$\dot{m}, \left(\dfrac{lbm}{sec}\right)$	Vel, kn	α, deg	β, deg	Comments
17	184	No	770	No	E	80	Sweep	0	
	185	No	↑	↑	↑	120	↑	↑	
	186	Sealed				80			
	187	Sealed				120			
18	180	NA				40			
	181	↑				80	Sweep		
	182					100	0		
	183					120	Sweep		
19	176					40	0, -5		
	177					60	↑		
	178					80	↓		
	179	↓				120	0, -5		
12A	264	↓	↓	↓	↓	80	Sweep	↓	
	265	NA	770	No	E	120	Sweep	0	

TABLE A-7. MISCELLANEOUS RUNS

HH Conf No.	LaRC Run No.	Hub Sealed	Hub rpm	Rotate Torque Link	$\dot{m}$, $\left(\dfrac{lbm}{sec}\right)$	Vel, kn	α, deg	β, deg	Comments
1	111	NA	1340	NA	0	40	Sweep	0	Engine tares, rotor on
1	112	↑	1340	↑	0	80	Sweep	0	Engine tares, rotor on
1	113		1340		0	120	Sweep	0	Engine tares, rotor on
10	227		770		Sweep	0	0	0	Engine tares, basic YAH-64 hub
↑	228		↑		0	80	Sweep	0	Engine tares
	229				0	120	Sweep	0	Engine tares
↓	230		↓		Sealed	80	Sweep	0	Engine tares
10	231		770		Sealed	120	Sweep	0	Engine tares
1	30		1340		E	40	0	0	Flow surveys at 0.21-scale stabilator position, small probe
↑	31		↑		↑	50	0	↑	
	32					60	0		
	33					80	0		
	34					80	+5		
	35					60	+5		
	36					50	+5		
	37					40	+10		
	38					50	+10		
	39					60	+10		
	40					80	+10		
	41					40	+5		
	42					40	+5		
	43					120	0	↓	
	44					120	+5	0	
	45					40	0	10,0, -10	
	46					60	0	10,0, -10	
	47					80	0	10,0, -10	
	48					80	0	-10	
	49					60	0	-10	
↓	50	↓	↓	↓	↓	50	0	-10	
1	51	NA	1340	NA	E	40	0	-10	

HH Conf No.	LaRC Run No.	Hub Sealed	Hub rpm	Rotate Torque Link	$\dot{m}$, $\left(\dfrac{lbm}{sec}\right)$	Vel, kn	α, deg	β, deg	Comments
1	52		1340			40	0	-10	
	53					50	0	-10	
	54					50	0	0	Flow surveys at 0.21-scale stabilator with large probe
	55					40	0	0	
	56					50	0	0	
	57					60			
	58					80			
	59					20			
	60					30			
	61					25			
	62					40			
	63					50			
	64					60	0		
	65					25	+10	0	
	66					30	+10		
	67					40	+10		
	68					50	+10		
	69					60	+10		
	70					40	0	0	Flow surveys at 0.30-scale stabilator position
	71					50	0	0	
	72					60			
	73					80			
	74					100			
	75					120	0	0	
	76					80	+5	0	
	77					100	+5	0	
	78					120	+5	0	
1	101						6, to -2	0	$i_t = 2.5$ deg
	102					120	6, to -2	0	$i_t = -2.5$ deg
	103					120	6, to -2	0	$i_t = -2.5$ deg
	104	Right panel only				120	6, to -2	0	$i_t = 2.5$ deg
	105					120	6, to -2	0	No stabilator
	118	NA	1340	NA	E	30	Sweep	0	21 percent tail empennage installed
	119				E	40	Sweep	0	
	120				E	40	Sweep	0	
	121				E	50	Sweep	0	

Stability runs with 0.30-scale stabilator. No flow surveys (for runs 101–104)

HH Conf No.	LaRC Run No.	Hub Sealed	Hub rpm	Rotate Torque Link	$\dot{m}$, $\left(\dfrac{lbm}{sec}\right)$	Vel, kn	α, deg	β, deg	Comments
1	122				E	30	Sweep	0	
	123				E	40	Sweep	0	
	124				E	50	Sweep	0	
	125				E	30	Sweep	0	
	126				E	30	Sweep	0	
	127	NA	1340	NA	E	50	Sweep	0	
9	132					20	0	0	Flow survey at 0.21-scale stabilator position
	133					30	0	↑	
	134					40	0		
	135					50	0		
	136					60	0		
	137					80	0		
	138					100	0		
	139					120	0		
	140					120	+5		
	141					80	+5		
	142					60	+5		
	143					40	+5	↓	Flow survey at 0.21-scale stabilator position
	144					20	+5	0	
10	240					120			Rotated sting for interference check
10	241			No		↑	0	0	Stabilator position
10	242						↑	↑	Stabilator position
10	243								Stabilator position
10	244								Stabilator position
10	245								Stabilator + 6 inches
10	247								Stabilator + 12 inches
10	248								Stabilator + 18 inches
11	249								Stabilator + 18 inches
11	250					↓			Stabilator + 12 inches
11	251					120	↓	↓	Stabilator + 6 inches
11	252					Sweep	0	0	Check calibration of wake

1856-81

134